DOCTORAL THESIS

Utilization and Reactivity Enhancement of Wood Ash in Cement–Based and Alkali–Activated Materials

Ece Ezgi Teker Ercan

Building Materials

LULEÅ UNIVERSITY OF TECHNOLOGY

DOCTORAL THESIS

Utilization and Reactivity Enhancement of Wood Ash in Cement–Based and Alkali–Activated Materials

Ece Ezgi Teker Ercan

Luleå, October 2025

Building Materials

Department of Civil, Environmental

and Natural Resources Engineering

Luleå University of Technology

SE-97187 Luleå, Sweden

Printed by Luleå University of Technology, 2025

ISSN 1402-1544

ISBN: 978-91-8048-887-7 (print)

ISBN: 978-91-8048-888-4 (electronic)

Luleå 2025

www.ltu.se

ACADEMIC THESIS

For the Degree of Doctor of Philosophy (Ph.D.) in Building Materials, which by due permission of the Technical Faculty Board at Luleå University of Technology will be publicly defended on:

Tuesday, October 28th, 2025, 10:00

Room E632, Luleå University of Technology

Opponent examiner:

Prof. **Lisbeth M. Ottosen**, Technical University of Denmark, Denmark

Examining committee:

Prof. **Edita Garskaite**, Vilnius University, Lithuania

Assoc. Prof. **Pablo García-Triñanes**, University of Cádiz, Spain

Assoc. Prof. **Fernando José Forte Garrido Branco**, University of Coimbra, Portugal

Principal supervisor:

Assoc. **Prof. Karin Habermehl-Cwirzen**, Luleå University of Technology, Sweden

Assistant supervisors:

Assoc. Prof. **Lale Andreas**, Luleå University of Technology, Sweden

Prof. **Andrzej Cwirzen**, Luleå University of Technology, Sweden

Chairperson:

Dr. **Thanyarat Buasiri**, Luleå University of Technology, Sweden

ACKNOWLEDGEMENTS

This PhD thesis has been prepared in the Building Materials group at Luleå University of Technology. This research was funded by the Development Fund of the Swedish Construction Industry (SBUF), Skanska, and LTU Creaternity. I would like to thank Stenvalls Trä AB and Holmen AB for providing the wood ash used in this project.

I would like to express my deepest gratitude:

To my main supervisor, Assoc. Prof. Karin Habermehl-Cwirzen, for her invaluable guidance and support throughout my entire PhD journey.

To my co-supervisors Assoc. Prof. Lale Andreas and Prof. Andrzej Cwirzen, for their insightful comments and advice.

To my colleagues in the Building Materials group: Klaudja, Thanyarat (Ploy), Ankit, Marcin, Vasiola, Magdalena, Ilda, Alaeddine, Sergio, David, Kyriaki, and Emmanuel for creating a warm working environment. Special thanks to Carina for her administrative guidance and to Rikard for his assistance in the laboratory.

To Yağmur, for her heartfelt friendship and invaluable help in Luleå from the very beginning.

To my best friend Eda, for being there, always.

Finally, to my family—my parents, Meltem and Volkan, and my brother, Bartu—for their unconditional love and unwavering support. Without them, none of this would have been possible. I am also deeply thankful to my other half, Umut, for his love, patience, and companionship while we were “strangers in a strange land, land of ice and snow” and to our lovely cat, Nobilis, for his comforting presence.

Ece Ezgi Teker Ercan

Luleå, October 2025

SUMMARY

Concrete is the most widely used construction material worldwide due to its good mechanical properties, durability, and affordability. However, Portland cement production contributes approximately 5–8% of global anthropogenic CO_2 emissions. Supplementary cementitious materials (SCM), which can partially replace Portland cement, present the greatest potential for reducing the environmental impact of the construction industry. Recently, there has been increasing interest in research on the potential use of wood ash (WA) as an SCM. Utilization of WA in concrete promotes waste reuse and offers a sustainable option for SCM. However, since the characteristics of WA can vary significantly depending on its source and production conditions, further research is needed to optimize its effective use.

This study aims to investigate the potential use of WA as an SCM and compare it with coal fly ash (FA), focusing on enhancing its reactivity and performance in both cement-based and alkali-activated materials through mechanochemical activation (MCA; high-energy grinding). The properties of WAs and the effect of MCA were examined, including Strength Activity Index (SAI), Frattini, R3 test, TGA/DTG, XRD and SEM-EDS analysis. WA was used to replace 10 wt% and 20 wt% of Portland cement in concrete and of ground granulated blast furnace slag (GGBFS) in alkali-activated mortars. Workability, strength, hydration behaviour, and microstructural properties were evaluated. The leaching behaviour of WA was evaluated through batch tests, and the environmental performance of selected concrete mixes containing WA was further investigated using dynamic surface leaching tests (DSLT) on monolithic concretes. The frost durability of these concrete mixes was examined using the de-icing salt frost scaling test.

MCA significantly increased the fineness and specific surface area of WA, resulting in enhanced reactivity. Depending on their chemical composition, some WAs exhibited predominantly pozzolanic behaviour, while others showed latent hydraulic properties. The use of WA after MCA in concrete and alkali-activated mortars led to improvements in strength, cumulative heat release and microstructure compared to unground WA. At lower replacement levels, the compressive strength improved compared with the control sample in certain mixes. In air-entrained concrete, it improves frost durability by reducing surface scaling. MCA improved the environmental compatibility by reducing the leaching of most heavy metals, despite stainless-steel grinding media increasing Cr and Ni concentrations. Principal Component Analysis (PCA) and Hierarchical Cluster Analysis (HCA) showed that, after MCA, WAs with higher pozzolanic oxide contents clustered more closely with FA.

Keywords: wood ash, mechanochemical activation, high-energy grinding, supplementary cementitious materials, pozzolanic activity, alkali-activated materials

SAMMANFATTNING

Betong är det mest använda byggmaterialet i världen på grund av dess goda mekaniska egenskaper, hållbarhet och överkomliga kostnader. Produktionen av portlandcement bidrar dock med cirka 5–8% av de globala antropogena koldioxidutsläppen. Kompletterande cementbaserade material, som delvis kan ersätta portlandcement, har stor potential att minska byggindustrins miljöpåverkan. Nyligen har intresset för forskning om den potentiella användningen av träaska som ett kompletterande cementbaserat material ökat. Användningen av sådana restmaterial i betong främjar återvinning av avfall och erbjuder ett hållbart alternativ till portlandcement. Eftersom träaskans egenskaper kan variera avsevärt beroende på källa och produktionsförhållanden krävs ytterligare forskning för att optimera dess effektiva användning.

Denna studie syftar till att undersöka den potentiella användningen av träaska som ett kompletterande cementbaserat material och jämföra den med kolflygaska, med fokus på att förbättra reaktivitet och prestanda i både cementbaserade och alkaliaktiverade material genom mekanokemisk aktivering (högenergimalning). Egenskaperna hos träaskor och effekten av mekanokemisk aktivering undersöktes med hjälp av Strength Activity Index, Frattini-test, R3-test, TGA/DTG, XRD samt SEM-EDS-analyser. Träaska användes för att ersätta 10 viktprocent respektive 20 viktprocent portlandcement i betong och mald granulerad masugnsslagg i alkaliaktiverade murbruk. Arbetbarhet, hållfasthet, hydratiseringsbeteende och mikrostrukturella egenskaper utvärderades. Träaskan analyserades även genom batchlaktester, och miljöprestandan hos utvalda betongblandningar innehållande träaska undersöktes vidare med dynamiska ytlakningstester (DSLT) på monolitisk betong. Frostbeständigheten hos dessa blandningar undersöktes med hjälp av frostskalningstester med avisningssalt.

Mekanokemisk aktivering ökade finheten och den specifika ytan hos träaska signifikant, vilket resulterade i förbättrad reaktivitet. Beroende på kemisk sammansättning uppvisade vissa träaskor främst pozzolanskt beteende, medan andra visade latenta hydrauliska egenskaper. Användning av träaska efter mekanokemisk aktivering i betong och alkaliaktiverade murbruk ledde till förbättringar i hållfasthet, kumulativ värmeutveckling och mikrostruktur jämfört med omald träaska. Vid lägre ersättningsnivåer förbättrades tryckhållfastheten i vissa blandningar jämfört med kontrollprovet. I luftporbildad betong förbättrades frostbeständigheten genom minskad ytavskalning. Mekanokemisk aktivering förbättrade även miljökompatibiliteten genom att minska urlakningen av de flesta tungmetaller, även om slipmedia i rostfritt stål ökade Cr- och Ni-halterna. Huvudkomponentanalys och hierarkisk klusteranalys visade att träaska med högre halter av pozzolanoxider, efter mekanokemisk aktivering, grupperades närmare flygaska.

Nyckelord: träaska, mekanokemisk aktivering, högenergimalning, kompletterande cementbaserade material, pozzolanaktivitet, alkaliaktiverade material

ÖZET

Beton, mekanik özellikleri, dayanıklılığı ve düşük maliyeti nedeniyle dünya genelinde en yaygın kullanılan yapı malzemesidir. Ancak, küresel antropojenik CO_2 emisyonlarının yaklaşık %5–8'i Portland çimentosu üretiminden kaynaklanmaktadır. Portland çimentosunun kısmen ikame edilebildiği mineral katkılar, inşaat sektörünün olumsuz çevresel etkilerini azaltma konusunda büyük potansiyele sahiptir. Son yıllarda, odun külünün mineral katkı olarak kullanılabilirliği üzerine araştırmalara olan ilgi artmaktadır. Beton içinde odun külünün değerlendirilmesi, atıkların yeniden kullanımını teşvik ederken aynı zamanda sürdürülebilir bir seçenek sunmaktadır. Ancak, odun külünün özellikleri kaynağına ve üretim koşullarına bağlı olarak önemli ölçüde değişiklik gösterebildiğinden, etkin kullanımını optimize etmek için daha fazla araştırmaya ihtiyaç vardır.

Bu çalışma, odun külünün tamamlayıcı çimentolu malzeme olarak potansiyel kullanımını araştırmayı ve kömür uçucu külü ile karşılaştırmayı; hem çimentolu hem de alkali ile aktive edilmiş malzemelerde reaktivitesini ve performansını mekanokimyasal aktivasyon (yüksek enerjili öğütme) yoluyla artırmaya odaklanmaktadır. Odun küllerinin özellikleri ve mekanokimyasal aktivasyonun etkileri; Dayanım Aktivite İndeksi, Frattini testi, R3 testi, TGA/DTG, XRD ve SEM-EDS analizleri aracılığıyla incelenmiştir. Beton içinde Portland çimentosunun %10 ve %20 ikame oranlarında, ayrıca alkali ile aktive edilmiş harçlarda yüksek fırın cürufu ikamesinde odun külü kullanılmıştır. İşlenebilirlik, dayanım, hidratasyon davranışı ve mikroyapısal özellikler değerlendirilmiştir. Ayrıca, odun külünün liç davranışı incelenmiş; seçilmiş beton karışımlarının çevresel performansı, monolitik numuneler üzerinde gerçekleştirilen dinamik yüzey liç testleri ile araştırılmıştır. Aynı beton karışımlarının donma-çözülme dayanıklılığı değerlendirilmiştir.

Mekanokimyasal aktivasyon, odun külünün inceliğini ve özgül yüzey alanını anlamlı ölçüde artırarak reaktivitesini geliştirmiştir. Kimyasal bileşimlerine bağlı olarak bazı odun küllerinin ağırlıklı olarak puzolanik davranış, bazılarının ise gizli hidrolik özellikler sergilediği görülmüştür. Mekanokimyasal aktivasyondan sonra odun külünün beton ve alkali ile aktive harçlarda kullanımı, öğütülmemiş odun külüne kıyasla dayanım, kümülatif ısı çıkışı ve mikroyapıda iyileşmelere yol açmıştır. Daha düşük ikame seviyelerinde, bazı karışımlarda kontrol numunesine kıyasla basınç dayanımında artış gözlenmiştir. Hava sürüklenmiş betonlarda, yüzey soyulmasını azaltarak donma-çözülme dayanıklılığını öğütülmemiş küle kıyasla artırmıştır. Mekanokimyasal aktivasyon ayrıca, paslanmaz çelik öğütme ortamının Cr ve Ni konsantrasyonlarını artırsa da, çoğu ağır metalin liç yoluyla salımını azaltarak çevresel uyumluluğu iyileştirmiştir. Temel Bileşenler Analizi ve Hiyerarşik Kümeleme Analizi, mekanokimyasal aktivasyon sonrası puzolanik oksit içerikleri daha yüksek olan odun küllerinin uçucu kül ile daha yakın kümelendiğini göstermiştir.

Anahtar Kelimeler: odun külü, mekanokimyasal aktivasyon, yüksek enerjili öğütme, tamamlayıcı çimentolu malzemeler, puzolanik aktivite, alkali ile aktive edilmiş malzemeler

Table of Contents

List of Figures

List of Tables

Terms and Abbreviations

Abbreviations	Description
AEA	Air-entraining admixture
C–A–S–H	Calcium aluminium silicate hydrate
C–S–H	Calcium silicate hydrate
CH	Portlandite
CTRL	Control sample
D10	10th percentile particle size
D50	Median particle size
D90	90th percentile particle size
DSLT	Dynamic Surface Leaching Test
DTG	Derivative Thermogravimetry
EC	Electrical conductivity
EDS	Energy Dispersive Spectroscopy
FA	Fly Ash
F–T	Freeze-thaw
GGBFS	Ground Granulated Blast Furnace Slag
HCA	Hierarchical Cluster Analysis
HM	Hydration modulus
Kb	Basicity coefficient
LOI	Loss on ignition
MCA	Mechanochemical Activation
Ms	Alkali modulus
N–A–S–H	Sodium aluminium silicate hydrate
OPC	Ordinary Portland cement
PCA	Principal Component Analysis
PSD	Particle Size Distribution
R3	Rapid, relevant, and reliable test
rpm	Revolutions per minute
s/b	Sand-to-binder ratio
SAI	Strength Activity Index
SC	Sodium carbonate
SCM	Supplementary Cementitious Material
SEM	Scanning Electron Microscopy
SH	Sodium hydroxide
SP	Superplasticizer
SSA	Specific Surface Area
SS	Sodium silicate
TGA	Thermogravimetric analysis
w/b	Water-to-binder ratio
WA	Wood Ash
WA1	Wood Ash 1 (unground)
WA1-10m	Wood Ash 1 (10 min ground)
WA1-20m	Wood Ash 1 (20 min ground)

WA2	Wood Ash 2 (unground)
WA2-10m	Wood Ash 2 (10 min ground)
WA2-20m	Wood Ash 2 (20 min ground)
WA3	Wood Ash 3 (unground)
WA3-10m	Wood Ash 3 (10 min ground)
WA3-20m	Wood Ash 3 (20 min ground)
WA4	Wood Ash 4 (unground)
WA4-10m	Wood Ash 4 (10 min ground)
WA4-20m	Wood Ash 4 (20 min ground)
wt%	Weight percent
XRD	X-ray diffraction

Chapter 1

Introduction

Concrete is the most used material in construction because it offers good mechanical properties, durability, and affordability (Monteiro et al., 2017; Teixeira et al., 2019). In 2020, 14 billion m^3 of concrete were produced worldwide (Global Cement and Concrete Association, 2022). Portland cement, the main component of concrete, has a high environmental impact because in clinker production limestone ($CaCO_3$) is decomposed into lime (CaO) and CO_2 in a process called calcination, which releases large amounts of greenhouse gases (Bakhoum et al., 2023; Teixeira et al., 2016; Ukrainczyk et al., 2016). Global cement production in 2023 was 4.07 billion tonnes (IEA, 2024). Cement production is a carbon-intensive process, emitting approximately 500–900 kg of CO_2 per tonne of cement (Tripathi et al., 2020), depending on the fuel type and production technology employed. According to data from the International Energy Agency (IEA), the global average emissions intensity of cement production has remained relatively stable at around 600 kg of CO_2 per tonne of cement since 2018 (IEA, 2025). It is estimated that the cement industry is responsible for approximately 5–8% of global anthropogenic CO_2 emissions. Reducing the CO_2 footprint of the construction industry by using supplementary cementitious materials (SCM) is therefore essential and aligns with the goals of the Paris Agreement to limit global warming to 1.5 °C (Hills et al., 2020; Scrivener et al., 2018).

SCMs are used to reduce the environmental impact of the construction industry by partially replacing Portland cement. They can reduce the clinker content and improve the performance of concrete (Scrivener et al., 2018b). For decades, coal fly ash has been the most common SCM due to its availability and pozzolanic behaviour. Today, its supply is decreasing because coal-based thermal power plants are being closed (Rumman & Alam, 2025). Therefore, there is a growing demand to explore alternative SCMs that are both

effective and more sustainable. Wood ash (WA) is one of the promising options (Gerges et al., 2021; Omran et al., 2018).

Globally, around 4600 million tonnes of wood-derived biomass are produced each year; about 60% is used for energy, 20% for industrial purposes, and the remaining 20% is lost during primary production and decomposes in the field (Tripathi et al., 2019). WA is the residue formed during the combustion of wood and wood-based products; most is landfilled, while some is used in agriculture and forestry (Ndahirwa et al., 2024; Rumman & Alam, 2025). However, landfilling leads to future costs and capacity challenges, and can cause the leaching of hazardous elements, potentially contaminating soils and groundwater (Bakhoum et al., 2023; Drljača et al., 2022; James et al., 2012). Fine ash particles may also become airborne and pose local health or nuisance risks, while some agricultural uses can be limited by heavy metal content and pH levels (Cheah & Ramli, 2011; Maresca et al., 2018; Sigvardsen et al., 2019). Compared to traditional disposal methods, incorporating WA into concrete can provide a more product-oriented approach by helping to immobilize contaminants within a hardened matrix and potentially reducing clinker consumption (Berra et al., 2019; Siddique, 2012).

Despite this potential, quality control is challenging because the composition depends on many factors, including tree species and parts, geographic origin, combustion technology and temperature, and collection and storage conditions (Berra et al., 2015; Etiégni & Campbell, 1991; Ottosen et al., 2016; Ukrainczyk et al., 2016). As a result, WA often does not meet the requirements of common standards developed for fly ash, such as EN 450-1 and ASTM C618. Typical characteristics, including irregular and porous particles, a broad particle-size distribution, and high loss on ignition (LOI), can reduce workability and may lower early strength if WA is used without any pre-treatment. Nonetheless, several studies show that WA can be used in construction materials under certain conditions (Abdullahi, 2006; Berra et al., 2015; Carević et al., 2019; Garcia & Sousa-Coutinho, 2013; Rajamma et al., 2009; Sigvardsen et al., 2019; Udoeyo et al., 2006).

In cement-based systems, WA can serve as a filler and, depending on its chemistry and amorphous content, may exhibit pozzolanic or latent hydraulic behaviour. The balance between physical filler effects and chemical reactivity depends on ash type, fineness, and cement replacement ratio (Carević et al., 2019; Demis et al., 2014; Rajamma et al., 2009; Wang et al., 2022).

Beyond cement-based systems, WA can also be used in alkali-activated systems. It can be used as a precursor alongside fly ash, granulated ground blast furnace slag (GGBFS), or metakaolin, or as an alkaline source (Abdulkareem et al., 2019; Bajare et al., 2011; Candamano et al., 2017; Cheah et al., 2015; Silva et al., 2022).

Pre-treatment methods can enhance the usability of WA in building materials (Amaral et al., 2022; Berra et al., 2015; Doudart de la Grée et al., 2016; Teker Ercan et al., 2023). In this context, mechanochemical activation (MCA) is a popular method for other SCMs to reduce particle size, increase specific surface area, and introduce structural disorder, all of which

might improve dissolution of reactive species and promote hydration (Donatello et al., 2010; Ke et al., 2023; Kumar & Kumar, 2011; Mucsi, 2016; Snellings et al., 2021). It could also be considered a potential pre-treatment option for biomass ashes, including WA (Kaminskas & Cesnauskas, 2014; Pantić et al., 2023; Rosales et al., 2017; Xu et al., 2015).

1.1. Aim and Objectives

This research aims to enhance the reactivity of wood ash through mechanochemical activation and to assess its potential for use in cement-based and alkali-activated materials, focusing on its impact on material properties, frost durability, and environmental performance.

The objectives of this research are as follows:

1. Assess the selected properties of wood ash before and after mechanochemical activation.
2. Evaluate the reactivity of different types of wood ash and investigate the effect of mechanochemical activation on its reactivity.
3. Evaluate the mechanical and microstructural properties, as well as the frost durability, of concrete containing unground and ground wood ash.
4. Investigate the environmental performance of wood ash-based concrete through leaching behaviour.
5. Investigate the mechanical and microstructural behaviour of alkali-activated mixes incorporating wood ash.

1.2. Scientific Approach

This research began with a comprehensive literature review to identify knowledge gaps concerning the use of wood ash in cement-based and alkali-activated systems. Based on the findings, a series of experimental studies were designed to investigate the effects of wood ash type, replacement level, and grinding duration on material performance. Following initial trials with various mechanochemical activation parameters, the final parameters were selected according to the research objectives and environmental considerations, including grinding duration and the ball-to-powder ratio.

In cement-based systems, wood ash was used as a partial replacement for Portland cement, while in alkali-activated systems, it was assessed as a partial substitute for ground granulated blast furnace slag (GGBFS). The experimental program focused on evaluating reactivity, mechanical performance, durability, and environmental behaviour to assess the feasibility of using wood ash as a sustainable alternative in construction materials. Additionally, the behaviour of wood ash was compared with that of fly ash (FA), with a particular focus on pozzolanic reactivity and its influence on the mechanical and durability performance of concrete.

To support the interpretation of the results, multivariate statistical analyses, including Principal Component Analysis (PCA) and Hierarchical Cluster Analysis (HCA), were conducted to identify dominant patterns and relationships among physical, chemical, and pozzolanic properties.

1.3. Research Questions

The following research questions were formulated for the project:

1. How does the utilization of wood ash in both cement-based and alkali-activated materials influence their mechanical properties, durability, and environmental impact? **(Paper I)**
2. How do wood ashes with varying chemical compositions respond to mechanochemical activation in terms of pozzolanic reactivity? **(Paper II)**
3. How does mechanochemical activation of wood ash affect the strength of concrete and hydration when used as a partial cement replacement, and what is the optimum grinding duration? **(Paper II, III)**
4. How does mechanochemical activation affect the leaching behaviour of heavy metals in wood ash and in concretes incorporating wood ash as a cement replacement? **(Paper III)**
5. How do wood ash incorporation and mechanochemical activation affect the freeze-thaw durability of concrete? **(Paper III)**
6. How does the incorporation of wood ash and mechanochemical activation affect the mechanical properties of alkali-activated mortars when used as a partial slag replacement, and what is the optimum grinding duration? **(Paper IV)**

1.4. Limitations

The following limitations were identified during this research:

- Only four different types of wood ash were obtained from two sources, and only one of them was available in enough quantity for concrete durability testing. The remaining samples were limited in volume and were therefore used only for selected experimental investigations.
- A comparative analysis was conducted between unground wood ash and wood ash ground for specific durations. Although different grinding parameters were tested in initial trials, material limitations, energy use concerns, and time constraints limited the study to two grinding durations.
- X-ray diffraction (XRD) analysis was performed to identify crystalline phases. However, due to limited resources, no Rietveld refinement was conducted. As a result, the XRD data should be considered semi-quantitative and do not provide accurate phase quantification.

- Freeze–thaw and leaching tests were performed only on one type of wood ash and for a single grinding duration due to material limitations. Additionally, leaching tests were conducted only at specific time intervals because of the limited resources. As a result, the outcomes do not fully represent other wood ash types or long-term leaching behaviour.
- This doctoral thesis focused only on laboratory-scale experimental investigations.

1.5. Structure of the Thesis

This PhD thesis is a compilation of three research papers and one review paper, and it is structured into five chapters:

		Key Papers
Chapter 1	**Introduction** Introduces the aim, scope, limitations, research questions and the list of appended publications.	
Chapter 2	**Literature Review** Presents literature review on the use of wood ash in both cement-based and alkali-activated materials and their fresh, strength and durability properties.	**Paper I**
Chapter 3	**Materials and Methods** Describes the materials and methods used in this project.	**Paper II – IV**
Chapter 4	**Results and Discussion** Presents and interprets experimental results related to using wood ash in alkali-activated and cement-based systems, focusing on reactivity, mechanical performance, durability, and environmental impact.	**Paper II – IV**
Chapter 5	**Conclusion** Summarizes the main findings and outlines key conclusions and suggestions for future research.	**Paper I – IV**

1.6. List of Appended Publications

The following publications are included in this doctoral thesis:

Paper I **Teker Ercan, E. E.**, Andreas, L., Cwirzen, A., & Habermehl-Cwirzen, K. (2023). Wood Ash as Sustainable Alternative Raw Material for the Production of Concrete – A Review. *Materials*. *16*(7), 2557. https://doi.org/10.3390/ma16072557

Paper II **Teker Ercan, E. E.**, Panek, R., Szeląg, M., Cwirzen, A., & Habermehl-Cwirzen, K. (2025). The Impact of the High-Energy Grinding of Wood Ash on Its Pozzolanic Activity. *Materials*, *18*(13), 3100. https://doi.org/10.3390/ma18133100

Paper III **Teker Ercan, E.E.**, Andreas, L., Cwirzen, A., Habermehl-Cwirzen, K. (2025). Ground Wood Ash as a Supplementary Cementitious Material: Effects on Strength, Durability and Environmental Performance of Concrete. *Construction and Building Materials,* Under Review.

Paper IV **Teker Ercan, E. E.**, Cwirzen, A., & Habermehl-Cwirzen, K. (2023). The Effects of Partial Replacement of Ground Granulated Blast Furnace Slag by Ground Wood Ash on Alkali-Activated Binder Systems. *Materials*, *16*(15), 5347. https://doi.org/10.3390/ma16155347

Conferences

"The Impact of Wood Ash Grinding Duration on the Mechanical Characteristics of Alkali-Activated Mortars" – ACI Spring Convention Poster Session, March 2024, New Orleans, LA, USA.

"Effect of Different Grinding Durations on the Pozzolanic Property of Wood Ash" – RILEM Spring Convention Poster Session, March 2025, Mendrisio, Switzerland.

Chapter 2

Literature Review

2.1. Supplementary Cementitious Materials

Supplementary Cementitious Materials (SCM) are derived from industrial byproducts, waste streams, or natural sources, and they exhibit either pozzolanic or hydraulic reactivity. These materials are commonly used to partially replace Portland cement in concrete, aiming to reduce environmental impact and improve strength and long-term performance. In cementitious systems, SCMs interact with water and/or cement hydration products, participating in different chemical or physical mechanisms that influence strength development, microstructure, and durability.

Pozzolanic SCMs, such as fly ash, silica fume, calcined clays, volcanic tuffs and rice-husk ashes are defined as siliceous or siliceous-aluminous materials that have little or no inherent cementitious value on their own but can chemically react with calcium hydroxide ($Ca(OH)_2$) in the presence of water (Snellings et al., 2012). According to EN 450-1, a material is classified as pozzolanic if the total content of pozzolanic oxides, which are SiO_2, Al_2O_3, and Fe_2O_3, exceed 70%. This pozzolanic reaction produces additional calcium silicate hydrate (C–S–H) gel, the primary strength-giving phase in hydrated cement, and consumes portlandite, leading to a denser and more durable microstructure.

Hydraulic or latent hydraulic SCMs, such as blast furnace slag, can react directly with water under alkaline conditions to form cementitious hydrates without requiring external $Ca(OH)_2$. In latent hydraulic reactions, $Ca(OH)_2$ mainly helps maintain a high pH rather than acting as a reactant (Skibsted & Snellings, 2019).

In addition to chemical reactivity, SCMs can affect hydration through physical effects. The filler effect describes how fine particles accelerate early hydration by creating nucleation sites, which are surfaces where hydration products such as C–S–H begin to precipitate. This

effect results from the high surface area of SCMs, reduced interparticle spacing, and enhanced shear conditions during mixing, all of which contribute to denser and more rapid hydrate formation. The filler effect involves two main mechanisms: dilution of cement and heterogeneous nucleation on the surfaces of SCM particles (Berodier & Scrivener, 2014; Lothenbach et al., 2011; Skibsted & Snellings, 2019; Snellings et al., 2012).

The dilution effect occurs when cement is partially replaced with less reactive or inert materials, lowering the overall clinker content and slowing down strength development. However, dilution also creates more space and water per unit of clinker, which can promote hydrate growth in the early stages. However, this effect can be countered over time by pozzolanic or hydraulic reactions. Heterogeneous nucleation depends strongly on the surface chemistry and fineness of SCM particles, which provide favourable sites for the early precipitation of C–S–H (Berodier & Scrivener, 2014; Lothenbach et al., 2011; Skibsted & Snellings, 2019; Snellings et al., 2012).

The reactivity and performance of an SCM depend on several factors, including its chemical composition, fineness, amorphous phase content, and the alkaline environment created by the cement paste. Understanding these mechanisms is crucial for optimizing blended cement formulations that achieve the right balance of early strength, durability, and sustainability.

There are many different test methods for assessing pozzolanic activity, which can be categorized as either direct or indirect. Direct methods include the Frattini test, the Chapelle test, the saturated lime method, and analytical methods such as X-ray diffraction (XRD) or thermogravimetric analysis (TGA). These methods observe the presence of $Ca(OH)_2$ and the reduction in calcium ion concentration over time due to the pozzolanic reaction (Donatello et al., 2010; Šídlová et al., 2023). Indirect methods, which include the strength activity index (SAI), electrical conductivity test, and rapid, relevant, and reliable (R3) test, among others, measure physical properties like compressive strength, electrical conductivity, or heat evolution through calorimetry (Juenger et al., 2019; Kramar & Ducman, 2018).

Over the past few decades, fly ash, an industrial by-product, has been widely used as a partial replacement for cement to decrease environmental impact and improve cost-efficiency in cementitious materials. However, the gradual shutdown of coal-fired thermal power plants around the world has caused a significant decrease in the availability of high-quality fly ash (Lazik et al., 2020). As a result, there is growing interest in alternative supplementary materials like biomass and wood ashes, which provide more sustainable and locally sourced options for cement replacement. Given their promising potential, research into the properties and performance of wood ash in cement-based systems has increased (Gerges et al., 2021; Omran et al., 2018).

2.2. Characteristics of Wood Ash

2.2.1. Physical Properties

The physical characteristics of wood ash (WA) significantly affects its water demand, workability, and reactivity when used as a supplementary cementitious material (Celik, 2009). Among these characteristics, surface area, particle fineness, and morphology significantly affect the kinetics of pozzolanic and hydraulic reactions, with finer particles generally improving reactivity (Carević et al., 2019).

Berra et al. (2015) reported particle sizes ranging from 86 to 176 μm for three WA samples, with real densities between 2.35 and 2.76 g/cm³. The inherently lower density of WA compared to Portland cement results in a reduction in the unit weight of mixtures, which can affect both fresh and hardened properties. Rajamma et al. (2009) highlighted differences between two fly ashes: one from forest residues (F1) with a specific surface area of 40.29 m²/g and another from the pulp and paper industry (F2) with 7.92 m²/g, despite similar densities. These differences were attributed to variations in shape and unburned carbon content, which directly impact water demand and workability.

Carević et al. (2019) emphasized that wood bottom ash (WBA) particles are generally coarser and more angular than wood fly ash (WFA) and Portland cement. Their study showed particle sizes ranging from 10 to 1000 μm for WBA and 0.2 to 100 μm for WFA, emphasizing the heterogeneity of ash fractions. Several studies consistently describe WA particles as porous, angular, and irregular in shape (Berra et al., 2015; Carević et al., 2019; Lescinskis et al., 2025; Rajamma et al., 2009; Ukrainczyk et al., 2016), features that are strongly associated with higher water demand and inconsistent workability (Baričević et al., 2021; Castrillón & Gil, 2020; Rajamma et al., 2009, 2015; Sigvardsen & Ottosen, 2019). Rumman & Alam (2025) observed that low and high temperature WFA samples had median particle sizes of 55.7 and 34.6 μm, respectively, both coarser than typical Class F coal fly ash (25.3 μm). These relatively large particle sizes, along with low amorphous content, were associated with delayed pozzolanic activity and decreased flowability.

Similarly, Šantek Bajto et al. (2021) reported particle size distributions ranging from 6.10 to 129.52 μm for WA and pointed out that the irregular and porous morphology increased water demand and negatively affected fresh-state properties. Abdulkareem et al. (2018) also confirmed that WFA has greater angularity and surface porosity than conventional coal fly ash, which may reduce packing efficiency and slow early hydration kinetics.

2.2.2. Chemical Properties

The chemical composition of supplementary cementitious materials is important in determining their performance in cementitious systems. Major oxides include CaO, SiO_2, Al_2O_3, and Fe_2O_3, which are directly related to the binder's hydraulic and pozzolanic properties. According to EN 450-1, fly ash used in concrete should contain a minimum of 70% of pozzolanic oxides ($SiO_2 + Al_2O_3 + Fe_2O_3$), more than 25% reactive SiO_2, less than 10% reactive CaO, alkali content ($Na_2O + K_2O$) below 5%, MgO under 4%, chloride content

below 0.10%, and SO_3 under 3%. While wood ash generally does not meet all these requirements, it can still contribute beneficially depending on its specific chemical and mineralogical compositions.

Etiégni and Campbell (1991) characterized WA as a highly alkaline material with pH values ranging from 9 to 13.5 due to the presence of hydroxides, carbonates, and bicarbonates. This observation was supported by Sklivaniti et al. (2017), who recorded a pH of 11.7 and attributed it to high hydroxide and carbonate content. When compared to coal fly ash, WA typically contains higher levels of LOI, CaO, K_2O, P_2O_5, and MgO (Carević et al., 2020; Štirmer et al., 2018), though these vary widely depending on feedstock, combustion method, and treatment. Vassilev et al. (2010) examined 28 WA samples and reported a general oxide distribution trend was $CaO > SiO_2 > K_2O > MgO > A_2O_3 > P_2O_5$. Wembe et al. (2024) further emphasized the species-dependent nature of WA, noting that only certain types met the pozzolanic oxide requirement, while others did not.

Sigvardsen et al. (2019) highlighted the importance of the production parameter, noting that WA produced by circulating fluidized bed (CFB) combustion exhibited chemical and physical characteristics favourable for hydraulic behaviour. In contrast, high-temperature grate combustion produced finer, inert particles better suited as fillers. However, none of the studied WAs exceeded the 70% pozzolanic oxide threshold, highlighting the limitations of EN 450-1 criteria for WA classification.

The combustion temperature also significantly influences the chemical composition of WA. According to Etiégni and Campbell (1991), increasing the combustion temperature from 538 to 1093 °C generally increases the levels of Ca, K, Mg, Si, and P, while reducing the amounts of more volatile elements like K, Na, and Zn. This occurs because some oxides decompose at lower temperatures. Rumman and Alam (2025) confirmed that high-temperature combustion (≥800 °C) increased the CaO content (up to 53.67%) and led to lower LOI and higher reactivity. On the other hand, ashes produced at lower temperatures contain more unburnt fractions and have less amorphous content.

The loss on ignition (LOI) reflects the unburned carbon and organic content in the ash, caused by uncontrolled or incomplete incineration, and it can vary depending on the analysis temperature. The maximum allowable LOI limits in ASTM C618 (2015) vary according to the type of fly ash, ranging from 6% to 10%, while EN 450-1 sets limits between 5% and 9%. According to ASTM C618, using Class F fly ash with up to 12% loss on ignition is permitted if acceptable performance results are provided.

High LOI in WA has been shown to negatively impact pozzolanic reactivity, workability, setting behaviour, and durability performance (Berra et al., 2016; Carević et al., 2020; Hamid & Rafiq, 2020). Ngueyep and Leroy (2019) noted that when LOI exceeds 12%, the unburnt carbon content interferes with the cement hydration and reduces pozzolanic performance, causing the ash to act mainly as a filler. Sklivaniti et al. (2017) attributed a 42% LOI in bottom ash to the formation of $CaCO_3$ and $K_2Ca(CO_3)_2$ from combustion carbonation. Carević et al.

(2021) mentioned that the decomposition of hydrated and carbonated wood ash phases also results in a high LOI.

2.2.3. Mineralogical Properties

X-ray diffraction (XRD) analyses have shown the presence of both crystalline and amorphous phases in WA. Etiégni and Campbell (1991) identified lime, calcite, portlandite, and calcium silicate as the main mineral components. Similarly, Elinwa and Mahmood (2002) reported a mineralogical profile primarily composed of silicates and carbonates in sawdust ash. Ngueyep and Leroy (2019) highlighted the presence of amorphous silica in WA, suggesting its potential pozzolanic reactivity. Along with the amorphous phase, their analysis also revealed various crystalline minerals, including calcite, gypsum, anhydrite, quartz, tridymite, magnetite, hematite, rutile, and muscovite. This diverse mineralogy reflects the heterogeneous nature and its dependence on combustion parameters. Chowdhury et al. (2015) confirmed that silica in WA exists in both amorphous and crystalline forms, further emphasizing its complex structure. Ukrainczyk et al. (2016) identified key mineral phases such as free lime (CaO), periclase (MgO), larnite ($2CaO \cdot SiO_2$), and calcium carbonate ($CaCO_3$), which may contribute to hydraulic or latent hydraulic behaviour. The effect of WA on cement hydration products was also studied using XRD of hydrated pastes. Rajamma et al. (2009) observed that pastes with 10 wt% and 30 wt% WA showed peaks corresponding to calcium hydroxide, calcium aluminate hydrate, and calcium silicate phases, along with ettringite, calcite, and silica. They noted that calcium silicate peaks were more prominent in samples with 10 wt% WA than in those with 30 wt%, indicating a dilution effect at higher replacement levels. The formation of ettringite was linked to increased alkali and water content associated with higher WA ratios.

2.2.4. Reactivity Potential

The pozzolanic potential of WA has been widely discussed in the literature, with reported values for the sum of pozzolanic oxides ranging from 13.03% (Jurić et al., 2021) to 88.32% (Ramos et al., 2013). Several studies have confirmed the pozzolanic behaviour of wood ash (Chowdhury et al., 2015; Elinwa & Mahmood, 2002; Fořt et al., 2020; Jurić et al., 2021; Rajamma et al., 2009). For example, Elinwa and Mahmood (2002) identified pozzolanic properties in sawdust ash with a pozzolanic oxide content of 73.55%. Rajamma et al. (2009) observed pozzolanic activity in wood fly ash based on Frattini test results, despite a lower oxide content of 53.2%. Likewise, Ramos et al. (2013) demonstrated the pozzolanic performance of wood ash through a strength activity index test in accordance with EN 450-1, using a 20 wt% replacement level of Portland cement. Kostanić Jurić et al. (2021) examined various wood ashes and observed pozzolanic and hydraulic properties in some longer-aged samples through the SAI and Frattini test.

In contrast, some studies have shown that certain WAs do not display pozzolanic behaviour. Garcia and Sousa-Coutinho (2013), for example, found no pozzolanic activity in various wood fly and bottom ashes based on Frattini test results. Demis et al. (2014) attributed the lack of reactivity to a low SiO_2 content (31.8%) and a high LOI of 27%.

Cheah and Ramli (2012) suggested that the high CaO content in WA may contribute to its hydraulic behaviour. Similarly, Berra et al. (2015), who found no pozzolanic activity according to EN 196-5, attributed the strength gains in concrete to the hydraulic properties of WA. Sigvardsen et al. (2021) also identified hydraulic characteristics in WA. Furthermore, Carević et al. (2019) noted that most of the studied WA are located near Portland cement in the $CaO–Al_2O_3–SiO_2$ ternary diagram, indicating a tendency toward hydraulic rather than pozzolanic reactivity.

The heterogeneous composition of WA presents challenges for maintaining consistent quality. However, various studies have reported improvements in concrete strength and durability when WA is incorporated (Chowdhury et al., 2015; Garcia & Sousa-Coutinho, 2013; Rajamma et al., 2009). These positive effects are associated with different pre-treatment methods, such as sieving, grinding, calcination, and washing, which help standardize the ash and enhance its performance in cement-based applications (Amaral et al., 2022; Berra et al., 2015; Doudart de la Grée et al., 2016; Rosales et al., 2017). A significant issue is the high unburnt carbon content, commonly measured as LOI. Doudart de la Grée et al. (2016) suggested sieving through a 500 μm mesh to remove coarse, carbon-rich particles and lower LOI. Amaral et al. (2022) used a re-calcination process, successfully reducing LOI from 24.30% to 10.60%. Besides decreasing LOI, pre-treatments like grinding and water washing can also positively modify the physical and chemical properties of wood ash, further improving its effect on concrete strength and durability (Berra et al., 2015; Sigvardsen et al., 2021). Grinding reduces particle size and increases reactivity (Couto et al., 2024; Donatello et al., 2010; Doudart de la Grée et al., 2016; Lescinskis et al., 2025), while water washing removes soluble components like chlorides, alkalis, and sulfates (Berra et al., 2015).

2.3. Using Wood Ash in Cement-Based Materials

2.3.1. Fresh Properties

Multiple studies commonly find that the workability decreases as the WA replacement ratio increases (Berra et al., 2015; Carević et al., 2018; Hamid & Rafiq, 2020; Šantek Bajto et al., 2021; Sharma & Lalotra, 2022; Udoeyo et al., 2006; Ukrainczyk et al., 2016). This reduction is usually due to the high specific surface area, irregular particle morphology, and porous structure of WA, which causes a higher water demand compared to Portland cement (Berra et al., 2015; Carević et al., 2018). Also, the presence of unburnt carbon, often indicated by high LOI values, has been linked to water absorption and slump loss (Berra et al., 2015; Yang et al., 2016). However, surface treatments such as water-washing (Berra et al., 2015) or using superplasticizers (Ukrainczyk et al., 2016) have been effective in reducing this impact.

Although a general tendency of decreased workability is observed, some studies have shown negligible or even slightly positive effects at low replacement levels. For instance, Rajamma et al. (2015) and Brazão Farinha et al. (2019) found that up to 10–5 wt% WA did not significantly impact the workability of mortars. Yang et al. (2016) observed a slight

improvement at 10 wt%, although higher levels (20–30 wt%) caused a decline due to water absorption by residual carbon in the ash.

Setting time is another parameter affected by WA incorporation, with most studies observing delayed setting, especially at higher replacement levels (Abdullahi, 2006; Berra et al., 2015; Carević et al., 2020; Elinwa & Ejeh, 2004; Hamid & Rafiq, 2020; Yang et al., 2016). This delay has been linked to the presence of alkalis, magnesium oxide, and unburnt carbon in the ash (Carević et al., 2020; Chen et al., 2019). High LOI ashes, for instance, have been shown to retard setting due to slower hydration reactions (Chen et al., 2019). However, Yang et al. (2016) found that at 10 wt% WA, the setting was even faster than the control sample, likely due to the reactive CaO and alkalis that accelerate the initial dissolution of cement phases. On the other hand, at 20–30 wt% replacement, the increased alkali content may inhibit Ca^{2+} dissolution, causing a delay in setting. Other studies have reported shorter setting times with increase WA content, explaining this by the formation of carboaluminates and carbonates, mineralogical composition, or finer particle sizes (Rajamma et al., 2009; Sklivaniti et al., 2017).

2.3.2. Mechanical Properties

The influence of WA on compressive strength has been extensively studied, with results generally pointing to a reduction in strength with increasing replacement levels. However, several exceptions have been reported depending on the WA properties and curing duration.

Most studies agree that early-age compressive strength decreases when WA replaces cement, especially at levels above 10–15%. For example, Šantek Bajto et al. (2021) found that concrete mixes with 15 wt% WA showed 1-day strength reductions ranging from 26% to 51%, while 28-day compressive strength values were 22–48% lower than those of the control mix. The negative impact was attributed to factors such as high LOI, free CaO and MgO, alkalis, and coarse particle size, which disrupt hydration and weaken the microstructural integrity. Similarly, Carević et al. (2018) observed a 19.6% reduction in compressive strength for concrete containing 15 wt% WA, while Carević et al. (2020), using mortar mixtures, reported average 7-day strength losses of 12%, 15%, and 22% for 5 wt%, 10 wt%, and 15 wt% WA replacements, respectively. However, at 28 and 90 days, several mixes with 5–10 wt% WA showed equal or even higher strength, demonstrating the contribution of pozzolanic and hydraulic activity over time.

This delayed strength development has also been noted by Štirmer and Carević (2022), who reported that mixtures containing 5 wt% and 10 wt% WA achieved equal or higher strength values than the control at 28 days. However, they emphasized that higher WA content reduces compressive strength and therefore recommended limiting WA replacement to 20 wt% in structural concrete.

Several authors also confirmed that optimal performance often reached at 10 wt% WA replacement. For instance, Elinwa and Ejeh (2004) reported a 60-day compressive strength of 21.45 MPa for concrete with 10 wt% sawdust ash, compared to 22.44 MPa for reference. On the other hand, Rajamma et al. (2015) observed an improvement of the 28-day strength at

10 wt% WA. Udoeyo et al. (2006) recorded compressive strengths of 28.66 MPa and 27.54 MPa for 5 wt% and 10 wt% WA, respectively, compared to 31.48 MPa for the control, while strength sharply decreased to 19.52 MPa at 30 wt% replacement. These findings highlight that while low to moderate doses of WA may slightly reduce strength, they are acceptable in structural applications, especially when considering sustainability or cost.

Furthermore, Garcia and Sousa-Coutinho (2013) showed that adding ground wood bottom ash to mortar at 5–10 wt% replacement levels can enhance long-term strength, with a 12% increase after 90 days compared to the control. In another study, Subramaniam et al. (2015) found that 15 wt% WA in concrete blocks resulted in a 21-day compressive strength of 3.66 MPa, higher than the 3.10 MPa of the reference, although strength declined when ash content exceeded 15 wt%.

Similar to compressive strength, split tensile and flexural strengths generally decrease with increasing WA content, though the reduction tends to be more gradual. Optimal performance is often seen at replacement levels (around 5–10 wt%), where tensile strength may remain close to or even slightly exceed that of the reference mixtures (Cheah & Ramli, 2013; Chowdhury et al., 2014, 2015; Naik et al., 2002; Raju et al., 2014). The decrease in tensile strength at higher dosages is commonly attributed to increased porosity and weaker bonding between the binder matrix and ash particles (Akinyemi & Dai, 2020; Chowdhury et al., 2015; Lessard et al., 2017). In some cases, early-age strength losses are partially recovered over time due to ongoing pozzolanic and hydraulic reactions. A similar trend is observed in flexural strength development, where low replacement levels (≤10 wt%) can sustain or improve long-term performance, while higher dosages tend to reduce strength (Cheah & Ramli, 2013; Chowdhury et al., 2015; Garcia & Sousa-Coutinho, 2013; Rajamma et al., 2009; Udoeyo et al., 2006; Wembe et al., 2024). Overall, it is generally recommended to limit WA content to 10–15 wt% to keep tensile and flexural properties within acceptable structural limits (Cheah & Ramli, 2013).

2.3.3. Frost Durability

Concrete structures in cold climates face freeze–thaw (F–T) cycles, where water in the pores freezes and expands, causing internal stresses that can lead to microcracking and surface scaling (Rissanen et al., 2020). This cycle of deterioration is worsened by the slower rate of cement hydration at low temperatures, which delays early strength development by about 20–40% (Kothari et al., 2020).

The incorporation of WA into concrete may affect its resistance to F–T cycles through both physical and chemical mechanisms. One major concern is the typically high LOI of WA, which can disrupt the performance of air-entraining admixtures (AEA) and weaken the durability of concrete, even when proper air content is initially maintained (Senneca et al., 2011).

The literature presents various results regarding the effect of WA on F–T performance. Some studies report minimal impact when WA is used at moderate replacement levels. For instance, the incorporation of WA at 5–12 wt% was not found to significantly affect the frost

resistance of concrete under certain conditions (Chowdhury et al., 2014; Naik et al., 2002). Similarly, Wang et al. (2008) investigated various combinations of wood fly ash (WFA) and coal fly ash (Class F and Class C), maintaining a constant fly ash ratio of 25 wt%. Their results indicated that the mixtures containing WFA had comparable or slightly reduced weight loss after F–T exposure compared to reference mixes, suggesting that WFA does not substantially deteriorate F–T resistance. Moreover, their findings on AEA compatibility ranked the air-entraining demand as follows: Class F > Wood F (WFA + Class F) > Wood C (WFA + Class C) > Class C > Portland cement.

However, other studies emphasize potential durability issues. Santek Bajto et al. (2021) observed that concrete mixes containing WA exhibited reduced F–T resistance relative to control mixtures. The poorest performance was linked to ashes with high alkali content, where the mass loss reached 3.09 kg/m^2 after 56 cycles. Nonetheless, increasing the air content to 6.5% effectively mitigated the damage, reducing the mass loss to 0.30 kg/m^2. These results highlight the importance of optimizing both AEA dosage and alkali content to ensure satisfactory durability (Šantek Bajto et al., 2021; Wang et al., 2008).

Rissanen et al. (2020) assessed the use of fluidized bed combustion fly ash (FBCFA) derived from peat and wood. Their findings showed that untreated and ground FBCFA improved F–T resistance compared to coal-derived fly ash and did not impair AEA functionality. Remarkably, untreated FBCFA at 10% air content provided 20% better F–T performance than the reference mortar. Lescinskis et al. (2025) evaluated mortar samples incorporating WA subjected to sieving, slaking, and ball milling. All WA-containing mortars experienced higher mass loss than the reference after 56 cycles, although slaked ash performed better among all WA mortars.

2.3.4. Leaching Behaviour

Wood ash has significant potential as a resource in a circular economy, especially in agriculture as fertilizer or in construction materials, but its sustainable use faces challenges due to concerns about the possible release of heavy metals into the environment (Ukrainczyk et al., 2016; Vassilev et al., 2012). Because trees absorb heavy metals from soils during growth, and soil concentrations result from both natural minerals and anthropogenic contamination, combustion residues inevitably contain accumulated metals such as Cd, Cr, Cu, Ni, Pb, and Zn (Ottosen & Sigvardsen, 2024). In waste-wood fly ash, finer fractions can carry higher levels of Zn, Pb, and Cd, which is important for screening and handling (Lanzerstorfer, 2017).

Ottosen and Sigvardsen (2024) investigated the leaching behaviour of heavy metals in wood fly ash. They observed that aging by hydration and carbonation significantly reduced the leaching of Cd, Cu, Ni, and Pb by trapping them in newly formed mineral phases, while Cr decreased less and remained the most concerning element. Leaching is strongly pH-dependent, typically higher at lower pH, though Cr may remain mobile even at high pH. The continued leaching of Cr indicates the presence of the toxic form Cr(VI), which requires targeted management and specific speciation assessments in reuse evaluations.

For product-stage evaluation, dynamic surface leaching tests (DSLT) are important because they capture the gradual, diffusion-controlled release of harmful substances from intact specimens over periods relevant to service life (Berra et al., 2019; Carević et al., 2020; Tosti et al., 2018). Berra et al. (2019) used a modified DSLT under controlled conditions and identified a two-stage process (early wash-off followed by diffusion), projecting 100-year releases of Cd, Cr, Cu, Ni, Pb, and Zn below Dutch regulatory limits. Berra et al. (2016) examined various wood-biomass fly ashes (WFA) and recommended long-duration monolithic testing as the proper product-based assessment, noting that granular tests on crushed material can be overly conservative. They also found that fly ash from treated wood contained significantly higher heavy metal contents and exhibited poorer leaching performance, with a 30 wt% treated-WFA monolithic samples failing product criteria. Tosti et al. (2018) also compared monolithic, batch, and percolation tests within a scenario-based framework, showing low releases for intact mortars but potential increases after crushing.

In cementitious composites, multiple studies confirm that adding WA into pastes or mortars generally keeps the cumulative releases of regulated metals within widely accepted benchmarks. The cement matrix offers alkaline conditions and physical encapsulation that immobilize metals such as Cr, Pb, and Zn, reducing their release to below regulatory limits (Berra et al., 2019; Carević et al., 2020; Tosti et al., 2018). Pre-treatments like water washing can further improve environmental compatibility by lowering soluble salts (chlorides, sulfates, alkalis), thus decreasing leaching risks (Sigvardsen, 2020). Around 15% replacement, monolithic mortars maintained Cd, Cr, Cu, and Pb at or below reference levels, with Zn slightly higher but still within Dutch limits, while eluates of the raw ashes alone did not meet inert criteria (Carević et al., 2020). Similarly, at about 10% WA replacement, both soluble-fraction and diffusion-controlled leaching remained very low, with Ni and Cr being the most detectable but still at safe levels (Sigvardsen, 2020).

2.4. Using Wood Ash in Alkali-Activated Materials

Alkali-activated binders, which are an eco-alternative to Portland cement, are created through a chemical reaction between an aluminosilicate precursor and alkali activators. In systems with high calcium content, the main reaction product is the formation of C–A–S–H gel, which is responsible for the strength development (Luukkonen et al., 2018; Provis, 2014). Alkali-activated materials have become a viable alternative to traditional Portland cement-based systems, mainly because of their substantial reduction in CO_2 emissions, reaching up to 80% (Flower & Sanjayan, 2017; Humad et al., 2019; Şanal, 2018). Energy consumption is reduced by 43%, and water usage decreases by about 25% (Jiang et al., 2014; Long, 2021). Additionally, they demonstrate increased strength, with certain durability features proving superior (Awoyera et al., 2020; Puertas et al., 2018). In addition to all these benefits, they also offers advantages in utilizing industrial waste materials and by-products such as slag or fly ash (Owaid et al., 2021). One of the most used industrial by-products as an alkali-activated precursor is GGBFS, which is produced during steel manufacturing. Alkali-activated slag systems show high mechanical strength; however, they face challenges like rapid setting

times and significant shrinkage. To address these properties, their use with other precursors has been studied, leading to promising improvements. The combination of slag and fly ash is the most researched binary system (Awoyera et al., 2020). Recent studies report extended setting times, reduced shrinkage, and ultra-high strength in this binary system (Cui et al., 2023; Lao et al., 2023; Luo et al., 2023).

Many studies explore incorporating WA into alkali-activated systems to assess effects on strength, microstructure, and setting, despite challenges like high crystallinity, residual carbon, and coarse particles that reduce reactivity. Methods such as mechanical treatment and hybrid binder design show promise in certain conditions. These studies highlight the challenges and opportunities related to WA's reactivity, binder compatibility, and curing methods.

The use of untreated WA in alkali-activated materials is often limited due to its low amorphous content, high crystallinity, and particle heterogeneity. Studies have shown that mortars made with 100 wt% WA without chemical activators or blended binders exhibit low mechanical strength and porous microstructures, with limited or no formation of C–A–S–H or N–A–S–H gels (Candamano et al., 2017; Silva et al., 2021). These deficiencies mainly result from the presence of unburnt carbon, coarse particles, and variability in oxide composition. For example, Silva et al. (2021) reported compressive strengths below 4 MPa in pastes containing 100 wt% WA and observed unreacted particles and high porosity. Additionally, WA's high absorptivity and calcium content can cause rapid setting (Cheah et al., 2015). While elevated-temperature curing can promote the formation of hydration products, it may also induce microcracking due to thermal gradients or accelerated reaction kinetics (Bajare et al., 2011). Consequently, untreated WA without any pretreatment or hybrid systems shows limited performance.

To enhance the poor reactivity and mechanical performance of WA, mechanical grinding and its incorporation into hybrid binder systems have been widely investigated. Grinding increases the surface area and promotes the dissolution of reactive oxides (Bajare et al., 2011). Hybrid systems that combine WA with materials like glass powder (Silva et al., 2021), metakaolin (Candamano et al., 2017), fly ash (Abdulkareem et al., 2019; Cheah et al., 2015) or ground granulated blast furnace slag (Cheah et al., 2017; De Rossi et al., 2020) demonstrate improved strength, reduced porosity, and better gel formation. Samsudin and Cheah (2015) achieved a compressive strength of 12.3 MPa with 30 wt% WA in GGBFS systems without activators. Cheah et al. (2017) observed that replacing part of a WA-GGBFS blend with fly ash (10–60 wt%) enhanced compressive strength and lowered water demand. De Rossi et al. (2020) highlighted the importance of activator composition and curing conditions in WA–metakaolin systems. Candamano et al. (2017) demonstrated that compressive strength values above 35 MPa were achievable at 30 wt% WA replacement despite increased porosity and drying shrinkage. In general, replacing more than 30–40 wt% of WA was found to reduce performance (Cheah et al., 2017; Owaid et al., 2021).

Curing conditions and activator chemistry significantly influence the behaviour of WA-based systems. Elevated curing temperatures (60–75 °C) enhance early strength and reduce water absorption but may lead to microcracking (Bajare et al., 2011; Owaid et al., 2021). For example, Bajare et al. (2011) reported that samples cured at 75 °C had a compressive strength of 9.3 MPa, while those cured at 20 °C reached only 2.3 MPa. However, microcracks were observed in high-temperature samples. De Rossi et al. (2020) found that hydrothermal curing at 40 °C reduced water absorption but resulted in lower compressive strength (18.3 MPa) than thermal curing (24.2 MPa). Room-temperature curing was considered more sustainable, although it required longer durations and optimized activator formulations.

The ratio and concentration of alkali activators also played a crucial role. Cheah et al. (2017) observed increased water demand with higher WA content in fly ash-based systems, which impacted strength development. Abdulkareem et al. (2019) reported that 10–20 wt% WA reduced porosity at early ages but increased water absorption after 28 days. Owaid et al. (2021) found the highest compressive strength at 25 wt% WA replacement when activated with 10M NaOH and sodium silicate, while higher WA contents decreased strength due to excess calcium interfering with gel formation. Cheah et al. (2015) and Owaid et al. (2021) both indicated that although high CaO in WA can promote C–S–H formation, it may also disrupt geopolymerization at higher levels.

2.5. Sustainability of Wood Ash

Using WA in cementitious systems offers environmental benefits, given the rising costs of landfills and the growing need for sustainable resource use (Amaral et al., 2022; Nader et al., 2020; Ottosen et al., 2016). This practice aligns with the principles of the circular economy, which emphasizes minimizing waste, promoting reuse, and reducing the environmental impact of industrial by-products (Ghufran et al., 2022; Norouzi et al., 2021; Turk et al., 2015; Usta et al., 2022).

Wood ash is a by-product of wood biomass combustion, a process generally considered CO_2-neutral, since the CO_2 released during combustion is approximately equal to the amount absorbed during biomass growth (Amaral et al., 2022; Carević et al., 2020; The European Commission's Knowledge Centre for Bioeconomy, 2018). Replacing part of the cement with WA not only diverts waste from landfills but also decreases clinker use, which reduces CO_2 emissions. Several life cycle assessment (LCA) studies have shown that using biomass fly ash as a cement replacement results in a significant reduction in environmental impacts (Celik et al., 2015; Gaudreault et al., 2020; Teixeira et al., 2016). In addition to ecological advantages, WA is readily accessible in many areas, promoting local material sources and decreasing transportation emissions. According to Abdulkareem et al. (2023), such local availability is also a social sustainability indicator, promoting supply security and reducing reliance on imported precursors.

Despite its potential, WA often needs pre-treatment, such as calcination, washing, or grinding, to meet performance standards. However, it is important to balance the benefits of improving reactivity with the energy use of these treatments. Grinding has been shown to be

more energy-efficient than recalcination, both in terms of environmental impact and technical performance (Amaral et al., 2022; da Costa et al., 2019). For instance, the average energy use for grinding and sieving is 11.0 and 2.2 kWh/t, respectively (da Costa et al., 2019), whereas recalcination can be considerably more demanding. Finally, the economic aspect of WA use has also been investigated. Kannan & Raja Priya (2021) reported that partial replacement of cement with WA can lower total concrete costs by over 30%, depending on the replacement level and the combination with other SCMs such as metakaolin.

In summary, although this study does not directly evaluate the environmental performance of WA, the existing literature emphasizes its substantial potential as a sustainable, low-cost, and circular alternative to traditional cementitious materials.

2.6. Mechanochemical Activation

Mechanochemical activation (MCA) is an advanced grinding method that uses mechanical energy to reduce particle size, and to cause structural changes such as amorphization, defect formation, and increased surface reactivity, which enhances the chemical reactivity of solid materials without the need for additional heat or solvents (Baki et al., 2022; Ke et al., 2023; Szczesniak et al., 2020; Tole et al., 2018). As a sustainable and environmentally friendly alternative to traditional pretreatment methods that depend on high temperatures or chemical additives, MCA is becoming increasingly popular for material activation (Baki et al., 2022; Bülbül & Courard, 2025; Ke et al., 2023; Tole et al., 2018).

The process is driven by mechanical forces, including shearing, compression, and impact, which induce lattice and plastic deformations in solid structures (Tole et al., 2018). These deformations create localized stress energy that can break chemical bonds and forming defects and active sites, especially at phase interfaces (Bülbül & Courard, 2025). The resulting disordered or amorphous structures have higher chemical reactivity than the original crystalline material (Ilić et al., 2016; Pálková et al., 2021; Seco et al., 2025; Vdovic et al., 2010).

MCA enables a mechanically driven chemical reaction, in which stress buildup, lattice distortions, and temporary temperature rises during grinding, which together promote bond rupture, increased surface area, and disruption of crystal structure (Baláž et al., 2013; Grabias-Blicharz & Franus, 2023; Michalchuk et al., 2021). These physical and structural changes accelerate the dissolution of reactive components and enhance pozzolanic or hydraulic reactions (Akmalaiuly et al., 2023; Ke et al., 2023; Kumar & Kumar, 2011; Mucsi, 2016).

Various types of milling devices have been used for MCA, including planetary ball mills, attrition mills, vibratory mills, and shaker mills. Planetary ball mills are the most commonly used in laboratory settings due to their short processing time, reproducibility, and efficiency (Baláž, 2008; Kumar et al., 2020; Tole et al., 2018). The effectiveness of MCA depends on key parameters such as ball-to-powder ratio, rotational speed, grinding duration, and grinding media characteristics (Cagnetta et al., 2018; Ke et al. 2023; Szczesniak et al. 2020).

Although, high-energy ball milling effectively increases the reactivity by promoting amorphization and increasing surface area, excessive grinding may cause agglomeration, particle caking, or contamination, which may decrease the specific surface area and limit performance (Ashrafizadeh & Ashrafizaadeh, 2012; Baki et al., 2024; Grabias-Blicharz & Franus, 2023; Ilić et al., 2016). Therefore, optimizing milling parameters, including duration, rotational speed, ball size, and vessel material, is essential to prevent ineffective activation or material degradation.

Additionally, the grinding medium and the use of additives influence MCA outcomes. Although dry grinding generally promotes more effective structural changes, wet milling or the addition of surfactants may be necessary to reduce agglomeration and ensure uniform particle size distribution, especially during extended grinding periods (Patil & Anandhan, 2015; Tole et al., 2018).

The structural and morphological changes caused by MCA are directly linked to improved performance in cementitious systems. For example, milled fly ash shows a higher specific surface area, greater solubility of Si and Al ions, and decreased crystallinity, all of which enhance the formation of cement hydration products like C–S–H and contribute to denser microstructures with greater strength (Bülbül & Courard, 2025; Kato et al., 2019; Seco et al., 2025). Furthermore, MCA has been demonstrated to stabilize heavy metals by incorporating them into newly formed amorphous phases, reducing environmental risks associated with ash-based binders (Fu et al., 2008; Wu et al., 2021; Yuan et al., 2021).

In recent years, MCA has gained attention as an effective technique for improving the reactivity of biomass ashes as well, including those from wood combustion. Several studies have demonstrated that grinding can significantly reduce particle size and increase surface area, thereby enhancing hydration kinetics and mechanical properties. For example, Kaminskas and Cesnauskas (2014) showed that vibratory milling of wood chip-based biomass fly ash reduced 70 wt% of the particles to below 63 μm, which facilitated the formation of C–S–H and portlandite, enabling up to 15 wt% cement replacement without losing strength. Similar improvements were reported for biomass bottom ash (Rosales et al., 2017) and rice husk ash (Xu et al., 2015), where decreased porosity and improved reactivity were observed after milling. Pantić et al. (2023) found that grinding promoted nucleation, refined pore structure, and improved particle packing, all of which contributed to faster hydration and increased durability. Likewise, Ohenoja et al. (2016) observed increased self-hardening behaviour in peat biomass fly ash after particle size refinement.

Besides physical refinement, the chemical composition of the ash also plays a critical role in the effectiveness of MCA. Šupić et al. (2021) reported that high-silica ashes exhibited significant reactivity gains with grinding alone, while low-silica ashes required additional chemical activation. In another study, Moraes et al. (2021) demonstrated that prolonged grinding increased the amorphous content and surface area of initially inert sugarcane bagasse ash, resulting in improved long-term strength. Ke et al. (2023) further revealed that mechanochemical activation could enhance the carbonation capacity of timber biomass ash

by disrupting polymerized Si–O–Si bonds and generating reactive oxygen sites, enabling partial mineral carbonation under ambient conditions within 1–2 hours. This led to up to 100% improvement in CO_2 uptake, even in low-alkali ashes. These findings indicate that mechanochemical activation not only improves pozzolanic or hydraulic performance but also offers potential for carbon capture in Ca- and Mg-rich silicate residues.

MCA can be also applied to stabilize heavy metals found in different waste ashes (Chen et al., 2019; Grabias-Blicharz & Franus, 2023; Yuan et al., 2021). Extended grinding of ash causes microstructural deterioration, lower crystallinity, and the formation of amorphous, melt-like phases. These amorphous structures are thought to immobilize heavy metals through absorption mechanisms (Li et al., 2010; Wu et al., 2021). The effective stabilization of heavy metals suggests that ashes processed with MCA can serve as safe SCM, ensuring environmental stability even under weathering conditions.

Yuan et al. (2021) found that 10-hour dry grinding of coal fly ash significantly reduced the leaching rates of heavy metals: Cu (52.10%), Cr (70.16%), Pb (89.80%), Zn (22.97%), Cd (3.15%), and Ni (23.49%). The process transformed water-soluble heavy metals into stable residual forms, notably reducing Cr(VI) to Cr(III) and encapsulating it. Chen et al. (2019) demonstrated that mechanochemical treatment through prolonged ball milling effectively stabilizes heavy metals in municipal solid waste incineration (MSWI) fly ash by decreasing their water and acid solubility, thereby reducing leachability and environmental risk. The study emphasizes the potential of this method as a low-temperature detoxification technique for hazardous ashes, although optimal conditions may vary depending on the waste’s composition and metal forms.

Chapter 3

Materials and Methods

This chapter presents the materials and methods used in the thesis. The research is based on three studies, each corresponding to a journal article. The appended papers are listed in Chapter 1.6.

3.1. Materials

3.1.1. Wood Ash

This thesis utilized four types of wood fly ash (WA) which are by-products of timber waste combustion, WA1, WA2, WA3, and WA4. WA1, WA2, and WA3 were sourced from Stenvalls Trä AB (Piteå, Sweden) and collected during different operational periods, while WA4 was obtained from Holmen AB (Skellefteå, Sweden). Production parameters including biofuel composition, combustion technology and temperature are summarized in Table 1.

Table 1. Production parameters of wood ash samples WA1, WA2, WA3 and WA4, including biofuel composition, combustion technology, and combustion temperature.

Wood ash	Biofuel composition	Combustion technology	Combustion temperature (°C)
WA1	60% bark, 30% sawdust, and 10% dry wood chips	Grate	1050
WA2	60% bark, 30% sawdust, and 10% dry wood chips	Grate	1050
WA3	60% bark, 30% sawdust, and 10% dry wood chips	Grate	1050
WA4	30% bark and 70% wood shavings	Grate	800–900

3.1.2. Ordinary Portland Cement (OPC)

Ordinary Portland cement (CEM I 42.5 N) was obtained from Heidelberg Materials (formerly Cementa) in Skövde, Sweden. Its chemical composition is given in Table 2.

3.1.3. Fly Ash (FA)

Fly ash (Type F) was obtained from Thomas Cement in Bremen, Germany. Its chemical composition is given in Table 2.

Table 2. Chemical composition of wood ashes (WA1, WA2, WA3, WA4), ground granulated blast furnace slag (GGBFS), fly ash (FA), and Portland cement (CEM I). Data adapted from Paper II, III, and IV (Teker Ercan et al., 2023b; Teker Ercan et al., 2025b; Teker Ercan et al., 2025a).

Chemical composition (%)	WA1	WA2	WA3	WA4	FA	CEM I	GGBFS
SiO_2	31.7	6.63	22.4	0.75	60.20	21.20	34.80
Al_2O_3	7.25	3.48	6.75	0.37	17.70	3.40	11.30
Fe_2O_3	4.19	1.11	2.62	0.17	2.78	4.10	0.42
CaO	14.7	22	15.1	29	1.37	63.30	40.80
K_2O	5.14	9.10	8.25	1.20	1.61	0.56	0.99
MgO	2.08	3.43	2.69	2.52	0.43	2.20	11.40
MnO	0.61	1.22	0.80	1.80	0.05	-	0.32
P_2O_5	1.39	2.63	2.81	2.11	0.07	-	<0.02
TiO_2	0.33	0.12	0.3	0.01	0.71	-	1.46
Na_2O	1.53	0.37	1.46	0.03	0.60	0.18	0.58
SO_3	-	-	-	-	-	2.70	-
LOI (1000 °C)	34.5	43.7	29.7	56.7	1.80	2.50	-1.81
$SiO_2 + Al_2O_3 + Fe_2O_3$	43.14	11.22	31.77	1.29	80.68	28.70	46.52
CaO/SiO_2	0.46	3.32	0.67	38.67	0.02	2.99	1.17
$(CaO + MgO)/SiO_2$	0.53	3.84	0.79	42.03	0.03	3.09	1.50
$(CaO + MgO + Al_2O_3)/SiO_2$	0.76	4.36	1.10	42.52	0.32	3.25	1.82
$K_2O + Na_2O$	6.67	9.47	9.71	1.23	2.21	0.74	1.57

3.1.4. Ground Granulated Blast Furnace Slag (GGBFS)

The ground granulated blast furnace slag (GGBFS) used in this study was obtained from SweCem (Helsingborg, Sweden), and its chemical composition is presented in Table 2. The basicity coefficient (Kb) of GGBFS was determined using the formula $Kb = (CaO + MgO)/(SiO_2 + Al_2O_3)$ and calculated as 1.13. Since this value exceeds 1, it indicates the basic nature of the slag (Aydin & Baradan, 2014; Humad et al., 2019; Y. Li & Sun, 2000; Tole et al., 2020). The pH of GGBFS was measured as 10.38. Additionally, the hydration modulus (HM) was calculated using the equation $HM = (CaO + MgO + Al_2O_3)/SiO_2$, yielding a value of 1.82 (Aydin & Baradan, 2014). This result suggests efficient slag hydration, as it surpasses

the recommended threshold of 1.4, which ensures the formation of effective hydration products (Aydin & Baradan, 2014; Chang, 2003).

3.1.5. Aggregates

Fine sand B15 (50 µm) and B35 (350 µm) were supplied by Baskarpsand AB (Habo, Sweden). Standard sand (0–4 mm) and natural granite aggregate (4–8 mm) were obtained from the Jehander Heidelberg Materials (Sweden).

3.1.6. Chemical Admixtures

In Study B, two types of chemical admixtures were used. A polycarboxylate ether-based superplasticizer (MasterGlenium ACE 30) was incorporated into all concrete mixes to improve workability. Additionally, an air-entraining admixture (MasterAir 105) was used in selected mixes for freeze–thaw resistance evaluation. Both admixtures were supplied by Master Builders (Rosersberg, Sweden).

3.1.7. Alkali Activators

Three different alkali activators were utilized in alkali-activated mortars (Study C): sodium silicate (SS), sodium carbonate (SC), and sodium hydroxide (SH). The liquid sodium silicate (Na_2SiO_3) was obtained from Sigma-Aldrich, with an alkali modulus (Ms) calculated as Ms = SiO_2/Na_2O of 2.5. Its composition consisted of 26.5 wt% SiO_2, 10.6 wt% Na_2O, and a total solid content of 43.82 wt%. The activator dosage was maintained at 10 wt% for all mixes activated with SS, with an Ms value of 1. The Ms value was adjusted by incorporating sodium hydroxide (NaOH) pellets (98% purity), which were also supplied by Sigma-Aldrich. Sodium carbonate (SC) powder (Na_2CO_3), used in the study, was supplied by CEICH SA in Warsaw, Poland. A 10 wt% concentration of SC was used in all SC-activated mixes. For the SH-activated mixtures, a 10 M solution of sodium hydroxide (NaOH) was prepared with distilled water. The pH values of the SS, SC, and SH alkali solutions were measured as 12.84, 11.24, and 12.95, respectively.

3.2. Mechanochemical Activation

The WAs used in all studies were first dried at 65 ± 0.5 °C for 24 hours and subsequently sieved through a 500 µm sieve to remove large particles (Doudart de la Grée et al., 2016; Teker Ercan et al., 2023b). Mechanochemical activation (MCA) was subsequently performed via high-energy grinding using a Retsch PM100 planetary ball mill, shown in Figure 1, operated at 500 rpm, with a ball-to-powder ratio of 5, for durations of 10 and 20 minutes. Study A and Study B used 30 stainless steel balls, each 10 mm in diameter, within the same type of jar. Study A included all four wood ash types (WA1, WA2, WA3, and WA4), while Study B focused on WA3 and WA4. In Study C, which involved only WA3, the grinding was conducted in a 500 mL stainless steel jar containing 10 stainless steel balls with a diameter of 20 mm.

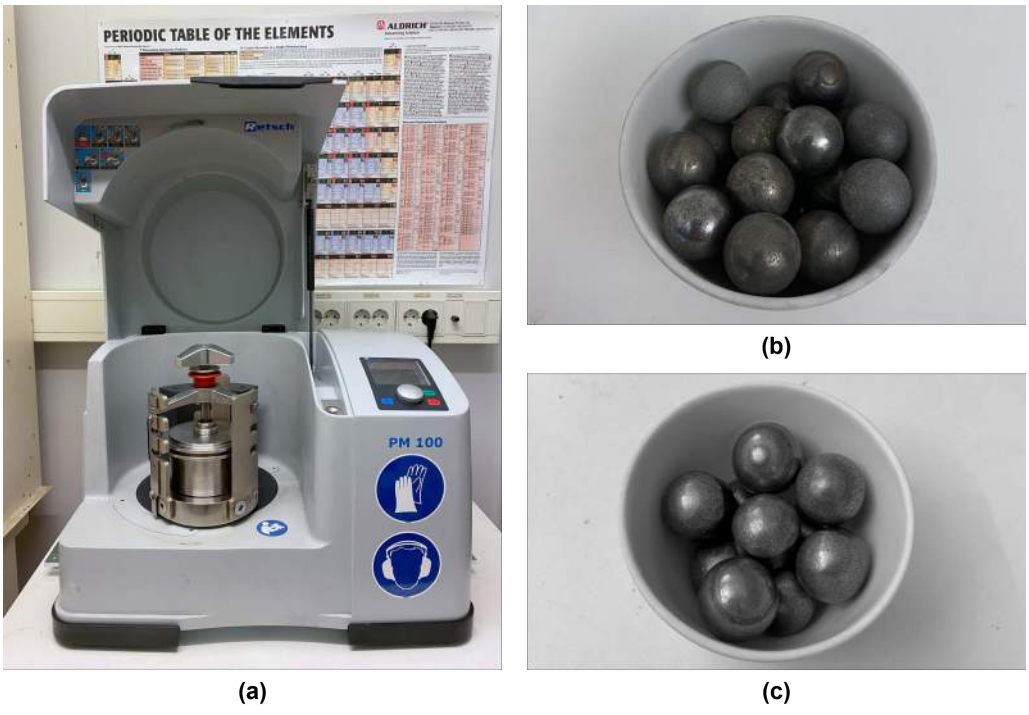

Figure 1. **(a)** Planetary ball mill, Retsch PM 100, **(b)** grinding media with 10 mm diameter, **(c)** grinding media with 20 mm diameter.

The overall processing steps for the wood ashes, including drying, sieving, and mechanochemical activation for 10 and 20 minutes, are illustrated in Figure 2. In this thesis, 'grinding' refers to MCA; 'ground' denotes wood ash after MCA, and 'unground' refers to the sieved-only wood ash. All WAs used in this PhD thesis, including those ground for 10 and 20 minutes, are presented in Figure 3.

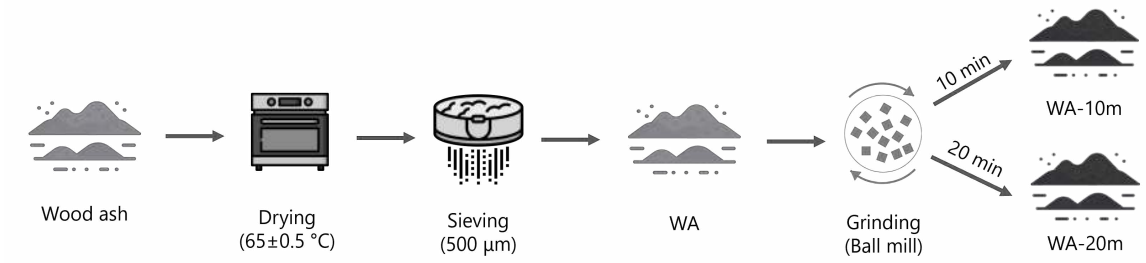

Figure 2. Processing of wood ash after receiving. Adapted from Paper IV (Teker Ercan et al., 2023b).

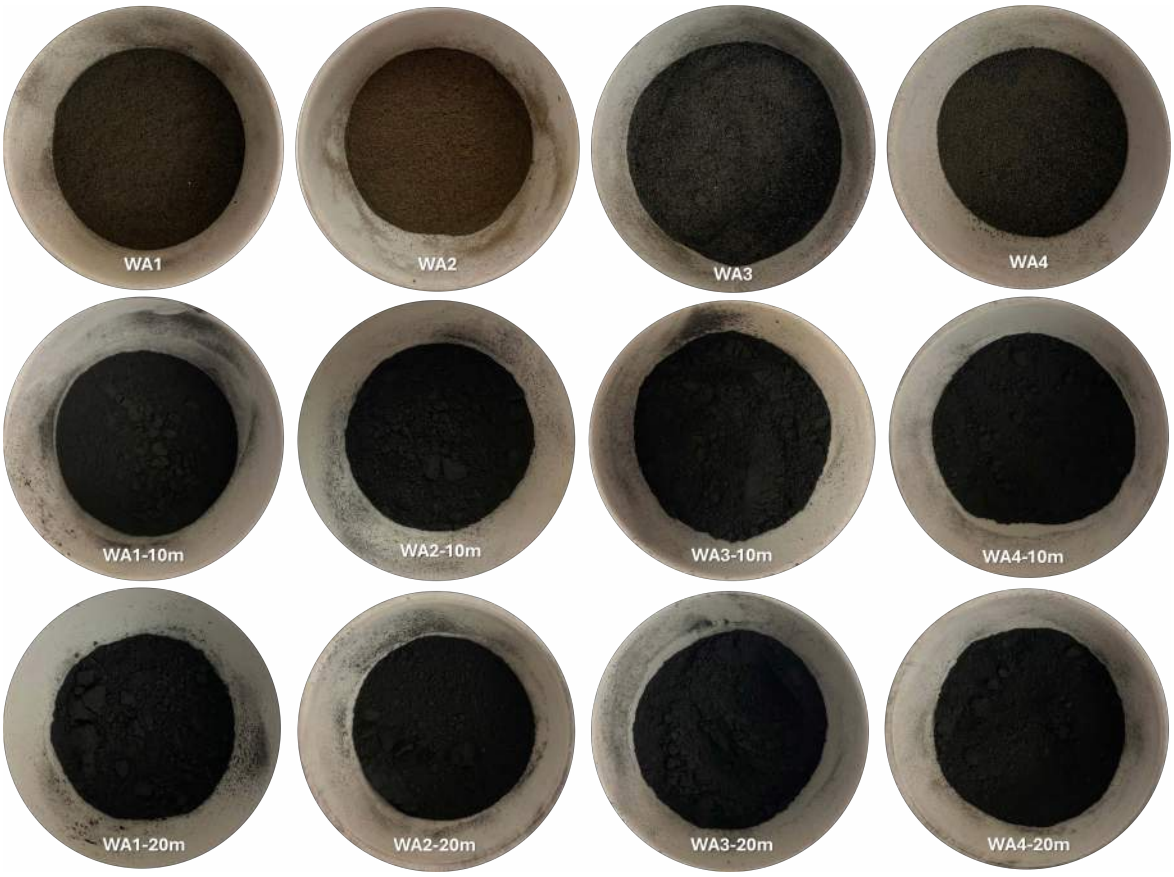

Figure 3. Unground and ground for 10- and 20-minutes wood ashes (WA1, WA2, WA3, WA4).

The materials used and the experimental methods applied in each study are summarized in Table 3.

Table 3. Studies and related experiments with materials.

Study (Paper)	Materials	Tests
Study A (Paper II)	WA1, WA2, WA3, WA4, FA, OPC	PSD, Frattini, Compressive strength, SAI, R3, SEM-EDS, XRD, TGA
Study B (Paper III)	WA3, WA4, FA, OPC	Workability, Compressive strength, Heat of hydration, SEM-EDS, XRD, Leaching, F–T
Study C (Paper IV)	WA3, GGBFS	Workability, Compressive strength, Flexural strength, SEM-EDS, XRD, Heat of hydration

3.3. Sample Preparation and Mix Design

In all studies, paste samples were mixed with a vacuum mixer (Ecovac, Bredent, Germany) at 600 rpm for 2 minutes. Mortars were mixed in a 3 L Hobart mixer, while concrete samples were prepared in an 8 L Hobart mixer. For both mortar and concrete mixes, the dry materials were mixed for 3 minutes, then liquids were added and mixed for an additional 2 minutes.

3.3.1. Assessment of Pozzolanic Activity (Study A)

Mortar mixes for the Strength Activity Index (SAI) were prepared in accordance with ASTM C311. A control mix containing 100 wt% Portland cement and test mixes containing 20 wt% of wood ash or fly ash were prepared. Sand-to-binder (s/b) ratio of 2.75 and standard sand (0–4 mm) was used. The water-to-binder (w/b) ratio was 0.484 for the control sample and 0.494 for the test samples. Fresh mortars were cast into 50 × 50 × 50 mm^3 cube molds, demolded after 24 hours, and cured in water until the day of testing. Paste samples were also prepared using the same replacement levels and a fixed water-to-binder ratio of 0.4, and were used for XRD, SEM-EDS, and TGA analyses.

3.3.2. Wood Ash in Concrete (Study B)

The concrete mix designs used in this study are presented in Table 4. In these mixes, 10 or 20 wt% of Portland cement were replaced with unground and ground wood ash (WA3 and WA4) or with fly ash (FA). A mix containing 100 wt% cement was used as the control sample (CTRL). All mixtures were prepared with a constant water-to-binder (w/b) ratio of 0.48, and a polycarboxylate-based superplasticizer was added at 1 wt% of the binder to enhance workability.

Workability, compressive strength, and microstructural properties were evaluated for all mixes. In addition, leaching and freeze-thaw (F–T) resistance tests were performed on selected mixtures, including those containing 20 wt% WA3 (unground and ground for 10 minutes), 20 wt% FA, and the CTRL mix. For the F–T test, 0.1 wt% air-entraining admixture was added to these mixes, and a separate set of samples was prepared accordingly. Paste samples were prepared using the same replacement levels and a constant water-to-binder ratio of 0.4 and were used for XRD analysis and isothermal calorimetry measurements.

Table 4. Concrete mix design. Data adapted from Paper III (Teker Ercan et al., 2025b).

Concrete Mix ID	Ash ratio (%)	Ingredient (kg/m³)							
		OPC	WA or FA	B15	0-4	4-8	Water	SP	AEA
CTRL[a,b]	0	400	-						
FA-10	10	360	40						
FA-20 [a,b]	20	320	80						
WA3-10	10	360	40						
WA3-20 [a,b]	20	320	80						
WA3-10m-10	10	360	40						
WA3-10m-20 [a,b]	20	320	80						
WA3-20m-10	10	360	40						
WA3-20m-20	20	320	80						
WA4-10	10	360	40	352	880	528	189	4	-
WA4-20	20	320	80						
WA4-10m-10	10	360	40						
WA4-10m-20	20	320	80						
WA4-20m-10	10	360	40						
WA4-20m-20	20	320	80						
CTRL-AE [a]	0	400	-						
FA-20-AE [a]	20	320	80						0.4
WA3-20-AE [a]	20	320	80						
WA3-10m-20-AE [a]	20	320	80						

Concrete mix IDs specify the type of ash (WA3, WA4, FA), the grinding duration in minutes when given (10m or 20m), and cement replacement ratio (10 or 20 wt%). If no grinding duration is included, the ash is unground. The presence of an air-entraining agent (AEA) is indicated by the suffix "-AE."
Mixes labeled with "-AE" are air-entrained concrete, while those without this suffix are non-air-entrained.
[a] Samples for air-content and freeze-thaw resistance.
[b] Samples for leaching test

3.3.3. Wood Ash in Alkali-Activated Mortars (Study C)

A total of 21 different alkali-activated mortar mixes were prepared for testing compressive and flexural strength by replacing GGBFS with 0, 10, and 20 wt% WA3, WA3-10m, and WA3-20m, respectively. Three types of alkali activators were used: SS, SC, and SH. Mix design details are given in Table 5. The alkali activator solutions (SS and SH) were prepared approximately 3 hours prior to casting by dissolving them in water. All mortar mixes had a constant water-to-binder (w/b) ratio of 0.5 and a sand-to-binder (s/b) ratio of 2. Fine sand B35 (350 µm) was used. Mortars were cast into 40 × 40 × 160 mm³ molds and sealed with plastic foil. After demoulding, samples were stored in sealed plastic bags under ambient conditions. For XRD analysis and isothermal calorimetry measurements, alkali-activated pastes were prepared with a constant water-to-binder (w/b) ratio of 0.5.

Table 5. Mix design of the alkali-activated mortars for the Study C (Teker Ercan, Cwirzen, et al., 2023).

Mortar Mix ID	Wood Ash Grinding Time (min)	Wood Ash Ratio (wt%)	Alkali Activator Type	Alkali Activator Dosage	Alkali Modulus (Ms)
SS-CTRL	-	0			
SS-10	0	10			
SS-20	0	20			
SS-10m-10	10	10	SS	10%	1
SS-10m-20	10	20			
SS-20m-10	20	10			
SS-20m-20	20	20			
SC-CTRL	-	0			
SC-10	0	10			
SC-20	0	20			
SC-10m-10	10	10	SC	10%	-
SC-10m-20	10	20			
SC-20m-10	20	10			
SC-20m-20	20	20			
SH-CTRL	-	0			
SH-10	0	10			
SH-20	0	20			
SH-10m-10	10	10	SH	10 M	-
SH-10m-20	10	20			
SH-20m-10	20	10			
SH-20m-20	20	20			

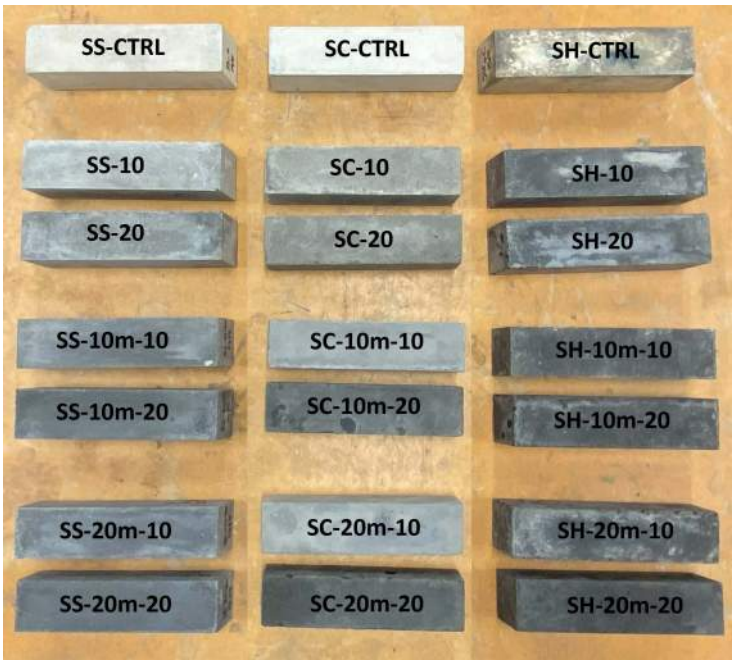

Figure 4. Alkali-activated mortar beams for the Study C.

3.4. Test Methods

3.4.1. Fresh Properties

a. Workability

In Study B, the slump was assessed by measuring it immediately after mixing the concrete, following EN 12350-2:2019. In Study C, the workability of fresh mortar was evaluated using the flow table test, in accordance with ASTM C1437-07.

b. Air Content

The air content of fresh concrete was determined in selected F–T mixes of Study B according to EN 12350-7:2019.

3.4.2. Mechanical Properties

a. Compressive Strength

The compressive strength was measured on different specimen types depending on the study: 5 × 5 × 5 cm^3 mortar cubes in Study A, 10 × 10 × 10 cm^3 concrete cubes in Study B, and 4 × 4 × 16 cm^3 mortar prisms tested at both ends with a loading area of 4 × 4 cm^2 in Study C. All tests were performed at 7 and 28 days with a Toni Technik compression testing machine, and the use of different specimen types followed the respective standards, all in compliance with EN 12390-3:2019. For each mix and testing age, compressive strength was measured on three replicate samples.

b. Flexural Strength

The flexural strength of the alkali-activated mortars in Study C was evaluated at 7 and 28 days in accordance with EN 196-1. The tests were conducted using a Wykeham Farrance mechanical testing machine, operated with a loading rate of 0.5 mm/min and controlled via Catman Easy software. For each mix and testing age, three replicate samples were tested.

3.4.3. Reactivity and Hydration Assessment

a. Strength Activity Index (SAI)

In Study A, the strength activity index (SAI) was assessed by conducting comparative compressive strength tests on mortar cubes with dimensions of 5 × 5 × 5 cm^3 at the age of 7 and 28 days. According to the ASTM C618, a material is considered to exhibit pozzolanic reactivity if the SAI exceeds 75% at both 7 and 28 days. The SAI was calculated using the following using the Equation (1):

$$\text{SAI}\ (\%) = \frac{\text{A}}{\text{B}}\ \text{x}\ 100 \tag{1}$$

where A is the compressive strength of the 20 wt% wood ash or fly ash containing mortar cubes and B is the compressive strength of the control mortar cubes containing 100 wt% Portland cement.

b. Frattini Test

In Study A, the pozzolanic reactivity was evaluated using the Frattini test according to EN 196-5. Test samples contained 80 wt% Portland cement and 20 wt% wood ash or fly ash, while the control sample used 100 wt% Portland cement. All samples were mixed with 100 ml of distilled water, which was initially boiled and then stored in sealed containers at 40 °C. After 8 days of curing, the paste samples were vacuum filtered through filter paper, and 50 mL of the filtrate was titrated with 0.1 M hydrochloric acid (HCl) using methyl orange as an indicator to determine the [OH^-] concentration. Subsequently, [Ca^{2+}] was titrated with a 0.3 M EDTA solution using Patton and Reeder's indicator.

The concentrations of [OH^-] and [Ca^{2+}] were then plotted on a Frattini diagram, illustrating the relationship between CaO solubility and [OH^-] concentration (Donatello et al., 2010; Tironi et al., 2013; Tole et al., 2022). For samples that did not exhibit pozzolanic behaviour on either day 8 or day 15, the test was repeated on day 15. While EN 196-5 specifies testing at 8 and 15 days, an additional measurement was conducted at 28 days for mixes that initially failed to meet the pozzolanic activity criteria. Since EN 196-5 provides lime solubility data for [OH^-] concentrations in the range of 35–90 mmol/L, the lime solubility curve was plotted for an extended [OH^-] range of 40–110 mmol/L, using a theoretical [CaO] concentration calculated by Equation (2) (Donatello et al., 2010).

$$\text{Max } [\text{CaO}] = \frac{350}{[\text{OH}]-15} \tag{2}$$

c. R3 Test

In Study A, the cumulative heat release of the R3 pastes was measured using an 8-channel TAM Air isothermal calorimeter, according to ASTM C1897–20. R3 pastes were prepared using a potassium solution by dissolving 20 g of potassium sulfate powder and 4 g of potassium hydroxide pellets in 1 L of distilled water. The potassium solution and all dry materials, including wood ashes, fly ash, calcium hydroxide, and calcium carbonate, were stored in airtight conditions at 40 ± 2 °C overnight. The mix proportions of the SCM, calcium hydroxide ($Ca(OH)_2$), and calcium carbonate ($CaCO_3$) were 1:3:0.5, and the liquid-to-solid ratio was 1.2:1 by mass. The dry and liquid materials were mixed for 2 minutes using a small-volume vacuum mixer (Ecovac, Bredent/Senden, Germany) at 600 rpm. Then, 15 g of freshly mixed paste was placed into a glass ampoule, which was sealed immediately. Isothermal measurements were performed at a base temperature of 40 ± 0.5 °C for 7 days. The cumulative heat release of the samples was calculated according to the standard, based on the heat release recorded between 75 minutes and 168 hours.

d. Heat of Hydration

The cumulative heat release and heat flow of the binder pastes were monitored using an 8-channel TAM Air isothermal calorimeter over 7 days. In Study B, cement pastes were prepared by partially replacing Portland cement with 10 wt% and 20 wt% of unground and ground wood ashes (WA3 and WA4) and fly ash (FA), along with a control paste containing

100 wt% Portland cement. 6 g of each mix was placed into glass ampoules and sealed. The isothermal calorimetry measurements were then carried out at a constant temperature of 20 ± 0.5 °C, following the standard EN 196-11.

In Study C, alkali-activated pastes incorporating 20 wt% of WA3 and WA3-10m, as well as a control sample with 100 wt% slag, were evaluated. Each paste sample had a mass of 8.3 g and was sealed in glass ampoules, with calorimetric measurements conducted at a constant temperature of 23 ± 0.02 °C in accordance with ASTM C1702-17.

3.4.4. Phase Development and Microstructural Analysis

a. X-ray diffraction (XRD)

X-ray diffraction (XRD) analysis was performed in all studies to evaluate the mineralogical composition of raw materials and phase development in pastes (7- and 28-day-old in Study A and B; 7-day-old in Study C). The measurements were conducted using a PANalytical Empyrean diffractometer equipped with a PIXcel 3D detector, operated at 45 kV and 40 mA. Cu-Kα radiation (λ = 1.54 Å) was employed with a step size of 0.02° and a 2θ scan range from 5° to 70° (Carević et al., 2019). Semiquantitative phase composition analysis was carried out using Profex software (v.5.2.8) in conjunction with the Crystallography Open Database (COD).

b. Thermogravimetric Analysis (TGA/DTG)

In Study A, thermogravimetric analysis (TGA) was performed on 28-day-old paste samples used for XRD, SEM-EDS. The samples were crushed to a particle size of ≤1 mm and then underwent a solvent-exchange procedure as described by (Scrivener et al., 2016). About 5 g of ground paste was immersed in 50 mL of isopropanol for 10 minutes. The suspension was vacuum filtered, washed with 10 mL of diethyl ether, and then subjected to a second filtration. The samples were oven-dried at 40°C for 8 minutes.

TGA measured weight loss from 20 to 1000 °C at 20 °C/min using a NETZSCH STA 449 F3 Jupiter. Approximately 50 mg of powder was placed in alumina crucibles with an argon flow rate of 50 mL/min. The horizontal step identified bound water and decomposition of ettringite and calcite, while the tangential method analysed portlandite (Kim & Olek, 2012; Scrivener et al., 2016). Equations and temperature ranges for quantifying bound water, portlandite, ettringite, and calcite are summarized in Table 6 (Scrivener et al., 2016; Sigvardsen et al., 2021). The phase content was normalized to the anhydrous binder based on residual mass at 550 °C. Mass loss between 50–120 °C estimated ettringite content, noting that contributions from C–S–H or AFm phases are possible (Sigvardsen et al., 2021).

Table 6. Equations and parameters used for quantifying contents of bound water, portlandite, ettringite, and calcite from TGA measurements.

Phase	Temperature Range (°C)	Measured (wt%)	Anhydrous (wt% of anhydrous binder)
Bound Water	50–550	$H_{measured} = WL_{50-550}$	$H_{anhydrous} = \frac{H_{measured}}{Weight\ at\ 550\ °C} x\ 100$
Portlandite ($Ca(OH)_2$)	400–550	$CH_{measured} = WL_{400-550}\ x\ \frac{74}{18}$	$CH_{anhydrous} = \frac{CH_{measured}}{Weight\ at\ 550\ °C} x\ 100$
Ettringite (estimated) ($C_6A\bar{S}_3H_{32}$)	50–120	$Ett_{measured} = WL_{50-120}\ x\ \frac{1255}{32\ x\ 18}$	$Ett_{anhydrous} = \frac{Ett_{measured}}{Weight\ at\ 550\ °C} x\ 100$
Calcite ($CaCO_3$)	600–800	$Cc_{measured} = WL_{600-800}\ x\ \frac{100}{44}$	$Cc_{anhydrous} = \frac{Cc_{measured}}{Weight\ at\ 550\ °C} x\ 100$

Molar masses (g/mol): $Ca(OH)_2$: 74, H_2O: 18, $C_6A\bar{S}_3H_{32}$: 1255, $CaCO_3$: 100, CO_2: 44.

c. Scanning Electron Microscopy (SEM)

The microstructure and morphology of both wood ash and hardened paste and concrete samples were examined using a scanning electron microscope (SEM), JSM-IT100 model (JEOL Ltd., Tokyo, Japan), equipped with an energy dispersive spectrometer (EDS) from BRUKER (JEOL Nordic AB, Sollentuna, Sweden), and ESPRIT software (v.2.1). 7- and 28-day-old samples immersed in isopropanol for 48 hours to stop ongoing reactions, and then stored in a desiccator for an additional 48 hours (Humad et al., 2019). Following this, the samples were impregnated with Struers EpoFix low-viscosity epoxy resin under vacuum conditions. Once the resin hardened, they were polished using grinding plates covered with diamond spray of particle sizes 9, 3, and 1 µm, applying a paraffin-based lubricant (Rossen & Scrivener, 2017). SEM analysis was performed in low vacuum mode using a backscattered electron detector (BSE) at an accelerating voltage of 15.0 kV and 500× magnification. EDS spot analysis was also carried out at 1000× magnification, with 100 points manually chosen based on the grey-level histogram corresponding to C–S–H (Rossen & Scrivener, 2017).

3.4.5. Frost Durability

a. Freeze–Thaw Resistance

Two sets of selected concrete mixes were tested for freeze-thaw resistance. The first set was prepared without any air-entraining admixture and included the CTRL, FA-20, WA3-20, and WA3-10m-20 mixes. The second set was prepared with 0.1 wt% air-entraining admixture and consisted of CTRL-AE, FA-20-AE, WA3-20-AE, and WA3-10m-20-AE mixes.

Concrete cubes measuring 15 × 15 × 15 cm³ were cast, demoulded after 24 hours, and cured in water until the 7th day. On the 7th day, they were moved to a climate chamber at a temperature of 20 ± 2 °C. By the 21st day, 50 ± 2 mm thick concrete samples were cut from each cube according to CEN/TS 12390-9 and stored in the climate chamber. On the 25th day,

the samples were taken out from the climate chamber, all surfaces except the test surface were sealed with a rubber sheet, and the samples were returned to the chamber.

On the 28th day, a 3 mm layer of de-ionized water was applied to the test surface of the samples, which were then stored in the climate chamber for another 72 ± 2 hours. All surfaces except for the test surface were thermally insulated with 20 ± 1 mm thick polystyrene cellular plastic.

At 31 days, the de-ionized water on the test surface was replaced with a 3 mm layer of freezing medium, which consisted of 97 wt% water and 3 wt% NaCl. To prevent evaporation, a polyethylene sheet was placed over the surface. The samples were then placed in a freezing chamber at an initial temperature of 20 ± 2 °C. Each 24-hour freeze-thaw cycle reached a minimum temperature of −20 °C, with the temperature profile (Figure 5) maintained within the limits specified by CEN/TS 12390-9.

The scaled material was collected using a paper filter, dried at 110 ± 10 °C, and weighed after 7, 14, 28, 42, and 56 cycles. After each measurement, the freezing medium was replaced. Then, the cumulative amount (kg) of scaled material per unit area (m^2) was calculated.

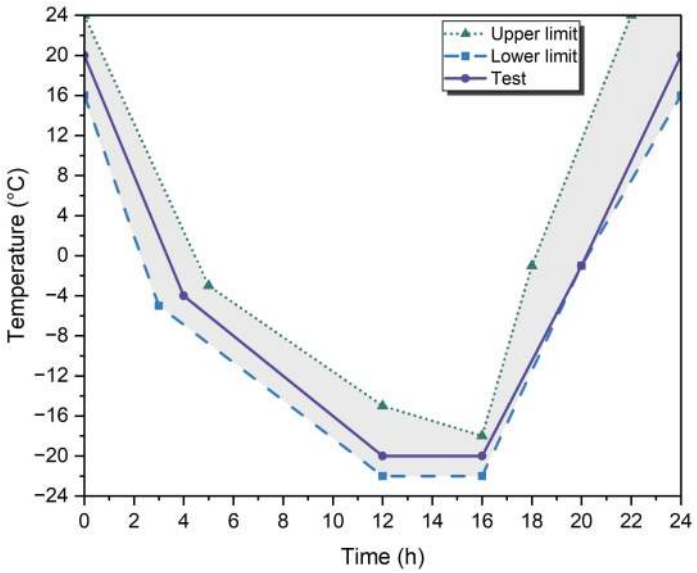

Figure 5. Test temperature profile and the range of upper and lower limits as specified by CEN/TS 12390-9.

3.4.6. Environmental Performance

a. Leaching

Leaching tests were conducted following the EN 12457-2 on WA3, WA3-10m, WA3-20m, WA4, WA4-10m, WA4-20m, FA, and CEM. For each test, 15 g of powdered sample was mixed with 150 mL of deionized water, maintaining a liquid-to-solid (L/S) ratio of 10, in a 250 mL closed bottle and rotated for 24 hours. After mixing, the mixtures were allowed to settle for approximately 15 minutes. The eluate was then filtered using a membrane filter

with a pore size of 0.45 µm; the pH and electrical conductivity (EC) of the filtrate were measured.

The dynamic surface leaching test (DSLT) was conducted following the EN 16637-2:2023 on selected monolithic concrete samples: CTRL, FA-20, WA3-20, and WA3-10m-20 mixes. Concrete specimens measuring 10 × 10 × 10 cm³ were cast, demoulded after 24 hours, and cured in water until the 7th day. After curing, the samples were suspended using polypropylene plastic rope from the lid of a polypropylene plastic vessel. As per the standard requirements, the distance between the sample and the vessel bottom and between the sample and the solvent surface had to be at least 20 mm.

The specimens were submerged in deionized water, maintaining a liquid-to-exposed surface area ratio (L/S) of 90 L/m². The liquid volume was determined following the EN 16637-2:2023. The test setup is illustrated in Figure 6. The samples were collected on the 9th and 64th days. The eluates were then filtered using a membrane filter with a pore size of 0.45 µm and their pH and electrical conductivity were measured.

The Relative Leaching Rate (RLR) was calculated using a simplified version of the formula employed by Yuan et al. (2021). to assess the relative leaching behaviour of heavy metals (Cd, Cr, Cu, Ni, Pb, and Zn). The equation was simplified with a fixed L/S of 10, and the RLR was expressed as:

$$\text{RLR}\ (\%) = \frac{C_{leachate}}{C_{total}} x\ 100 \tag{3}$$

where $C_{leachate}$ and C_{total} are the concentrations of a given heavy metal in the leachate and the ash, respectively (mg/kg). This ratio represents the leached fraction of the total content.

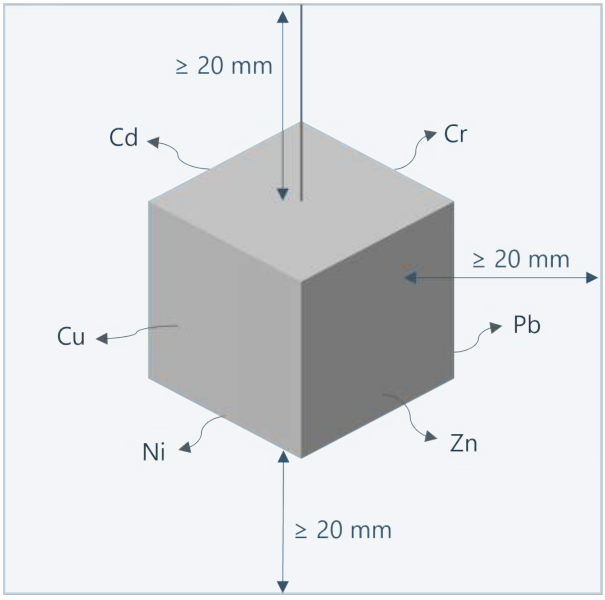

Figure 6. The dynamic surface leaching test setup.

Chapter 4

Results and Discussion

4.1. Chemical and Physical Characteristics of Wood Ash

The wood ash samples (WA1, WA2, WA3 and WA4) showed significant variability in both chemical and physical properties, which directly affected their potential as supplementary cementitious materials. None of the samples met the pozzolanic oxide criterion ($SiO_2 + Al_2O_3 + Fe_2O_3 \geq 70\%$) outlined in EN 450-1, with total contents ranging from as low as 1.29% (WA4) to 43.14% (WA1). It should be noted that EN 450-1 formally applies to coal fly ash; in this context, it is used as a comparative indicator.

WA2 and WA4 had notably high CaO contents exceeding 20%, indicating a tendency toward hydraulic reactivity. These samples also met the EN 197-1 requirement of $CaO/SiO_2 > 2$ and exhibited high hydraulic index (K_3), calculated as $(CaO + MgO + Al_2O_3)/SiO_2$, indicating limited pozzolanic but significant latent hydraulic potential (Berra et al., 2015; Sigvardsen et al., 2019).

The LOI values of WAs in this study ranged from 29.7% to 56.7%, indicating a generally high content of both organic and inorganic residues. Elevated LOI values are typically attributed to residual unburnt carbon. However, they may also result from pre-combustion organic matter or the formation of carbonates such as $CaCO_3$ and $K_2Ca(CO_3)_2$ during combustion (Carević et al., 2020; Sklivaniti et al., 2017). Several factors can affect these values, including the type of biomass, combustion conditions (temperature, technology), and the methods and timing of ash collection. Irregular furnace performance and longer residence times may lead to the accumulation of volatile components or partially reacted phases (Vassilev et al., 2010).

The cumulative particle size distribution curves of unground and ground wood ashes, fly ash, and Portland cement (CEM I) are presented in Figure 7, while the particle size

distribution parameters (D10, D50, D90) and specific surface areas (SSA) are summarized in Table 7.

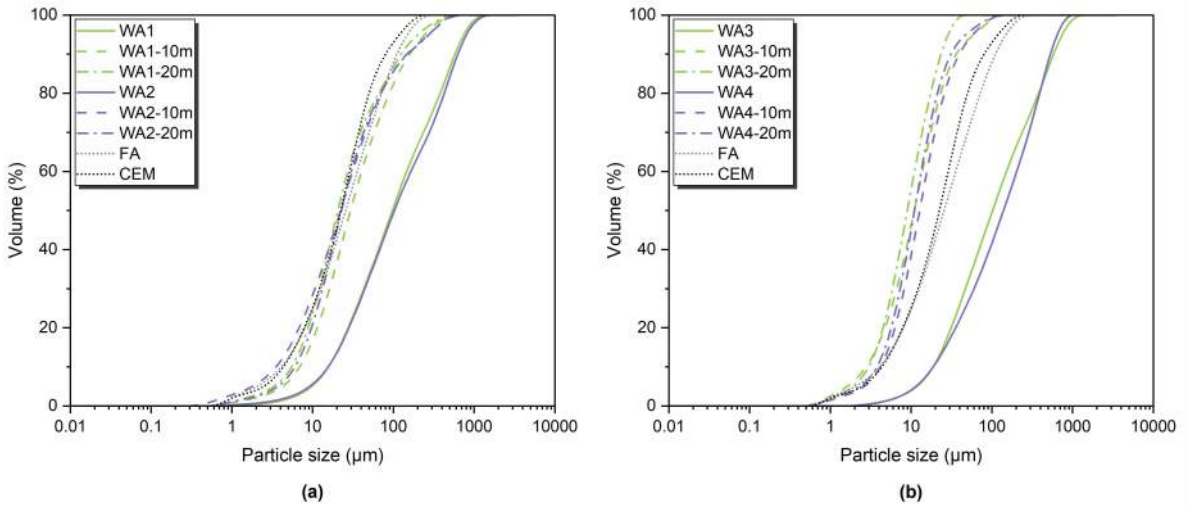

Figure 7. Cumulative particle size distribution curves of unground and ground wood ashes **(a)** WA1 and WA2, and **(b)** WA3 and WA4, compared to fly ash (FA) and Portland cement (CEM I). Data adapted from Paper II (Teker Ercan et al., 2025a).

The initial particle sizes (D50) of the wood ash samples ranged from 97.2 µm to 139 µm, which were significantly larger than fly ash (25.6 µm) and cement (22.4 µm). Grinding for 10 minutes caused a substantial size reduction, resulting in D50 values of 29.5 µm for WA1, 22.2 µm for WA2, 10.3 µm for WA3, and 12.7 µm for WA4. When grinding was extended to 20 minutes, the particle sizes of WA1, WA3, and WA4 further decreased to 20.6 µm, 8.98 µm, and 11 µm, respectively. In contrast, WA2 showed a slight increase to 22.8 µm, likely due to particle agglomeration. Additionally, D10 values, which represent the finer particle fractions, declined notably with grinding, especially in WA3 and WA4. As particle size decreased, the SSA of the wood ash samples increased significantly. The unground WAs had SSA between 131.9 to 186.6 m^2/kg. Grinding increased SSA across all samples, with the highest value observed for WA3 after 20 minutes (WA3-20m: 1048 m^2/kg). After 20 minutes of grinding, WA2 had a minor drop in SSA compared to its 10-minute value, consistent with its slight increase in particle size. Meanwhile, WA1, WA3, and WA4 continued to show a trend of decreasing particle size along with an increase in surface area.

The morphological transformation of wood ash particles is evident in the SEM images shown in Figure 8. While all unground wood ashes display larger and more irregularly shaped particles, the ground samples look visibly smaller and smoother, showing the refining effect of the grinding process.

Table 7. Particle size distribution parameters (D10, D50, D90) and specific surface areas (SSAs) of unground and ground wood ashes (WA1, WA2, WA3, WA4), fly ash (FA), and Portland cement (CEM I). Data adapted from Paper II (Teker Ercan et al., 2025a).

Material	Grinding time	D10 (µm)	D50 (µm)	D90 (µm)	SSA (m²/kg)
WA1	0	15.7	97.2	581	172.4
WA1-10m	10	6.91	29.5	159	444.3
WA1-20m	20	5.49	20.6	125	566.5
WA2	0	15.6	103	629	186.6
WA2-10m	10	3.53	22.2	147	829.6
WA2-20m	20	6.03	22.8	150	519.3
WA3	0	18.7	102	581	143
WA3-10m	10	2.77	10.9	36.3	1021
WA3-20m	20	2.98	8.98	23.5	1048
WA4	0	18.8	139	532	131.9
WA4-10m	10	4.16	12.7	39.5	782.1
WA4-20m	20	3.78	11	31.1	882.9
FA	0	4.09	25.6	111	666.6
CEM I	0	4.34	22.4	80.3	672.9

X-ray diffraction (XRD) analysis of both unground and ground wood ashes showed differences in crystalline phase composition and peak intensities, depending on the type of wood ash and grinding duration (Figure 9). Because of the similarity in the diffractograms, WA1, WA1-10m, and WA1-20m were grouped with WA3, WA3-10m, and WA3-20m in Figure 9a, while WA2, WA2-10m, WA2-20m, WA4, WA4-10m, and WA4-20m were shown together in Figure 9b.

Quartz (Q) became the main crystalline phase in the WA1 and WA3 series (except unground WA3), with its peak intensity increasing with longer grinding times. This pattern likely results from quartz's inherent hardness, which makes it less prone to breaking down structurally during grinding, leading to slower amorphization compared to other minerals (Sanna et al., 2023). Additionally, quartz can function as a grinding medium, speeding up the amorphization of softer minerals during extended milling (Makó et al., 2001), which makes it appear more dominant in the residual crystalline phases (Zhang et al., 2015). Calcite (C) was also consistently found in both ground and unground WA1 and WA3 samples, while arcanite (Ar) was observed in all WA3 samples.

In contrast, calcite was the main crystalline component in the WA2 and WA4 series. However, a reduction in calcite peak intensity was observed after grinding. WA4 showed an initial increase in calcite intensity after 10 minutes of grinding, followed by its complete disappearance after 20 minutes. Other phases such as quartz, portlandite, and hematite (in low intensity) were detected in the WA2 and WA4 samples, although hematite was absent in WA4-20m.

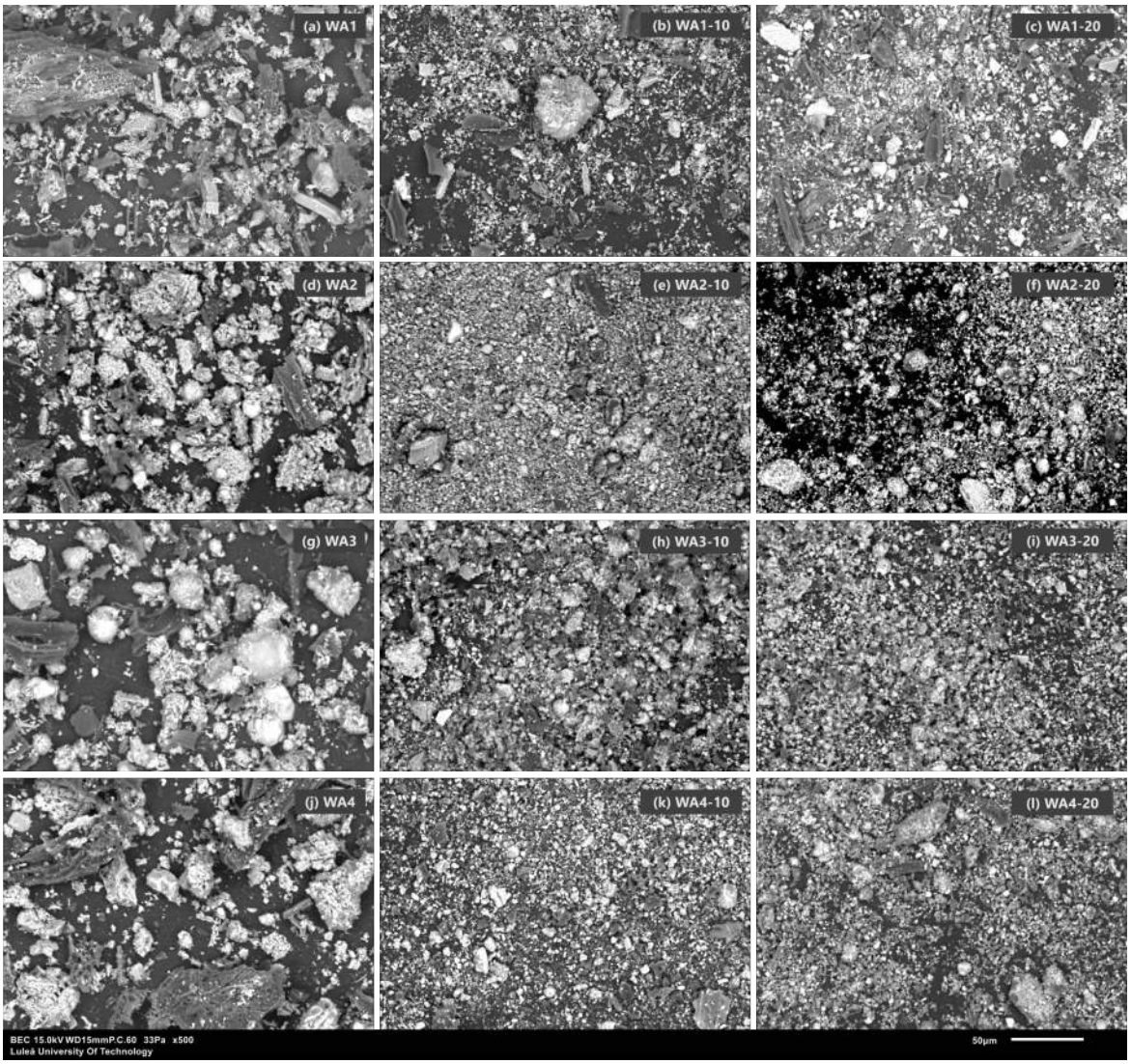

Figure 8. SEM images of wood ash powders before and after grinding for 10 and 20 min at 500× magnification. Data adapted from Paper II (Teker Ercan et al., 2025a).

The observed decrease in peak intensities indicates increased amorphization caused by high-energy grinding. This aligns with findings by Ke et al. (2023), who reported that intense milling decreases mineral crystallinity by changing the surface bonding of Al–O and Si–O groups. Kato et al. (2019) further described the mechanochemical activation process in three stages: the initial reduction of large ash particle size, subsequent amorphization during grinding, and finally, particle agglomeration that can be re-ground. These changes highlight the need to optimize grinding time and energy input to improve activation efficiency.

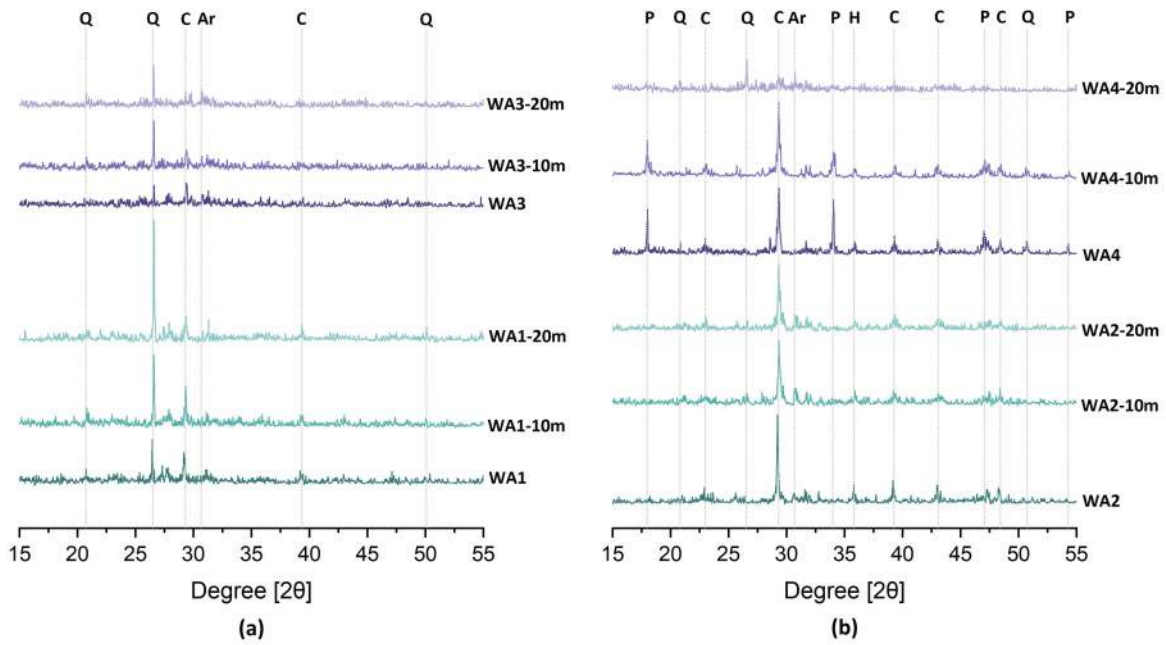

Figure 9. XRD patterns of unground and ground wood ashes: **(a)** WA1 and WA3; **(b)** WA2 and WA4 (P: Portlandite, C: Calcite, Q: Quartz, Ar: Arcanite, H: Hematite). Data adapted from Paper II (Teker Ercan et al., 2025a).

4.2. Assessment of Pozzolanic Activity of Wood Ash

4.2.1. Strength Activity Index (SAI)

The compressive strength and strength activity index (SAI) values were used to assess the mechanical performance and pozzolanic reactivity of mortars incorporating WA, following ASTM C618 criteria. The compressive strength results are presented in Figure 10, while the SAI values are shown in Figure 11.

At both 7 and 28 days of curing, all mortars containing WA or FA showed lower compressive strength than CTRL. Compared to mixes with unground WA, all mortars containing ground ash showed higher strength values. Mortars with WA ground for 10 minutes consistently performed better than those with an unground WA or WA ground for 20 minutes. Moreover, WA4-10m even exceeded the compressive strength of the CTRL mortar at 7 days.

According to ASTM C618, materials can be classified as pozzolanic if their SAI exceeds 75% at both 7 and 28 days. Mortars with ground WA1, WA3, and WA4 met the minimum SAI requirement of 75%, as defined by the standard. For instance, WA1-10m achieved SAI values of 88.88 ± 3.3% (7 days) and 78.52 ± 1.7% (28 days), WA3-10m reached 87.74 ± 1.8% and 82.66 ± 0.9%, and WA4-10m showed the highest SAI of 104.11 ± 2.9% at 7 days and 92.77 ± 2.5% at 28 days. These results emphasize the effectiveness of grinding in increasing the reactivity of wood ash. In contrast, all unground ashes (WA1, WA2, WA3, WA4) and FA stayed below the 75% threshold. WA2 also did not surpass the limit even after 10 or 20 minutes of grinding.

Among all samples, WA4-10m showed the best performance with a SAI of 104.11% at 7 days. However, its chemical properties suggest this improvement is more likely due to filler effects or latent hydraulic activity rather than true pozzolanic behaviour. WA4 had a high CaO/SiO_2 ratio (38.67), indicating a strong hydraulic character. The improvement in compressive strength observed after grinding may result from several mechanisms: a reduction in water demand, a larger surface area of amorphous silica in the ash that enhances pozzolanic reactivity, filler effects from fine particles, or a combination of these factors (Donatello et al., 2010).

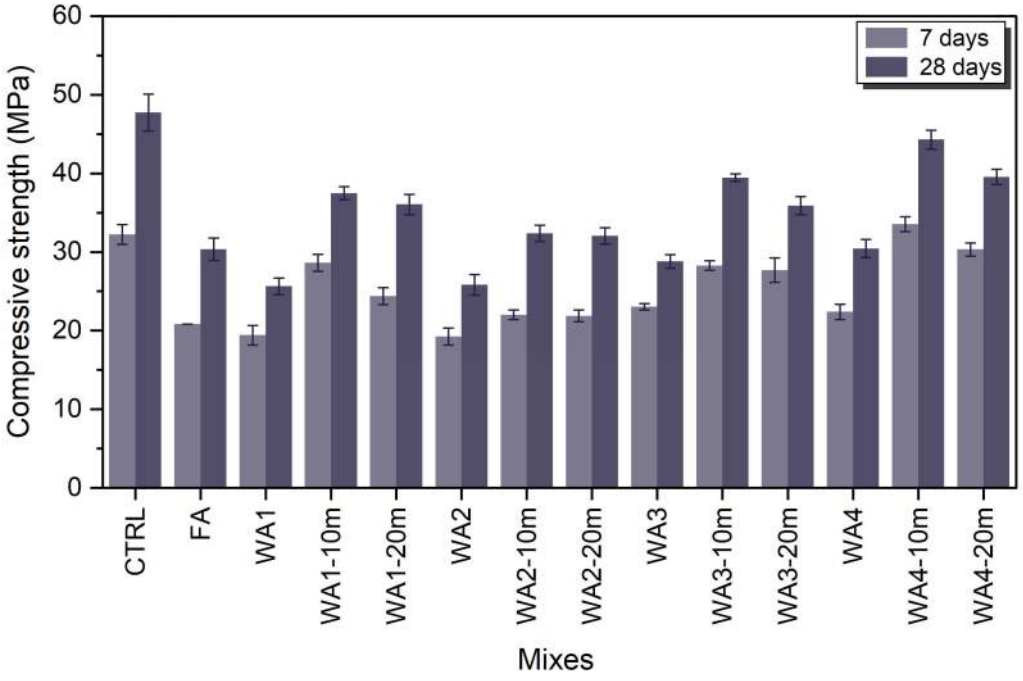

Figure 10. Compressive strength of mortars with 20 wt% fly ash or unground and ground wood ash, compared to a control sample with 100 wt% cement. Data adapted from Paper II (Teker Ercan et al., 2025a).

Despite the widespread use of the SAI test as an indirect indicator of pozzolanic activity (Garcia & Sousa-Coutinho, 2013; Jurić et al., 2021; Sigvardsen et al., 2021), it has certain limitations. The test results can be misleading due to physical effects such as improved particle packing or increased nucleation sites (Berodier & Scrivener, 2014), which do not necessarily indicate chemical reactivity. Additionally, some SCMs may exhibit delayed pozzolanic reactivity, requiring longer curing times for a more accurate evaluation (Dimter et al., 2022; Pantić et al., 2023). Donatello et al. (2010) suggested revising ASTM C618 by either increasing the minimum SAI threshold or raising the replacement level to 25–30% to reduce misclassification of low-reactive materials. Furthermore, it is often challenging to distinguish the contribution of pozzolanic reaction products from other hydration phases in strength development (Sigvardsen et al., 2021). Therefore, additional tests are needed to better assess the pozzolanic and hydraulic potential of materials.

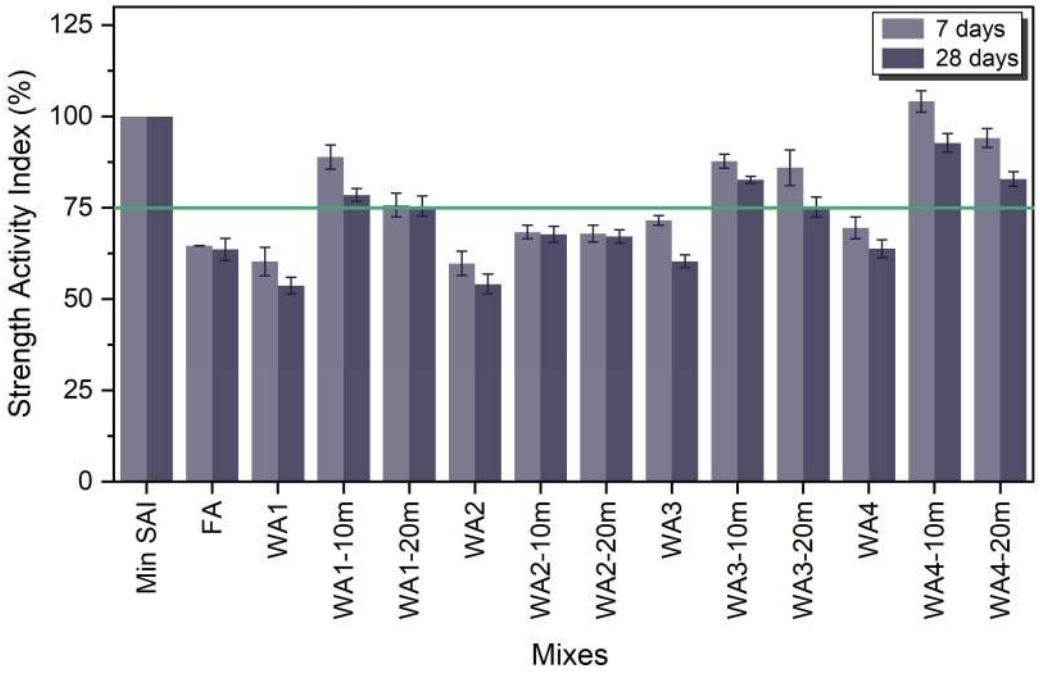

Figure 11. SAI (%) at 7 and 28 days. The green line marks the minimum SAI requirement (75%) according to ASTM C618 for a material to be classified as pozzolanic. Data adapted from Paper II (Teker Ercan et al., 2025a).

4.2.2. Frattini Test

The pozzolanic reactivity of the WAs and FA was assessed using the Frattini test at 8 and 15 days, with the results shown in Figure 12. According to EN 196-5, materials are considered pozzolanic when the results fall below the lime solubility curve; values above the curve indicate insufficient reactivity and are therefore classified as non-pozzolanic.

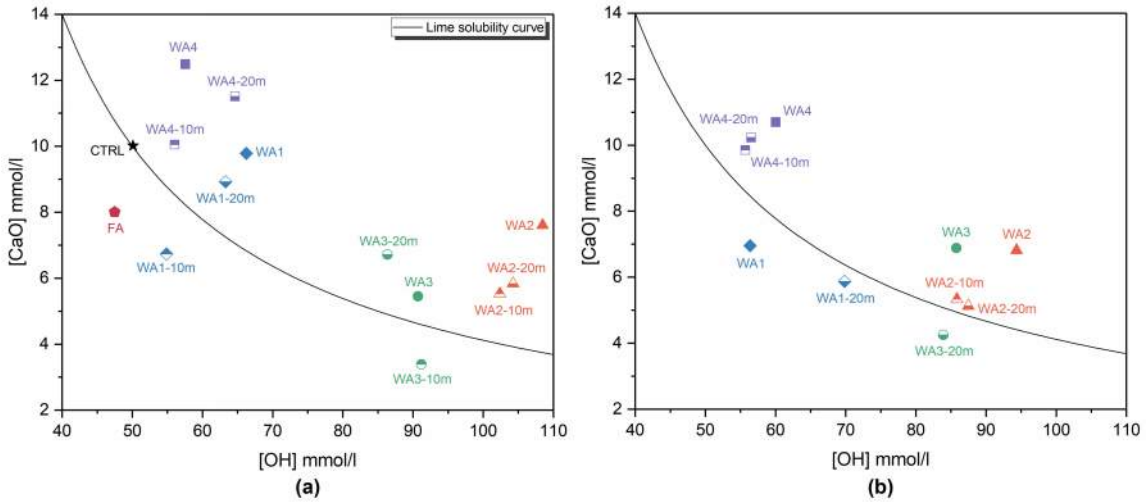

Figure 12. Frattini test results for pastes containing 20 wt% of unground and ground wood ash and fly ash and a control sample of 100 wt% Portland cement (CTRL), are shown **(a)** after 8 days, and **(b)** after 15 days. Data adapted from Paper II (Teker Ercan et al., 2025a).

To evaluate longer-term reactivity, an additional Frattini test was conducted at 28 days, with results shown in Figure 13. At this age, ground WA2 and WA4 fell below the lime solubility curve, indicating that their reactivity is likely linked to latent hydraulic behaviour rather than pozzolanic activity, given their high CaO content and low pozzolanic oxide ratios.

To support the diagrams, CaO reduction values were also calculated (Table 8). This approach, also recommended by Donatello et al. (2010), offers a quantitative way to assess pozzolanic activity, as it indicates the consumption of Ca^{2+} ions from the solution. The highest CaO removal at 8 days was observed in WA3-10m (26.3%), followed by FA (25.7%) and WA1-10m (23.3%), confirming early reactivity in these systems. By day 15, continued CaO reduction was seen in WA1 (17.8%) and WA3-20m (16.3%), supporting their slower but ongoing pozzolanic response.

On the 15-day Frattini test period, several samples showed negative CaO reduction values. Although these are often normalized to zero for simplicity, their presence offers valuable insight into the system's chemical environment (Donatello et al., 2010; Jurić et al., 2021; Tole, 2022). Negative values indicate oversaturation of the solution with Ca^{2+}, possibly due to unreacted free CaO or early-age hydraulic reactions, especially in high-CaO systems (Sigvardsen et al., 2021a). Such conditions may inhibit Ca^{2+} consumption from the pore solution and slow down pozzolanic activity. Donatello et al. (2010) pointed out that these results expose the limitations of the Frattini method under these circumstances and should not be interpreted as definitive indicators of inertness.

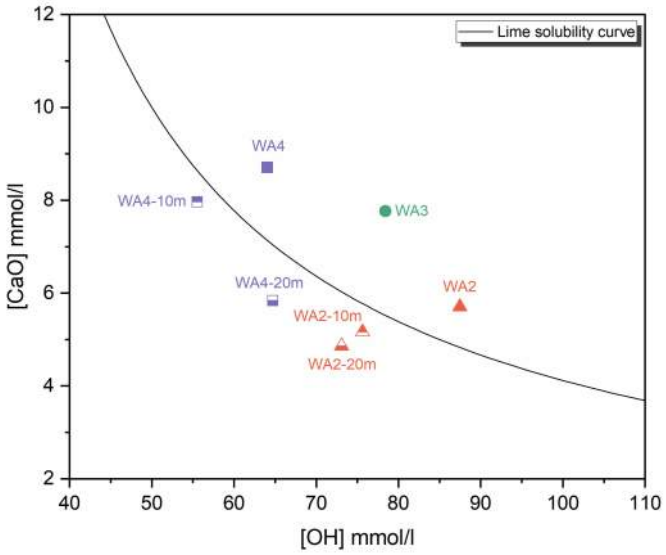

Figure 13. Frattini test results for pastes containing 20 wt% of unground and ground wood ash after 28 days. Data adapted from Paper II (Teker Ercan et al., 2025a).

At 28 days, CaO reductions of 10.5% and 19.3% were observed in WA2-10m and WA2-20m, respectively, while WA4-10m and WA4-20m showed reductions of 7.8% and 17.0%. These results confirm their relatively delayed but ongoing reactivity. However, Kramar and Ducman (2018) emphasized that reactive SiO_2 content plays a more critical role in controlling

pozzolanic performance than total CaO, highlighting the importance of chemical composition in long-term pozzolanic reactivity assessment.

A similar pattern was reported by Kostanić Jurić et al. (2021), who observed that wood ashes with limited pozzolanic oxide content showed reactivity only after extended curing time, suggesting that such materials may develop reactivity over time through the combined effects of pozzolanic and latent hydraulic mechanisms.

Table 8. Frattini test results with [CaO] reduction after 8, 15, and 28 days. Data adapted from Paper II (Teker Ercan et al., 2025a).

Sample	[CaO] Reduction (%)		
	8 days	15 days	28 days
CTRL	0 (-0.5 ± 0.15)	-	-
FA	25.7 ± 0.18	-	-
WA1	0 (-43.2 ± 0.13)	17.8 ± 1.35	-
WA1-10m	23.3 ± 1.39	-	-
WA1-20m	0 (-23.1 ± 1.74)	8.0 ± 0.95	-
WA2	0 (-103.1 ± 3.73)	0 (-54.6 ± 2.59)	0 (-18.1 ± 2.43)
WA2-10m	0 (-38.0 ± 2.57)	0 (-7.9 ± 0.63)	10.5 ± 0.5
WA2-20m	0 (-48.9 ± 2.66)	0 (-6.2 ± 2.46)	19.3 ± 1.43
WA3	0 (-17.9 ± 0.82)	0 (-39.2 ± 0.22)	0 (-40.7 ± 2.2)
WA3-10m	26.3 ± 1.88	-	-
WA3-20m	0 (-36.9 ± 1)	16.3 ± 1.75	-
WA4	0 (-51.8 ± 5.25)	0 (-37.6 ± 0.05)	0 (-22.0 ± 0.18)
WA4-10m	0 (-17.8 ± 1.5)	0 (-14.6 ± 3.82)	7.8 ± 2.71
WA4-20m	0 (-63.2 ± 0.71)	0 (-21.4 ± 2.66)	17.0 ± 0.86

4.2.3. R3 Test

R3 (rapid, relevant, reliable) test evaluates SCM reactivity based on the heat of hydration in an isothermal calorimeter. Although originally developed for calcined clay–limestone blends, it is now commonly used for other SCMs (Avet et al., 2016; Parashar & Bishnoi, 2020). Figure 14 shows the cumulative heat (J/g SCM) over 168 hours (at 40 °C) as follows: FA (168.15) > WA3-20m (109.73) > WA3-10m (106.73) > WA1-10m (101.66) > WA4-20m (101.56) > WA1-20m (71.22) > WA3 (58.57) ≈ WA1 (58.31) > WA2-20m (47.75) > WA2-10m (42.93) > WA4-10m (34.79) > WA2 (32.81) > WA4 (24.54).

ASTM C1897-20 does not specify a pass or fail limit; however, Suraneni (2021) proposes a benchmark of 100 J/g. Based on this, FA, WA3-20m, WA3-10m, WA1-10m, and WA4-20m exceed this value and can be considered reactive in the R3 system. Generally, longer grinding increased heat release, except for WA1, where WA1-10m exceeds WA1-20m, aligning with an optimal 10-minute duration and potential agglomeration or water-demand effects at longer grinding. WA4-10m exhibited low heat despite its relatively high strength, indicating filler/nucleation or hydraulic effects that do not necessarily increase R3 heat. In contrast, WA4-20m showed unexpectedly high heat compared to WA4 and WA4-10m, likely due to amorphization effects and its high CaO content (29%) combined

with very low SiO_2 (0.75%), supporting a latent hydraulic reaction rather than pozzolanic (Cheah, 2011; Jurić et al., 2021; Sigvardsen et al., 2021b; Ukrainczyk et al., 2016).

WA4-10m released very low R3 heat but maintains relatively high strength. Kalina et al. (2019) further classified materials based on their heat release: inert if below 100 J/g SCM, moderately pozzolanic if between 100 J/g and 200 J/g SCM, and highly pozzolanic if above 200 J/g SCM. R3 indicates chemical heat, while strength can also increase due to physical effects as previously discussed: finely ground WA acts as an inert filler and hydrate-nucleation surface (Berra et al., 2015; Sigvardsen et al., 2019). By filling voids and initiating early C–S–H formation, it accelerates hydration and enhances strength even when the ash itself has low reactivity (Berra et al., 2015; Sigvardsen et al., 2019; Sklivaniti et al., 2017; Vu et al., 2019). Similar improvements are reported in cement systems (Sigvardsen et al., 2019; Snellings et al., 2021).

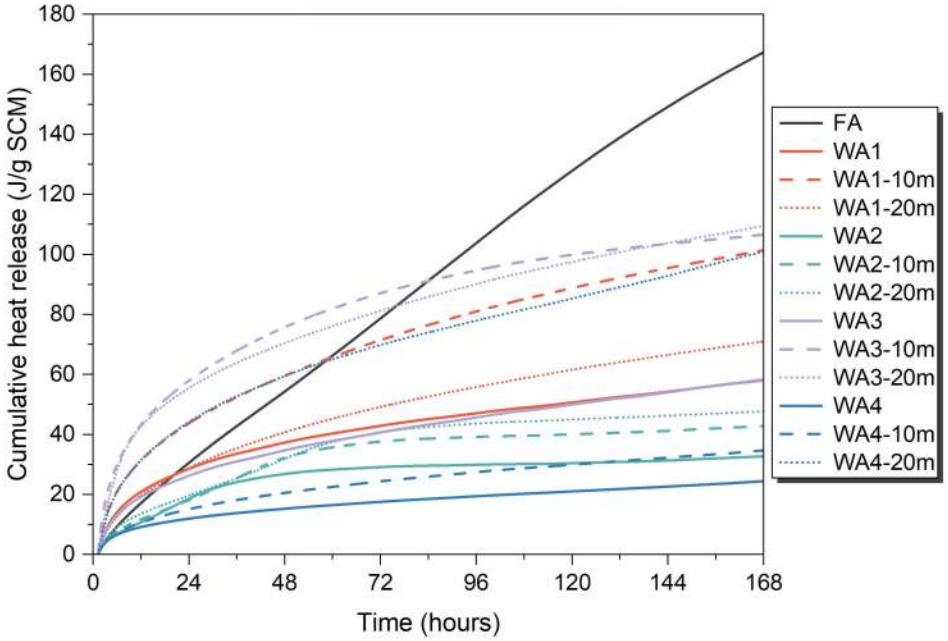

Figure 14. Cumulative heat release over 7 days at 40 °C for R3 paste samples containing unground and ground wood ashes (WA3 and WA4), with different grinding durations (10 and 20 minutes), and fly ash (FA). Data adapted from Paper II (Teker Ercan et al., 2025a).

The relationship between cumulative heat and relative strength was analysed by categorizing the WAs based on CaO content, given in Figure 15; low-CaO (<20%): WA1, WA1-10m, WA1-20m, WA3, WA3-10m, WA3-20m; high-CaO (>20%): WA2, WA2-10m, WA2-20m, WA4, WA4-10m, WA4-20m. For the low-CaO group, cumulative heat showed a strong correlation with 28-day relative strength, and this correlation improved over time (R^2 = 0.725, 0.767, 0.844, 0.865 at 12, 24, 72, 168 hours) (Koufany et al., 2025). This indicates that, for relatively silica rich WAs, R3 heat reflects pozzolanic reactions that influence strength at later ages (Londono-Zuluaga et al., 2022). In contrast, the correlations in the high-CaO group were weak across all intervals ($R^2 \leq 0.22$), aligning with the idea that filler and/or latent hydraulic mechanisms, rather than pozzolanic activity, primarily govern strength.

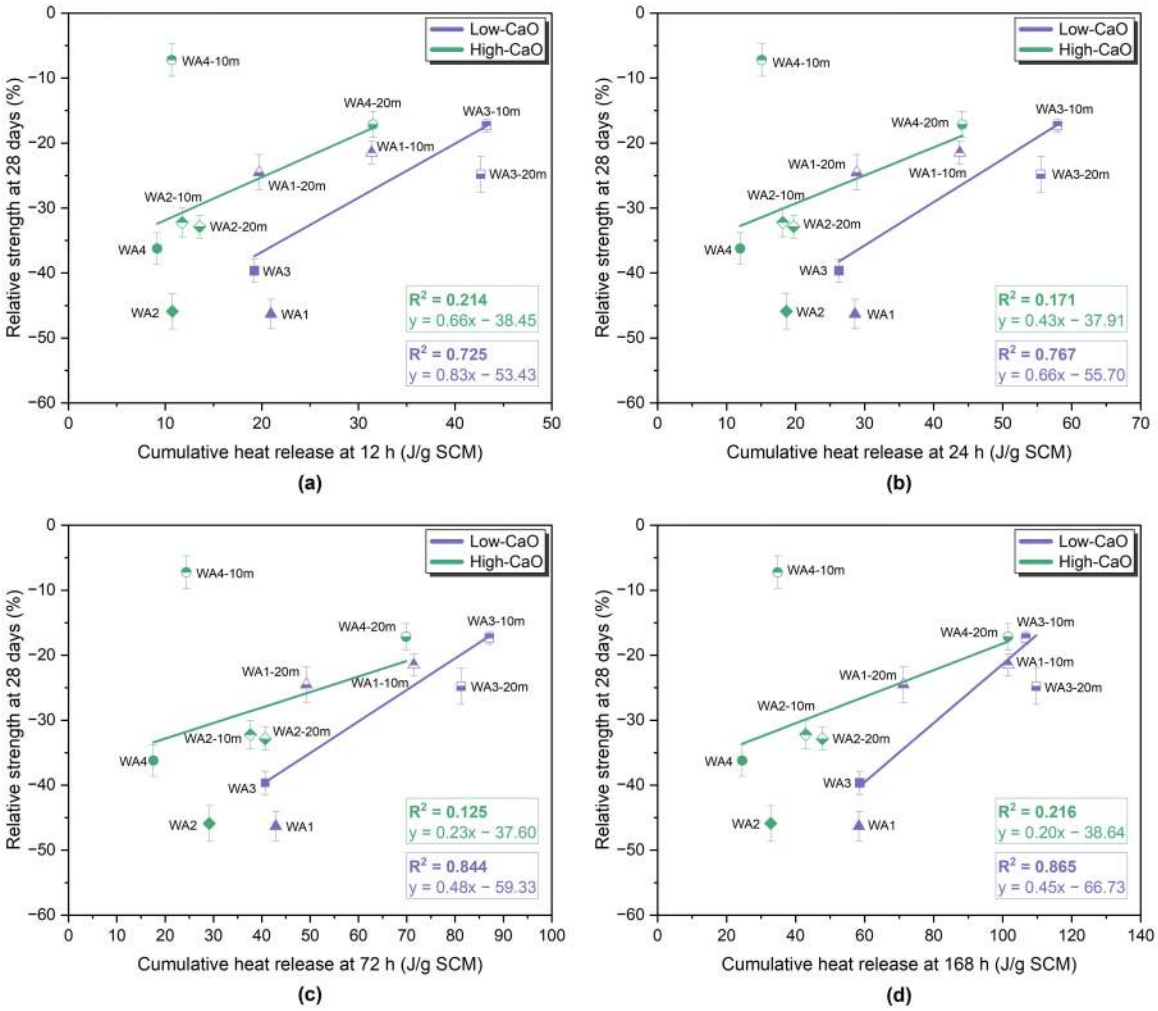

Figure 15. Correlation between the relative compressive strength at 28-day and cumulative heat release in the R3 test at **(a)** 12 h, **(b)** 24 h, **(c)** 72 h, and **(d)** 168 h. Data adapted from Paper II (Teker Ercan et al., 2025a).

4.2.4. Phase Development and Microstructural Investigation

Phase development at 28 days was assessed using TGA/DTG and XRD; SEM-EDS was used for microstructural investigation. The DTG curves (Figure 16) show three main regions: 50–120 °C for dehydration of ettringite and loosely bound C–S–H (and other phases that may decompose within this range), 400–550 °C for dehydroxylation of portlandite (CH), and 600–800 °C for decarbonation of calcite and other carbonates (Scrivener et al., 2016; Taylor, 1997). Figure 17 shows the quantified contents of portlandite and bound water, while Figure 18 displays ettringite and calcite contents. The XRD patterns at 7 and 28 days are shown in Figure 19. Since all ash-containing pastes replace 20 wt% of cement, part of the CH reduction results from dilution, and the interpretation considers this effect (Scrivener et al., 2016; Snellings et al., 2021; Suraneni & Weiss, 2017; Taylor, 1997).

XRD patterns of 7-day old pastes show that, compared to CTRL-7, FA-7 displays reduced CH reflections while ettringite remains present, indicating early pozzolanic reaction. In the WA series, WA3-10m-7 exhibits a reduction in CH compared to WA3-7 while still

showing ettringite, suggesting that 10 min of grinding activates WA3 at early ages. WA1-10m-7 demonstrates a slight decrease in CH peak intensity. On the other hand, WA2-7 maintains strong CH peaks alongside more prominent calcite, indicating carbonation rather than pozzolanic or hydraulic reactions. In WA4, a decrease in CH peak intensity appears in WA4-20m-7, along with an increase in calcite, which aligns with limited hydraulic activity due to its high CaO content.

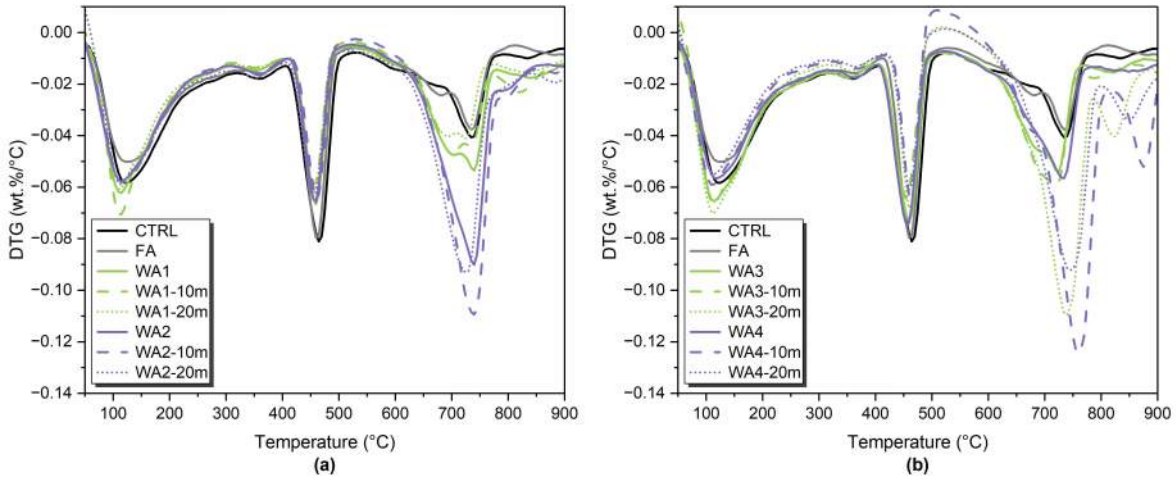

Figure 16. DTG curves for 28-day-old pastes with unground and ground samples of **(a)** WA1 and WA2, and **(b)** WA3 and WA4, compared to CTRL and FA-containing pastes. Data adapted from Paper II (Teker Ercan et al., 2025a).

The CTRL sample exhibits the highest hydration level, with 16.95% bound water and 16.04% CH; strong CH peaks and the presence of ettringite in XRD confirm OPC hydration and provide a benchmark for comparison (Snellings et al., 2021; Suraneni & Weiss, 2017; Wang et al., 2022). FA shows lower CH (13.68%), and bound water (14.65%) compared to CTRL; ettringite (4.76%) and calcite (10.39%) are also slightly reduced. XRD indicates a decreased CH peak intensity while ettringite remains detectable. These patterns align with the low early reactivity of low-Ca (Class F) fly ashes (Kramar & Ducman, 2018; Y. Wang et al., 2022).

WA3 exhibits the highest pozzolanic activity among WAs. In WA3-10m, CH decreases from 13.07% to 10.53%, while bound water remains high at 15.67%; AFt is 5.76%, and calcite increases slightly. XRD shows weaker CH peaks compared to unground WA3, with the ettringite peak still present. WA3-10m and WA3-20m show the highest R3 heat for the WAs and the highest strength for WA-containing mortars. The lower bound water and higher calcite content in WA3-20m (14.16% and 25.96%) correspond with its reduced strength relative to WA3-10m.

WA1 responds moderately to grinding. After 10 minutes of grinding, CH decreased from 11.86% to 9.49%, and ettringite increased to 6.57%, while bound water decreased slightly from 14.31% to 13.75%. XRD shows reduced CH with ettringite still visible. R3 heat increases from 54.52 to 95.6 J/g SCM at 10 min and then declines at 20 min to 67.65 J/g

SCM, aligning with the strength trend and indicating combined chemical and packing/nucleation effects (Avet et al., 2022).

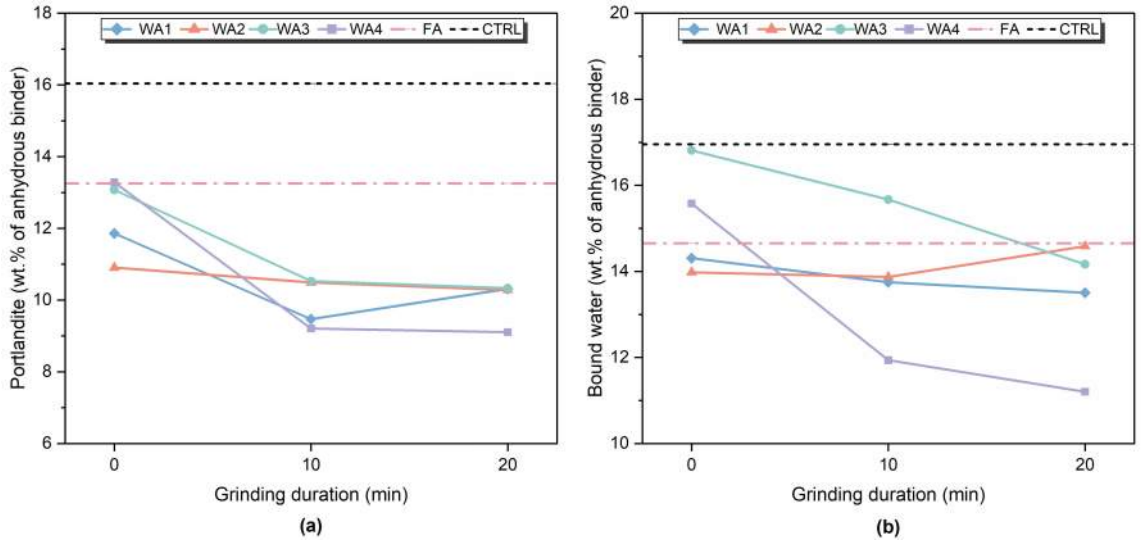

Figure 17. Quantification of **(a)** portlandite, and **(b)** bound water content of 28-day-old pastes based on TGA analysis. Data adapted from Paper II (Teker Ercan et al., 2025a).

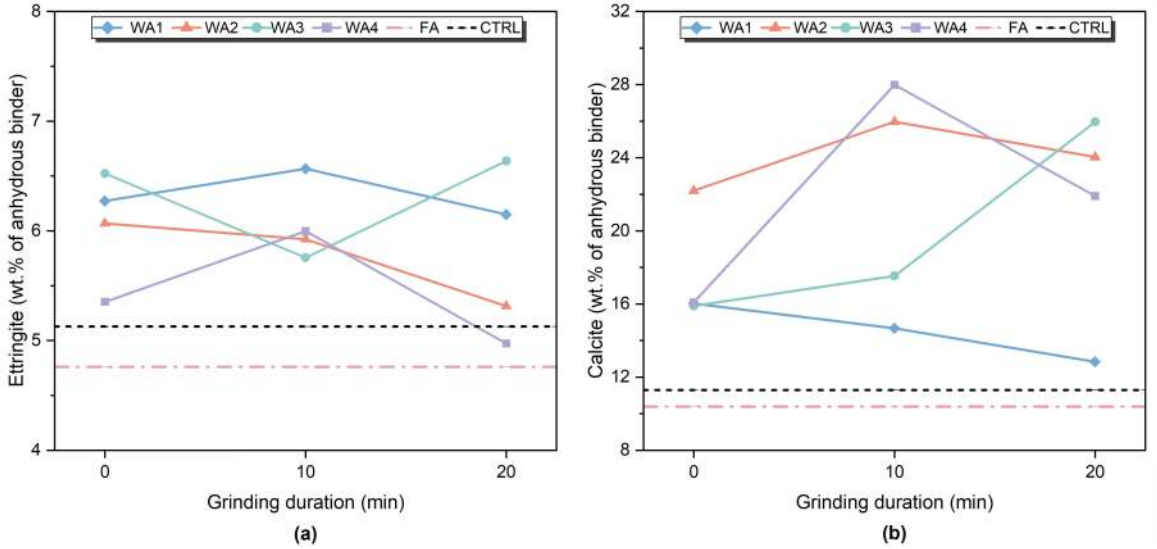

Figure 18. Quantification of **(a)** ettringite (estimated), and **(b)** calcite content of 28-day-old pastes based on TGA analysis. Data adapted from Paper II (Teker Ercan et al., 2025a).

The unground WA2 paste already shows lower CH (10.83%), bound water (13.98%), and higher calcite (22.20%) than CTRL. After grinding, CH decreases only slightly (10.40% at 10 min; 10.28% at 20 min), whereas calcite increases to 25.97% at 10 min and remains high at 24.04% at 20 min. XRD displays persistent CH reflections along with stronger calcite peaks. The combination of minimal change in bound water, pronounced calcite growth, and low R3 heat indicates that the observed CH loss results from carbonation rather than pozzolanic or hydraulic reactions (Taylor, 1997).

WA4 exhibits mixed behaviour. Grinding decreases CH (9.90% in WA4-10m; 8.87% in WA4-20m) but bound water stays low (11.94–11.20%); ettringite remains (~5–6%), and calcite is high in WA4-10m (27.99%) before decreasing in WA4-20m (21.90%). XRD indicates weakened CH and prominent calcite in WA4-10m. R3 heat is low for WA4-10m (32.28 J/g SCM) despite its strong mortar performance, whereas WA4-20m shows much higher R3 (101.56 J/g SCM); along with its high CaO (29%) and very high CaO/SiO_2 (38.67), this supports a filler/nucleation and latent-hydraulic contribution (Sigvardsen et al., 2021a, 2021b).

Alite (C_3S) and belite (C_2S) are detected by XRD in all WA2- and WA4-containing pastes and, to a lesser extent, in some WA1 and WA3 pastes, indicating limited clinker hydration under these conditions (Scrivener et al., 2016; Taylor, 1997).

Resin-impregnated, polished sections imaged at 500× (Figure 20) show that all pastes contain some unreacted WA particles. Mixes WA1-20m-28, WA3-10m-28, and WA4-20m-28 exhibit denser, more uniform matrices with fewer visible voids, consistent with finer particle size and higher reactivity, which promotes improved hydration and better particle packing. In contrast, pastes with unground WA are more porous and heterogeneous, with discontinuous hydrates, indicating limited reactivity and slower microstructural development.

SEM-EDS box plots of Si/Ca and Al/Ca at 7 and 28 days (Figure 21 and 22) were used as indicators of C–S–H composition (Rossen & Scrivener, 2017). At 7 days, CTRL shows a narrow, low Si/Ca distribution with low Al/Ca, which is typical of early cement hydration. FA already presents broader Si/Ca and Al/Ca ranges, indicating the start of pozzolanic reactions and the incorporation of additional silica and alumina into the gel. Within the wood-ash series, WA1-10m and WA3-10m display locally elevated Si/Ca and Al/Ca; this suggests partial transformation toward C–A–S–H or AFt-like compositions in some areas (Rossen & Scrivener, 2017; Scrivener et al., 2016). WA2 exhibits only a slight shift with grinding, while WA4 remains similar to CTRL, indicating limited chemical changes in the gel. By 28 days, the trends become more pronounced. FA shows the widest spread and highest medians in both ratios, indicating a sustained pozzolanic reaction and ongoing gel development (Scrivener et al., 2016). WA3-20m and WA1-20m shift upward, especially in Si/Ca, suggesting that grinding gradually activates their pozzolanic potential. WA2 remains relatively unchanged; along with the increased calcite observed elsewhere, this supports a carbonation-dominated response rather than significant gel evolution. WA4 stays close to CTRL with low variability, consistent with mainly filler or nucleation effects and only limited hydraulic contribution.

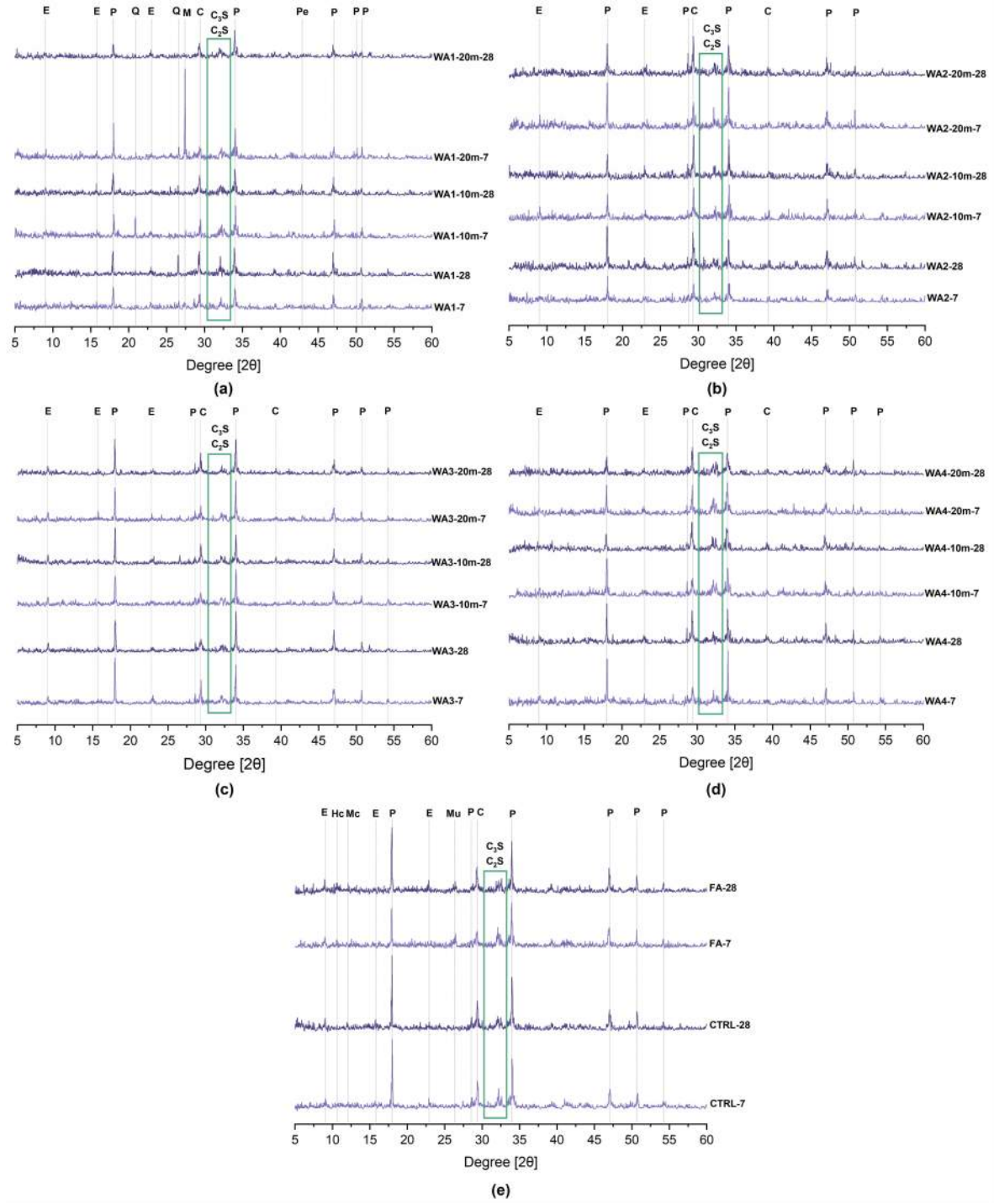

Figure 19. XRD patterns of 7- and 28-day-old pastes containing: **(a)** WA1, WA1-10m, WA1-20m; **(b)** WA2, WA2-10m, WA2-20m; **(c)** WA3, WA3-10m, WA3-20m; **(d)** WA4, WA4-10m, WA4-20m; and **(e)** CTRL and FA-containing pastes. (P: Portlandite, C: Calcite, Q: Quartz, E: Ettringite, Pe: Periclase, M: Microcline, Mu: Mullite, C_3S: Alite, C_2S: Belite, Hc: Hemicarbonate, Mc: Monocarbonate). Data adapted from Paper II (Teker Ercan et al., 2025a).

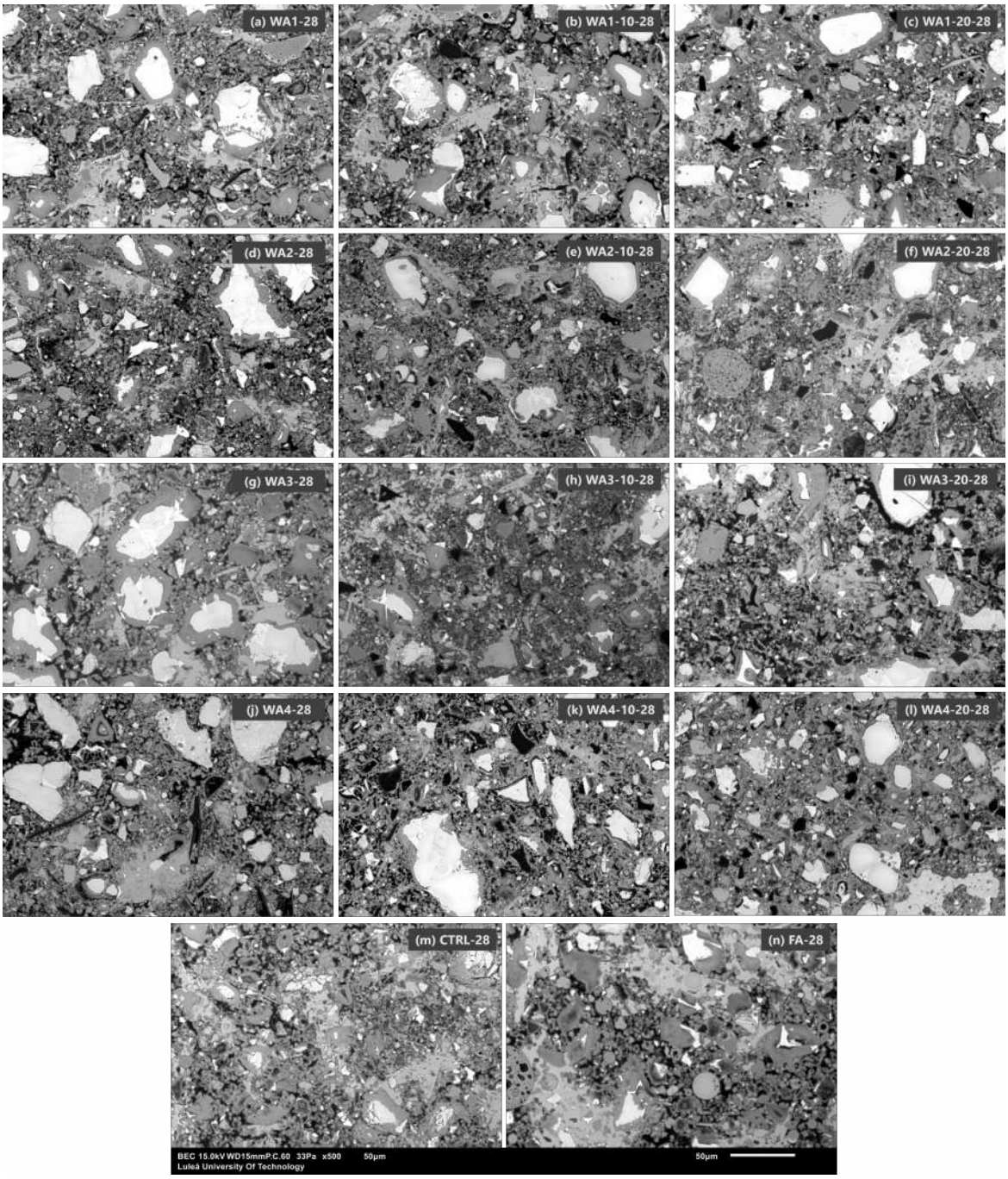

Figure 20. SEM images of 28-day-old paste samples containing 100 wt% cement, 20 wt% fly ash, and unground and ground wood ash at 500× magnification. Data adapted from Paper II (Teker Ercan et al., 2025a).

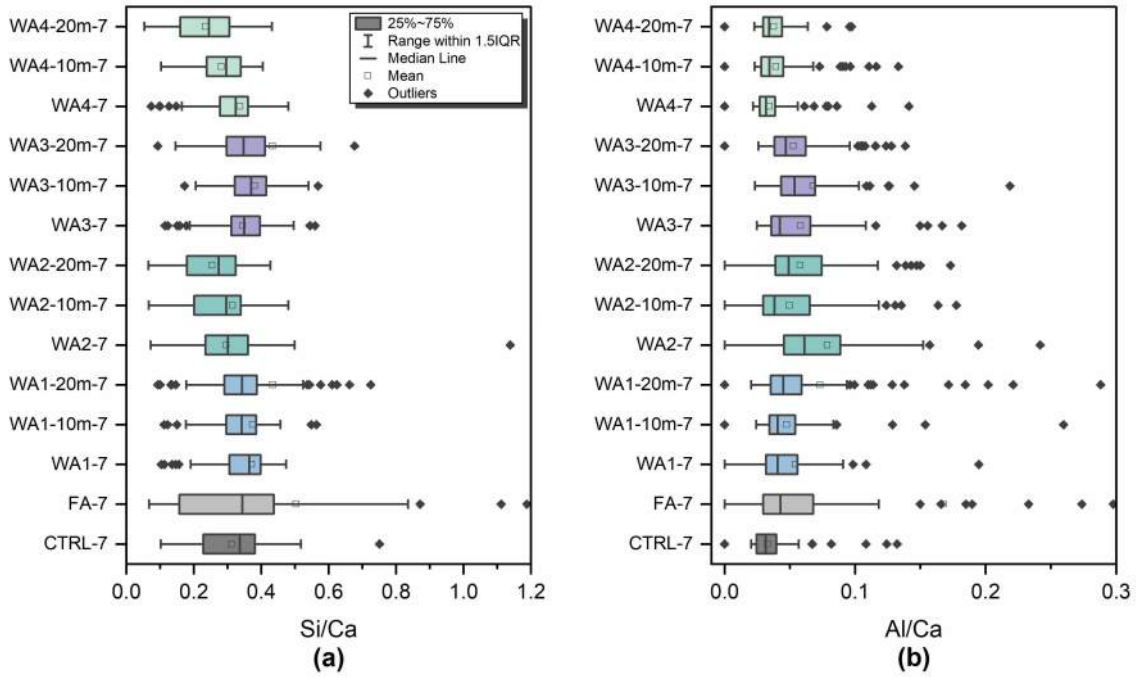

Figure 21. Distribution of Si/Ca and Al/Ca atomic ratios obtained from EDS point analyses at 7 days. Data adapted from Paper II (Teker Ercan et al., 2025a).

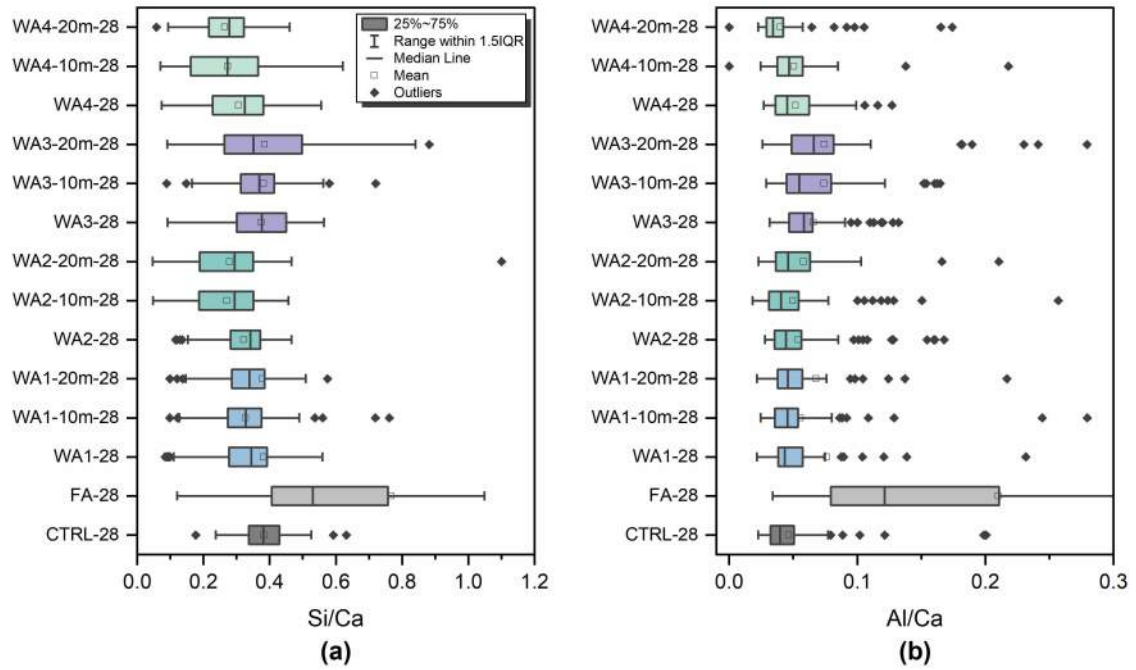

Figure 22. Distribution of Si/Ca and Al/Ca atomic ratios obtained from EDS point analyses at 28 days. Data adapted from Paper II (Teker Ercan et al., 2025a).

4.3. Wood Ash in Concrete

4.3.1. Fresh Properties

Measured slump values are given in Figure 23. In general, the incorporation of WA reduced the workability compared to CTRL. Mixes containing unground WA4 had the lowest workability. This was attributed to the coarser and more porous particle morphology, which likely impaired packing efficiency and increased water demand. Additionally, the high LOI of WA4 contributed to further workability loss, consistent with previous findings (Berra et al., 2015).

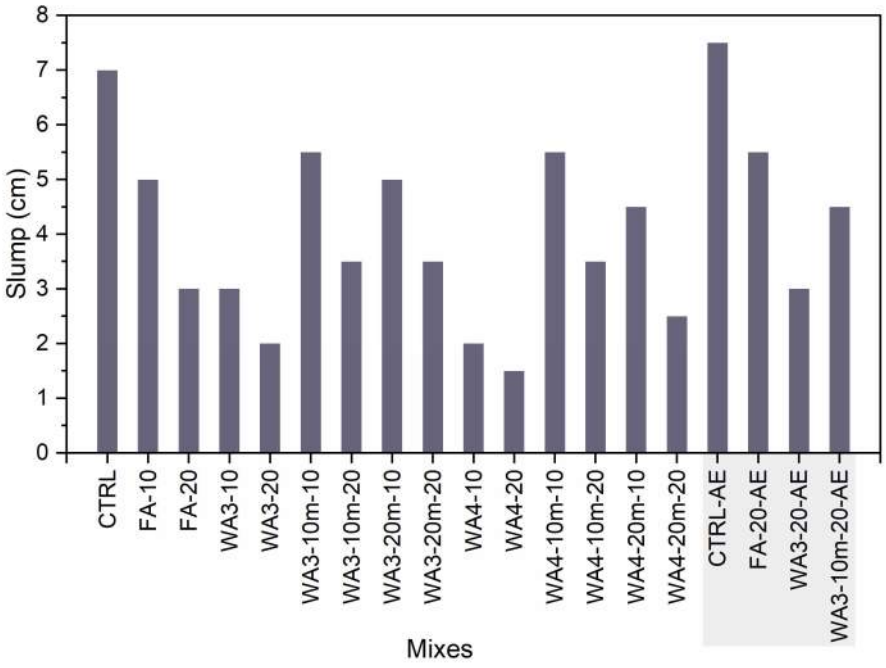

Figure 23. Measured slump values of all concrete mixes. Data adapted from Paper III (Teker Ercan et al., 2025b).

Grinding of WA significantly enhanced the workability across all mixes. The most notable improvement occurred after 10 min of grinding. This benefit is attributed to better particle shape and packing density, which decrease inter-particle voids and enable more efficient water dispersion within the mix. However, grinding for more than 10 min offered minimal additional benefits, particularly for WA4, likely due to increased surface area leading to higher water absorption.

The type of WA also played a significant role. WA3, which had a lower LOI, and finer initial particle size compared to WA4, responded more positively to grinding in terms of workability. These trends align with previous findings by Gabrijel et al. (2021) and Kara De Maeijer et al. (2020) who observed that finer and less porous ashes improve flow properties due to better particle packing. Similarly, Rissanen et al. (2018) emphasized that grinding reduces inter-particle voids and enhances water distribution, thereby increasing the slump.

The use of an air-entraining admixture (AEA) further enhanced workability in all selected mixes. The presence of microbubbles is known to decrease internal friction within the fresh paste, allowing for better flow. This effect was especially clear in fly ash and ground wood ash mixtures. These findings align with Rissanen et al. (2020), who also observed improved slump with AEA addition in mixes containing SCMs.

Air content of non-air-entrained and air-entrained mixes given in Figure 24. All air-entrained concrete showed a significant increase compared to non-air-entrained samples as expected. Unground wood ash resulted in higher entrapped air even without AEA, due to its irregular and porous structure. However, the effectiveness of AEA addition was limited in mixes with high LOI, such as those containing unground WA3, indicating that unburned carbon can inhibit the formation of stable air voids (Rissanen et al., 2020; Wang et al., 2008). On the other hand, ground WA3 responded more effectively to AEA, forming a more uniform and well-distributed air-void system.

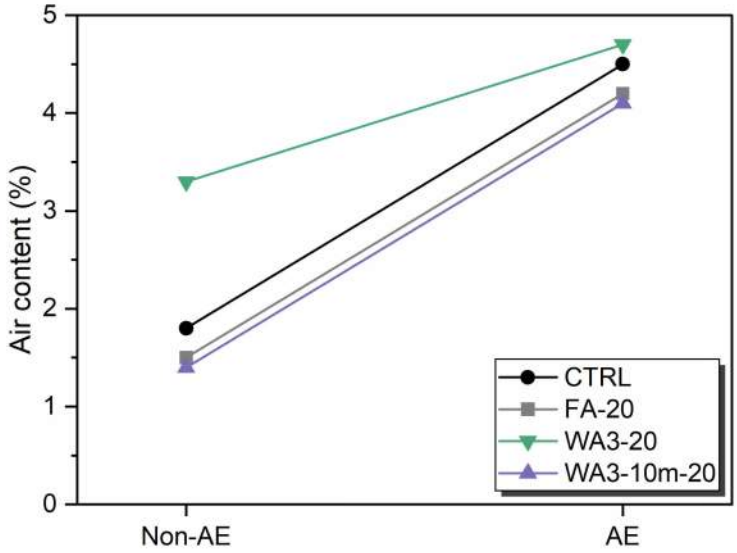

Figure 24. Air content of non-air-entrained (non-AE) and air-entrained (AE) concrete mixes. Data adapted from Paper III (Teker Ercan et al., 2025b).

4.3.2. Compressive Strength

Compressive strength results at 7 and 28 days are shown in Figure 25. Grinding of WA significantly improved strength at both ages, with the highest gains at the 10 wt% replacement level. Compared to unground WA mixes at the same replacement level, strengths increased by approximately 9–19% at 7 days and 11–15% at 28 days, consistent with better particle packing, larger surface area, and higher nucleation density typically seen in finely ground SCMs (Kapeluszna et al., 2020; Pantić et al., 2023).

The highest strengths were observed for WA4-10m-10 and WA3-10m-10, with values of 44.96 ± 0.66 MPa and 41.27 ± 0.20 MPa at 7 days, and 51.00 ± 0.43 MPa and 48.78 ± 0.31 MPa at 28 days, respectively. Although 20 min grinding also enhanced compressive strength, it was consistently slightly lower than the 10 min grinding; for example, WA3-20m-10 and

WA4-20m-10 achieved 48.22 ± 0.25 MPa and 50.37 ± 0.55 MPa at 28 days, compared to 48.78 MPa and 51.00 MPa for the 10 min ground, indicating over-grinding effects such as increased water demand and potential agglomeration.

Increasing the replacement from 10 wt% to 20 wt% lowered strength in all systems due to clinker dilution and the limited binder contribution of the ashes. For WA3, the 28-day strength decreased from 48.78 ± 0.31 MPa (WA3-10m-10) to 41.05 ± 0.46 MPa (WA3-10m-20); for WA4, from 51.00 ± 0.43 MPa (WA4-10m-10) to 41.84 ± 1.03 MPa (WA4-10m-20). A similar decline was seen with fly ash, where FA-10 reached 41.62 ± 0.23 MPa and FA-20 dropped to 37.01 ± 0.41 MPa. These trends align with the different chemical compositions: WA3, higher in pozzolanic oxides (31.77%), mainly contributes through pozzolanic reactions, whereas WA4, with high CaO (29%) and low pozzolanic oxide content, acts primarily as a latent hydraulic material, providing additional hydrates and early strength but remaining sensitive to dilution at higher replacements (Suraneni et al., 2019).

Air-entrained concretes (CTRL-AE, FA-20-AE, WA3-20-AE, WA3-10m-20-AE) exhibited slightly lower strengths than their non-air-entrained versions, consistent with uniformly distributed air voids enhancing the frost resistance while reducing load-bearing capacity and possibly causing microcracking at the paste–aggregate interface (Kothari et al., 2020).

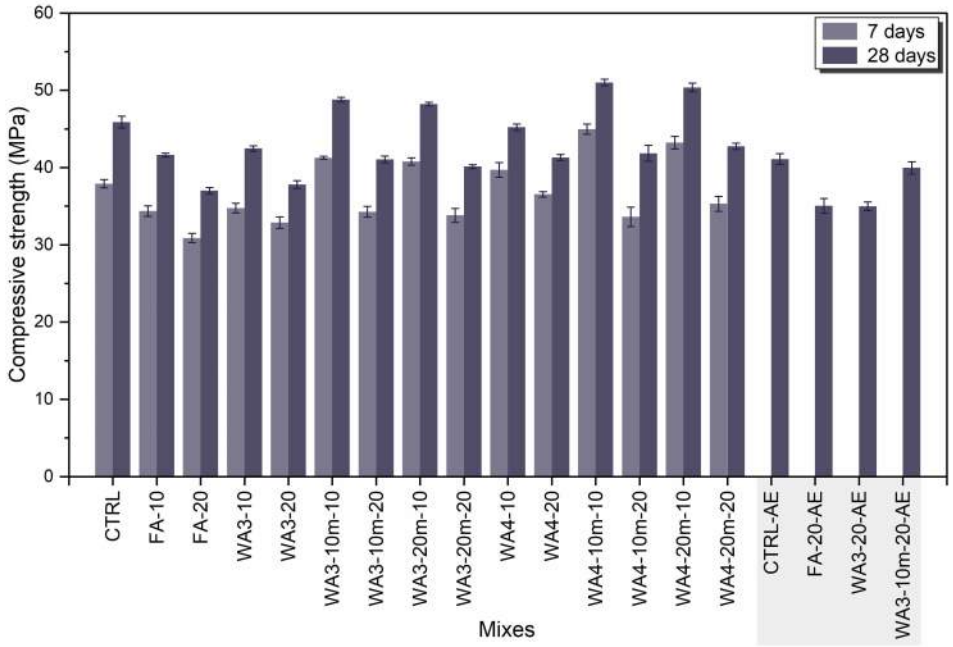

Figure 25. Compressive strength of concrete mixes using unground and ground wood ash (WA3, WA4) and fly ash (FA) at 7 and 28 days. Mixes include different replacement levels (10 wt% and 20 wt%) and grinding durations (10 and 20 minutes). Air-entrained (AE) mixes are included as well, with only 28-day compressive strength results provided for these samples. Data adapted from Paper III (Teker Ercan et al., 2025b).

4.3.3. Heat of Hydration

The heat of hydration was monitored by isothermal calorimetry for 168 h and normalized to cement mass (Figure 26). The first 30 minutes were excluded because initial wetting and mixing occurred outside the calorimeter. All mixtures showed the typical induction (dormant) period, followed by an acceleration peak mainly linked to C_3S hydration, and then a deceleration stage. In CTRL, the main peak occurred at 13.81 h; FA-10 and FA-20 peaked at 13.85 and 12.83 h, respectively. The lower heat output of FA-20 is attributed to dilution and the low early-age reactivity of fly ash (Lothenbach et al., 2011; Snellings et al., 2021).

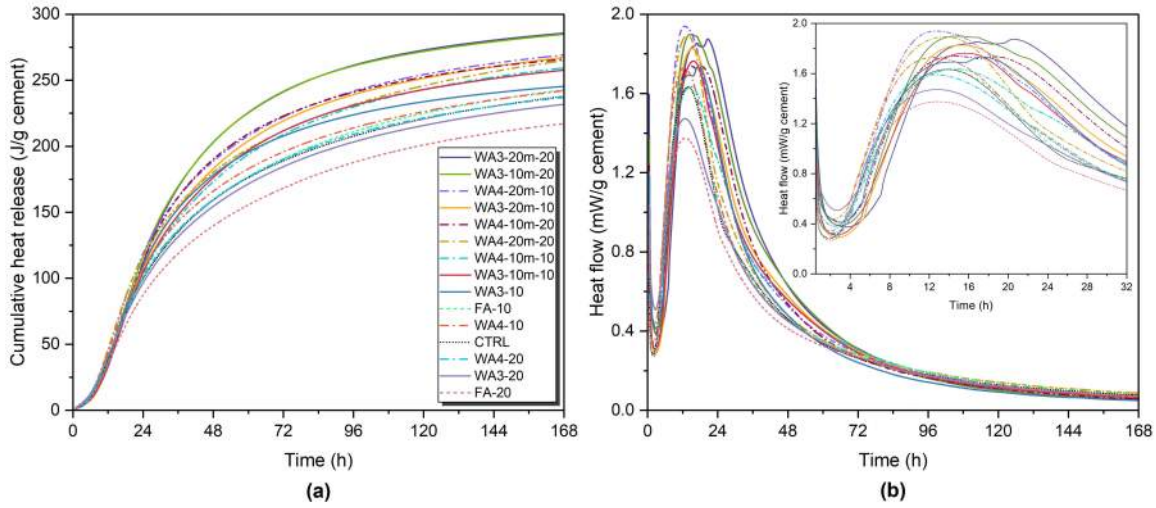

Figure 26. (a) Cumulative heat release and **(b)** heat flow curves of CTRL, FA-containing, unground and ground WA3-, and WA4-containing samples. All values are normalized per gram of cement. The legend is arranged in descending order based on the cumulative heat release in subfigure (a), and the same legend is used in subfigure (b). Data adapted from Paper III (Teker Ercan et al., 2025b).

For unground WA3-containing mixes, the peak time varied with replacement level: the peak occurred at 14.07 h in WA3-10 and 12.73 h in WA3-20. This behaviour is linked to the alkali content, which may enhance C_3S dissolution and promote early $Ca(OH)_2$ formation (Hewlett & Liska, 2019; Huang & Yan, 2019; Rajamma et al., 2009). However, the porous and irregular morphology of WA3 can absorb mixing water and restrict effective hydration (Castro et al., 2012; Yang et al., 2016). Therefore, although WA3-20 peaks earlier, its peak intensity is lower than that of WA3-10, likely due to increased clinker dilution and lower reactive cement content (Snellings et al., 2021). When WA3 was ground, the induction period lengthened: WA3-10m-10 and WA3-20m-20 peaked at 15.66 and 16.87 h, respectively. Increased fineness and SSA accelerate the early dissolution of alkalis and aluminates, temporarily disturbing pore-solution equilibrium and delaying the onset of C_3S hydration. In contrast, the greater number of nucleation sites increases peak intensity (Moraes et al., 2021; Šantek Bajto et al., 2021). In WA3-10 and WA3-20m-20, a clear shoulder after the main peak indicates delayed aluminate hydration (AFt to AFm transition) under sulfate depletion, influenced by WA3's alkali and alumina content (Skevi et al., 2022; Snellings et al., 2021).

Unground WA4-containing mixes exhibited shorter induction periods, with peaks at 12.42 and 12.55 h, respectively. This early response aligns with the high CaO content of WA4, which can rapidly supply Ca^{2+} to the pore solution and accelerate C_3S hydration (Carević et al., 2021; Teixeira et al., 2019). Grinding WA4 for 10 min delayed the peak (WA4-10m-10: 14.63 h; WA4-10m-20: 14.67 h), whereas 20 min of grinding shifted it earlier again (WA4-20m-10: 12.75 h; WA4-20m-20: 13.65 h). This trend suggests that short-duration grinding may partially activate surfaces while disrupting early processes. In contrast, longer grinding exposes encapsulated Ca-rich phases in the wood ash, increasing their accessibility and dissolution, which facilitates an earlier onset of hydration (Baričević et al., 2021; Šantek Bajto et al., 2021).

Regarding cumulative heat, pastes containing wood ash generally produced higher values than CTRL and the FA-containing mixes. In WA3-containing mixes, the increase was more pronounced with higher replacement and especially with grinding; the highest values were measured for WA3-20m-20 (283.6 J/g) and WA3-10m-20 (282.9 J/g). High SSA provides abundant nucleation sites and promotes early, dense C–S–H formation through filler and pozzolanic effects; however, the delayed central peak indicates that greater heat release does not necessarily imply faster kinetics, highlighting the dual role of particle fineness and surface chemistry (Berodier & Scrivener, 2014; Moraes et al., 2021; Šantek Bajto et al., 2021; Skevi et al., 2022; Snellings et al., 2021). Conversely, the compressive strengths of mixes with 20 wt% WA3 remained lower than those with 10 wt% consistent with dilution and the limited hydraulic contribution given the composition of WA3 (Lothenbach et al., 2011; Snellings et al., 2021). Grinding WA4 also consistently increased cumulative heat (WA4-20m-10: 268.2 J/g; WA4-10m-20: 264.3 J/g), exceeding that of unground WA4 (241.2 J/g), FA-containing mixes (FA-10: 242.1 J/g; FA-20: 216.5 J/g), and CTRL (237.2 J/g) corroborating that grinding enhances heat release and reactivity in Ca-rich ashes (Carević et al., 2021; Šantek Bajto et al., 2021; Skevi et al., 2022; Teixeira et al., 2019).

4.3.4. Microstructural Investigation

At 28 days, SEM images were captured at 500× magnification and given in Figure 27. Unreacted WA particles are still present in all WA mixes. Among them, WA4 shows a higher concentration of unreacted particles, and a more heterogeneous matrix compared to WA3. Grinding enhances particle dispersion and matrix density in WA3. A lower WA replacement of 10 wt% results in a denser matrix with fewer pores, while 20 wt% replacement increases porosity. CTRL is compact and well-hydrated, whereas fly ash (FA) mixes display partially reacted spherical particles, characteristic of FA.

Si/Ca and Al/Ca ratios can act as simple indicators of C–A–S–H chemistry (Rossen & Scrivener, 2017). The ratios at 7 days and 28 days are shown in Figures 28 and 29, respectively. In CTRL, Si/Ca increases over time while Al/Ca decreases, reflecting ongoing C–S–H formation and the retention of Al in other hydrates (Lothenbach et al., 2011). In FA-10, both ratios increase with age, which aligns with pozzolanic consumption of CH and the formation of additional C–A–S–H (Rossen et al., 2015). For FA-20, the initially higher Si/Ca

may stabilize or slightly decrease, and Al/Ca might drop slightly, indicating that dilution limits further Al uptake.

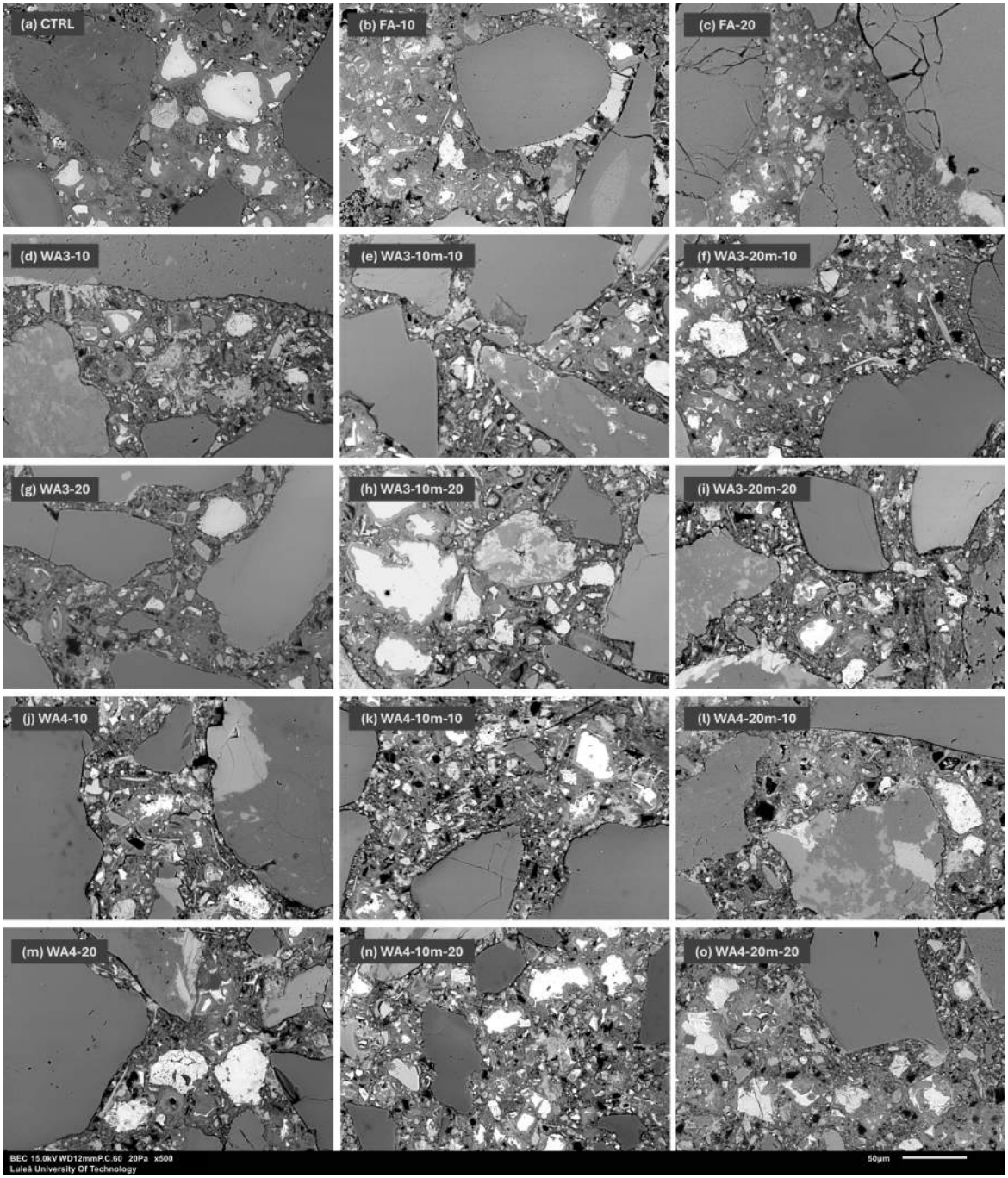

Figure 27. SEM images of 28-day-old concrete samples containing 100 wt% cement (CTRL), 10 and 20 wt% fly ash (FA), and 10 and 20 wt% unground and ground wood ash (WA3 and WA4) at 500× magnification. Data adapted from Paper III (Teker Ercan et al., 2025b).

Unground WA3 shows only minor changes in these ratios, while grinding WA3 generally increases Si/Ca and often Al/Ca, indicating that higher fineness promotes dissolution and nucleation. WA4, which is rich in calcite and low in Si and Al, mainly acts as a calcite-rich filler or hydraulic additive. After grinding, nucleation on calcite and formation of carbonate-

AFm phases may be enhanced, potentially reducing CH content and making the gel appear more Si-rich with higher Si/Ca ratios, while Al/Ca remains low due to limited Al input (Berodier & Scrivener, 2014; Lothenbach et al., 2011).

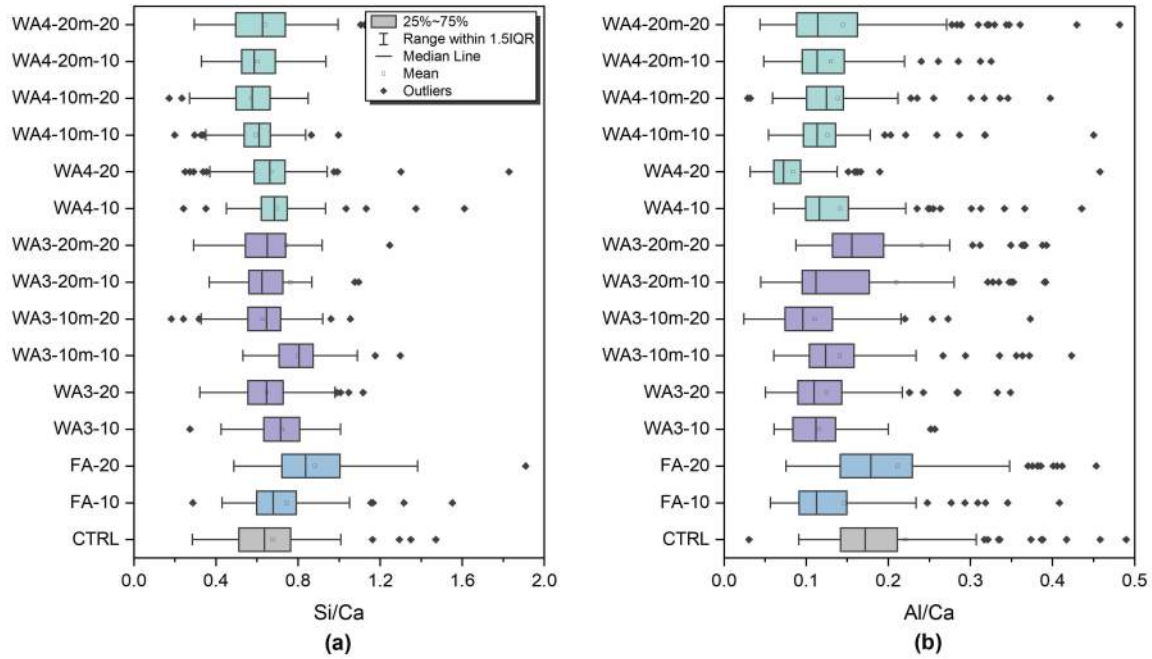

Figure 28. Distribution of Si/Ca and Al/Ca atomic ratios obtained from EDS point analyses at 7 days. Data adapted from Paper III (Teker Ercan et al., 2025b).

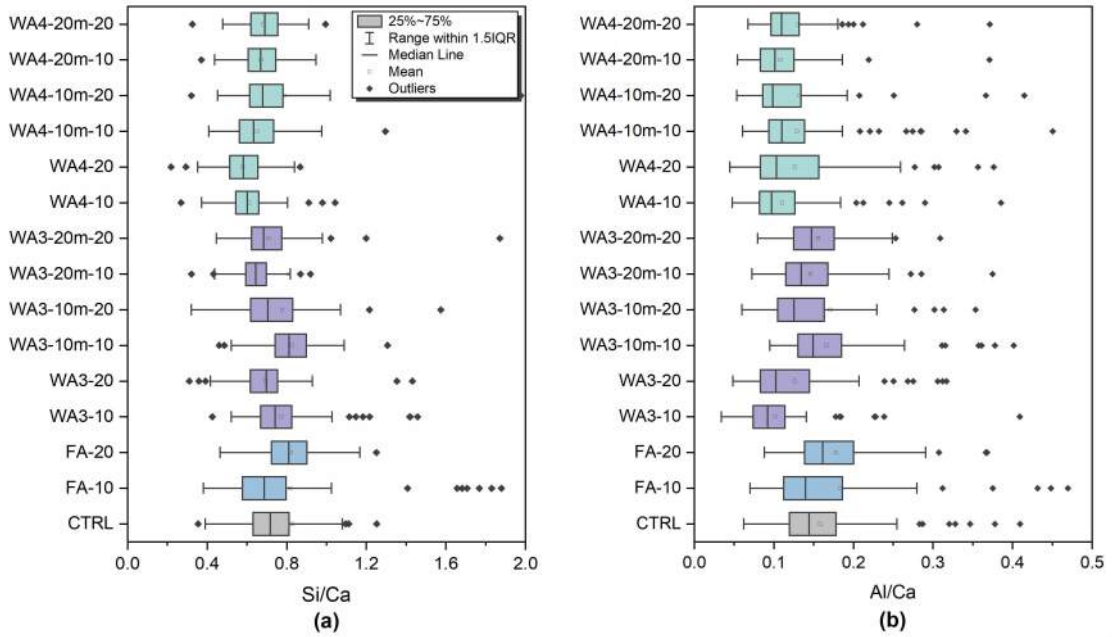

Figure 29. Distribution of Si/Ca and Al/Ca atomic ratios obtained from EDS point analyses at 28 days. Data adapted from Paper III (Teker Ercan et al., 2025b).

4.3.5. Freeze-Thaw Resistance

The freeze–thaw durability of selected mixtures was evaluated by measuring cumulative surface scaling after 7, 14, 28, 42, and 56 cycles (Figure 30). To examine the effect of air entrainment on wood ash-containing mixes, both non-air-entrained and air-entrained concretes modified with 0.1 wt% AEA were compared. As shown in Figure 24 in Section 4.3.1., the addition of AEA caused a significant increase in total air content across all mixtures.

CTRL demonstrated superior resistance with only 0.32 ± 0.12 kg/m^2 surface scaling after 56 cycles. However, replacing cement with FA and WA3 and WA3-10m without AEA significantly increased surface scaling. WA3-10m-20 showed the highest scaling (3.20 ± 0.12 kg/m^2), followed by WA3-20 (2.02 ± 0.18 kg/m^2) and FA-20 (1.18 ± 0.05 kg/m^2). While grinding typically improves matrix density and homogeneity, it also reduces entrapped air, limiting the system's ability to accommodate expansive pressures from freezing water. As noted by Chung et al. (2010), although highly fine SCMs can reduce freezable water by refining pores, they may trap moisture and intensify internal stresses during freeze–thaw cycles. A similar mechanism likely contributed to the poor performance of WA3-10m-20.

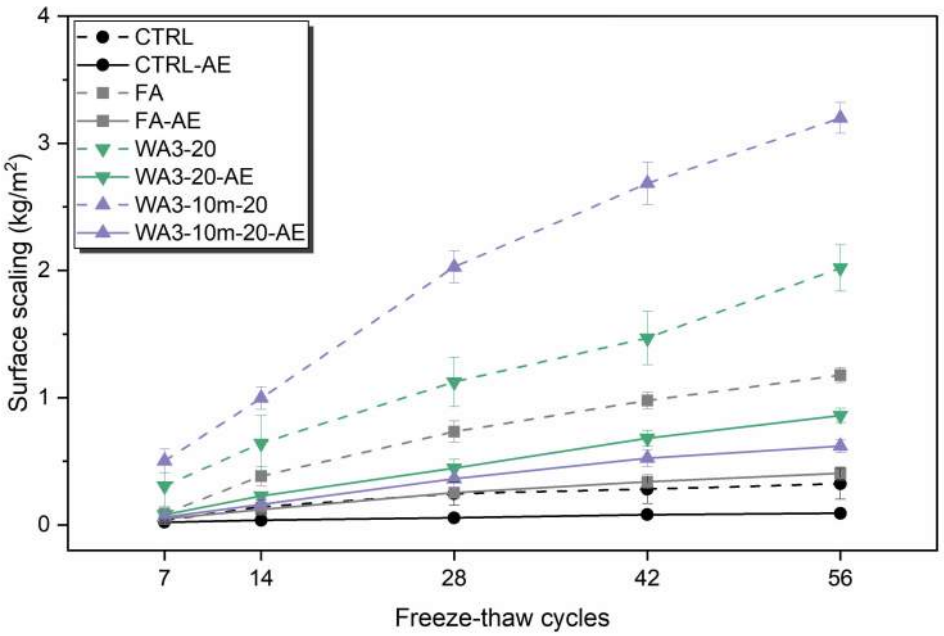

Figure 30. Surface scaling of concrete during freeze–thaw cycles. Data adapted from Paper III (Teker Ercan et al., 2025b).

WA3-20, despite its higher entrapped air, may not have developed an efficiently distributed air-void system, which could explain reduced its resistance to the F–T cycle. However, with the use of AEA, all mixes showed significant improvement. CTRL-AE and FA-20-AE recorded the lowest surface scaling (0.09 ± 0.01 and 0.41 ± 0.05 kg/m², respectively). Among the WA systems, WA3-10m-20-AE (0.62 ± 0.05 kg/m²) performed better than WA3-20-AE (0.86 ± 0.05 kg/m^2), indicating that a finer and more uniform air-void distribution compensated for its slightly lower total air content. This finding further

supports the positive effect of grinding on air-void system stability and compatibility with admixtures (Rissanen et al., 2020; Wang et al., 2008).

Table 9. Freeze-thaw resistance categories according to SS 137244:2019.

Freeze-thaw resistance	Requirements
Very good	$m_{56} < 0.10$ kg/m²
Good	$m_{56} < 0.20$ kg/m² **or** $m_{56} < 0.50$ kg/m² and $m_{56}/m_{28} < 2$
Acceptable	$m_{56} < 1.00$ kg/m² and $m_{56}/m_{28} < 2$
Not acceptable	If the requirements are not met.

m_{56}, m_{28}: scaled mass after 56 and 28 freeze-thaw cycles, respectively.

According to the classification criteria of SS 137244:2019, as summarized in Table 9, CTRL-AE was classified as *Very good*; CTRL and FA-20-AE as *Good*; WA3-10m-20-AE, and WA3-20-AE as *Acceptable*; while FA-20, WA3-20, and WA3-10m-20 were classified as *Not acceptable*. These classifications confirm that AEA is essential for all mixtures, especially those containing WA, to achieve acceptable F–T durability, with mechanochemical activation further improving performance when combined with AEA.

4.3.6. Leaching

To evaluate the environmental compatibility of wood ash (WA3 and WA4) as supplementary cementitious materials, both the total heavy metal contents (mg/kg) and the leaching at L/S = 10 (mg/kg) were assessed. The regulatory limits for total heavy metals were obtained from the Swedish Forest Agency (SFA) for forestry and agricultural use (Hjerpe, 2008) while the Swedish Environmental Protection Agency (Naturvårdsverket, 2010), provides separate limits for total and leached heavy metals under the "Very Low Risk" category for construction applications. EU landfill Waste Acceptance Criteria (Council of the European Union, 2003), applicable to leached heavy metals at L/S = 10, were also considered, with separate thresholds for inert, non-hazardous, and hazardous waste.

The total heavy metal concentrations in FA and unground and ground WAs, along with reported literature values for WA (Berra et al., 2015; Lanzerstorfer, 2017; Carević et al., 2020; Grau et al., 2015; Ottosen & Sigvardsen, 2024; Rajamma et al., 2009; Sigvardsen, 2020; Tosti et al., 2018; Zając et al., 2018) and the regulatory limits set by the SFA and EPA, are shown in Table 10.

WA3 exhibited the highest Cd and Cr levels, while WA4 and FA showed lower concentrations in comparison, though still surpassing EPA limits for several metals such as Cd, Cu, and Zn. A slight decrease in Cu, Pb, and Zn was seen after grinding, whereas Ni showed a moderate increase and Cr rose sharply, especially in WA3, likely due to contamination from stainless steel grinding media.

Table 10. Total heavy metal concentrations (mg/kg) in ground and unground wood ashes (WA3, WA4) and fly ash (FA), compared with literature values for wood ash and with regulatory limits for forestry and agricultural use (Swedish Forest Agency, SFA) and construction applications ("Very Low Risk" category, Swedish Environmental Protection Agency, EPA). Data adapted from Paper III (Teker Ercan et al., 2025b).

Samples and limit values	Total heavy metals concentration (mg/kg)					
	Cd	Cr	Cu	Ni	Pb	Zn
WA3	37	115	142	20.2	194	5260
WA3-10m	36.8	512	136	22.4	200	4850
WA3-20m	36.2	886	128	28	193	4820
WA4	5.55	<10	63.4	19.6	14.2	1390
WA4-10m	5.4	46.4	64.8	21.3	12.9	1370
WA4-20m	5.75	100	61.8	21.7	12.2	1420
FA	0.263	34.2	40.8	54.9	19.6	83.7
Literature values	1–60	13–160	27–920	0.03–176.3	0.01–5318	34–17,470
SFA limit	30	400	300	70	300	7000
EPA limit	0.2	40	40	35	20	120

While the concentrations of Cu, Pb, and Zn stay below the SFA limits, they significantly exceed the EPA limits. Cd exceeds both regulatory limits. Unground and ground WA4 and FA meet all SFA limits, but when compared to EPA limits, FA slightly exceeds the thresholds for Cd and Cu, and WA4 exceeds the limits for Cd, Cu, and Zn. For Ni, all samples are below both limits except for FA, which exceeds the EPA limit. A slight increase in Ni and a significant increase in Cr concentrations are observed with prolonged grinding for both wood ashes. WA4 and FA remain below both limits for Cr, but WA3 exceeds the EPA limit. Notably, Cr concentrations in WA3 and WA4 increase significantly with longer grinding, with ground WA3 even surpassing the SFA limit. This increase is likely due to contamination from the stainless steel grinding medium. Compared to literature values for WA (Berra et al., 2015; Lanzerstorfer, 2017; Carević et al., 2020; Grau et al., 2015; Ottosen & Sigvardsen, 2024; Rajamma et al., 2009; Sigvardsen, 2020; Tosti et al., 2018; Zając et al., 2018), most heavy metal levels are within reported ranges, but the elevated Cr levels after grinding exceed reported values.

The leached heavy metal concentrations, leachate pH, and electrical conductivity, together with the corresponding limits from the Swedish EPA and the EU Waste Acceptance Criteria at L/S = 10 for inert, non-hazardous, and hazardous waste categories are given in Table 11. All samples are below the EPA limit and classified as inert waste in terms of Cd, Cu, Pb, Ni, and Zn. WA4 was the only material that did not exceed the Cr limit and was classified as inert for Cr. Unground WA3 is classified as hazardous waste. However, after grinding, WA3 shifts from hazardous to non-hazardous, indicating that MCA can reduce environmental risks and improve classification (Chen et al., 2019). WA4 was categorized as

inert waste, and leaching was also reduced with MCA. FA also exceeds both EPA and inert waste limits.

Table 11. Leached heavy metal concentrations (mg/kg, L/S = 10) from ground and unground WAs, FA, and CEM I. "<" indicates values below the detection limit. Leachate pH and electrical conductivity are also presented. Results are compared with regulatory limits from the Swedish Environmental Protection Agency (EPA) and the EU Directive 1999/31/EC Waste Acceptance Criteria for inert, non-hazardous, and hazardous waste at L/S = 10. Data adapted from Paper III (Teker Ercan et al., 2025b).

Samples and limit values	Heavy metals concentration (mg/kg)						pH	EC (mS/cm)
	Cd	Cr	Cu	Ni	Pb	Zn		
WA3	<0.0008	13.6	0.049	<0.005	0.006	0.11	10.15	12.4
WA3-10m	<0.0005	5.2	0.021	<0.005	<0.002	0.032	10.54	11.01
WA3-20m	<0.0005	9.51	0.025	0.01	0.005	0.023	10.73	11.33
WA4	<0.0005	0.389	0.013	<0.005	0.011	0.501	12.19	10.41
WA4-10m	<0.0005	0.241	<0.01	<0.005	0.008	0.648	12.25	10.19
WA4-20m	<0.0005	0.277	0.016	<0.005	0.008	0.963	12.3	9.81
FA	<0.0008	1.11	0.016	<0.005	0.002	0.031	11.66	1.33
CEM I	<0.0005	4.89	0.027	<0.005	0.028	0.117	12.25	12.57
EPA limit	0.02	1	0.8	0.4	0.2	4		
Inert	0.04	0.5	2	0.4	0.5	4		
Non-hazardous	1	10	50	10	10	50		
Hazardous	5	70	100	40	50	200		

The relative leaching rate (RLR, %) was used to determine the proportion of each heavy metal released relative to its total content, serving as an indicator of leaching extent and the impact of MCA on heavy metal mobility (Yuan et al., 2021). RLRs are shown in Figure 31. For WA3, the Cr RLR dropped sharply from around 11.8% (unground) to about 1% after 10–20 minutes of grinding; for WA4, it decreased from approximately 3.9% to about 0.5% at 10 minutes and to approximately 0.3% at 20 minutes. These suggest that MCA reduces the amount of leachable material and may promote immobilization through encapsulation, changes in surface energy, or entrapment in new agglomerates (Montinaro et al., 2008; Nomura et al., 2010). In WA3, leaching of Pb and Cu significantly declined, while Zn decreased gradually; in WA4, Zn leaching increased, indicating differences in mineralogy and surface properties (Wang et al., 2020). Cd remained very low across all ashes, with a moderate decrease in WA3, and Ni increased slightly in WA3 after extended grinding, possibly due to increased surface exposure or the release of previously bound species (Grabias-Blicharz & Franus, 2023).

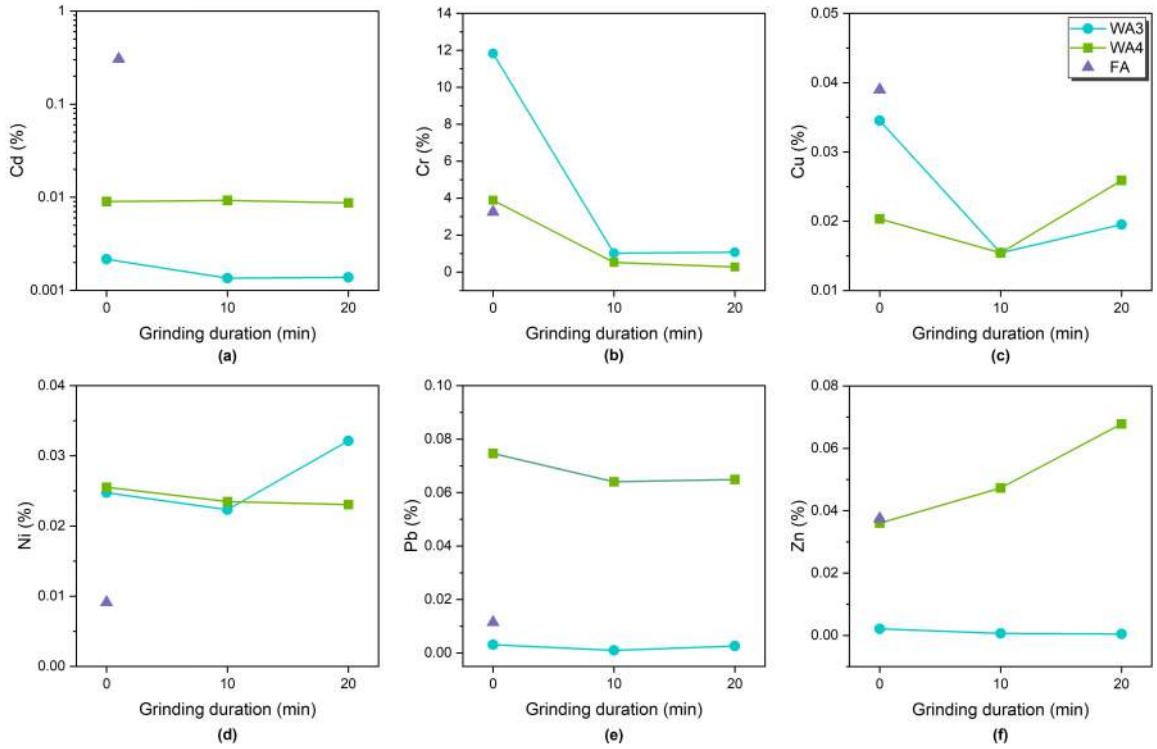

Figure 31. Relative leaching (RLR, %) of **(a)** Cd, **(b)** Cr, **(c)** Cu, **(d)** Pb, **(e)** Ni, and **(f)** Zn from wood ash (WA3, WA4) and fly ash (FA) as a function of grinding duration (0, 10, and 20 min).

The cumulative leaching of heavy metals from monolithic concrete samples is shown in Table 12, while Figure 32 illustrates their release at 9 and 64 days. Cd concentrations were consistently near the detection limit, with lower release in the ash-containing concretes compared to CTRL. In CTRL, most Cd leaching occurred within the first 9 days, aligning with early surface-governed processes (Carević et al., 2020). For the other mixes, the distribution between early and later stages appeared more balanced, although this partly reflects values close to detection thresholds. Ni and Zn behaved similarly, with leaching primarily during the initial stage and little variation among mixtures.

Cr leaching decreased in all ash-containing mixes compared to CTRL. Most of the release occurred within the first 9 days, after which leaching slowed significantly, indicating a two-step process involving initial surface wash-off followed by slower diffusion (Berra et al., 2015; Carević et al., 2020). The WA3-10m-20 released slightly more Cr than WA3-20.

Cu release was lowest in WA3-10m-20. Compared to CTRL, a lower proportion of Cu was leached within the first 9 days in the wood ash concretes, suggesting improved immobilization. This behaviour aligns with increased particle fineness, enhancing pozzolanic reactivity, which leads to matrix densification and stronger binding of Cu in hydration products.

Pb showed a contrasting trend. While FA-20 and WA3-10m-20 demonstrated reduced leaching, WA3-20 released slightly more Pb than CTRL. In WA3-10m-20, most Pb was released during the first 9 days, whereas in CTRL, the release was more gradual. This

behaviour supports a two-phase mechanism where early dissolution of more mobile Pb species is followed by diffusion-controlled release (Berra et al., 2019). The higher Pb release in WA3-20 may be linked to differences in ash chemistry or less effective immobilization early on. Over time, sorption onto hydration products and the maintenance of a high internal pH further reduces Pb mobility.

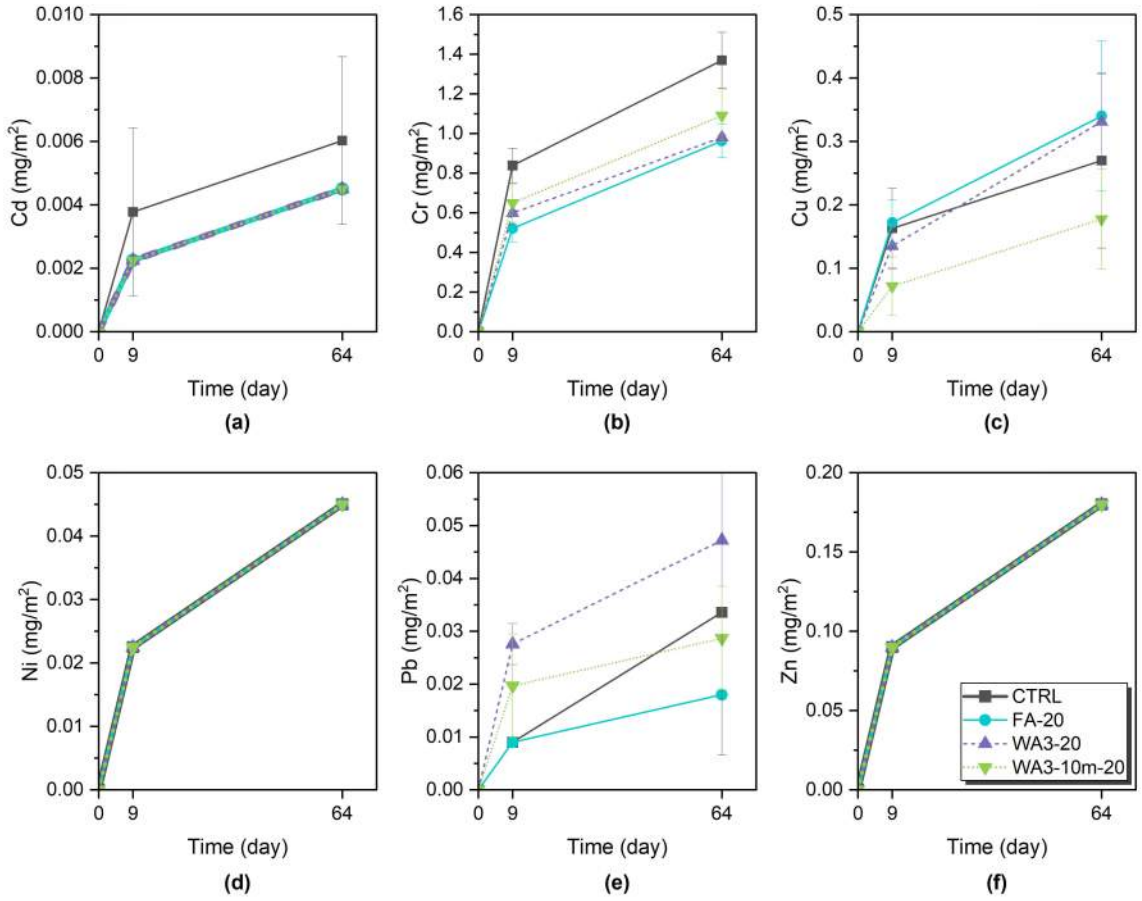

Figure 32. Cumulative leaching from monolithic samples at days 9 and 64 for **(a)** Cd, **(b)** Cr, **(c)** Cu, **(d)** Pb, **(e)** Ni, and **(f)** Zn.

All samples showed highly alkaline leachates, with pH values increasing over time (Table 13). Ash-containing mixes reached higher pH levels than CTRL, with WA3-20 showing the highest values. This aligns with earlier studies that report the dissolution of portlandite, and the release of alkali ions increase pore solution pH (Carević et al., 2020; Fava et al., 2018; Marion et al., 2005). The additional contribution of wood ash, rich in $Ca(OH)_2$ and alkalis, likely enhanced this buffering effect (Drljača et al., 2022). Since metal mobility generally decreases as pH increases, the higher alkalinity in the ash concretes contributed to reducing leaching at later stages (Udoeyo et al., 2006).

The cumulative leaching of all tested heavy metals remained far below the threshold values set by the Dutch Building Materials Decree, which is commonly used in environmental assessments in the literature (Berra et al., 2019; Carević et al., 2020; Tosti et al., 2018). These

findings confirm that using both fly ash and wood ash at a 20 wt% replacement level produces environmentally safe concrete with effective immobilization of heavy metals.

Table 12. Cumulative leaching concentrations of heavy metals from selected concrete samples after 64 days, based on DSLT, values are expressed as mean ± standard deviation. The table also includes the regulatory limit values are provided in accordance with the Dutch Building Materials Decree. Data adapted from Paper III (Teker Ercan et al., 2025b).

Heavy metal	Cumulative heavy metal concentration (mg/m^2)				
	CTRL	FA-20	WA3-20	WA3-10m-20	Limit Values
Cd	<0.006 ± 0.003	<0.004 ± 0	<0.004 ± 0	<0.005 ± 0	12
Cr	1.369 ± 0.140	0.963 ± 0.084	0.980 ± 0.013	1.090 ± 0.135	1500
Cu	0.270 ± 0.138	0.340 ± 0.118	0.331 ± 0.075	0.178 ± 0.078	540
Ni	<0.045 ± 0	<0.045 ± 0	<0.045 ± 0	<0.045 ± 0	525
Pb	0.034 ± 0.027	<0.018 ± 0	0.047 ± 0.013	<0.028 ± 0.010	1275
Zn	<0.180 ± 0	<0.180 ± 0	<0.180 ± 0	<0.180 ± 0	2100

Table 13. pH and electrical conductivity (EC, mS/cm) of the leachates at 9 and 64 days. The values are expressed as mean ± standard deviation. Data adapted from Paper III (Teker Ercan et al., 2025b).

Samples	pH		EC (mS/cm)	
	9 days	64 days	9 days	64 days
CTRL	11.74 ± 0.08	12.00 ± 0.23	1.64 ± 0.23	1.64 ± 0.07
FA-20	11.80 ± 0.08	12.12 ± 0.02	1.61 ± 0.39	1.36 ± 0.22
WA3-20	12.04 ± 0.05	12.40 ± 0.13	2.91 ± 0.10	2.37 ± 0.53
WA3-10m-20	11.96 ± 0.06	12.30 ± 0.10	2.49 ± 0.12	1.56 ± 0.45

4.4. Wood Ash in Alkali-Activated Mortars

4.4.1. Workability

Figure 33 presents the measured flow diameters for all mixes. SS-activated systems showed the highest flowability, followed by SC and SH (SS > SC > SH). CTRL mixes have the highest flow diameters, while increasing the WA content or extending its grinding time decreased flowability across all activator types. The only exception was the mix with 10 wt% WA ground for 10 minutes, which exhibited a similar flow to the unground WA mix for all activator types. The reduction in flow with higher WA content is often linked to its high LOI, which can absorb part of the mixing water or activator solution, and to the higher SSA, which raises water demand.

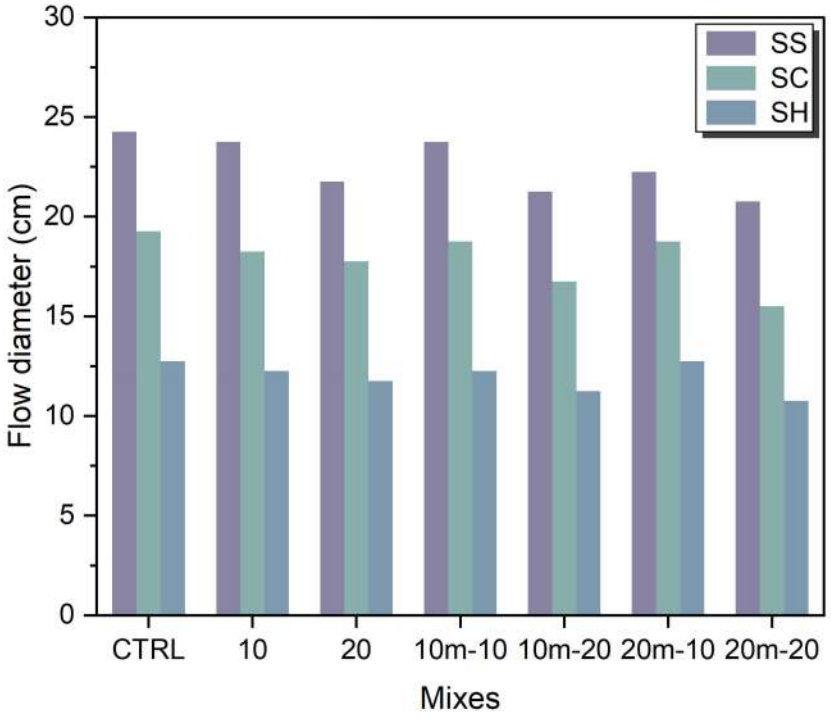

Figure 33. Flow diameters of the SS-, SC-, SH-activated fresh mortar mixes. Data adapted from Paper IV (Teker Ercan et al., 2023b).

The activator chemistry also played a significant role. SH activation is characterized by higher alkalinity and faster early reactions, which tend to reduce workability and lower flow (Provis et al., 2014). SC activation occurs at lower pH and shows an extended induction period during which transient carbonate phases, such as gaylussite can form. These early products can stiffen the paste and lead to intermediate flow values (Ke et al., 2016; Provis et al., 2014). In SS-activated mixes, the fresh behaviour is influenced by the silicate modulus and the viscosity and composition of the soluble-silicate solution (Ouyang et al., 2020; Provis et al., 2014).

4.4.2. Mechanical Properties

The compressive strength of the alkali-activated mortars is shown in Figure 34. SS-activated mixes achieved the highest values at both 7 and 28 days. Incorporating unground WA reduced compressive strength compared with all the CTRL mixes, mainly due to its high unburned carbon content and the presence of large, low-reactivity particles (Carević et al., 2019; Silva et al., 2022). For all activator types and grinding times, higher WA content decreased strength. MCA improved strength for all WA-containing mixes, consistent with the nucleation effect of finer particles and higher SSA, which accelerates C–A–S–H formation (Doudart de la Grée et al., 2016; Marjanović et al., 2014; Senneca et al., 2011).

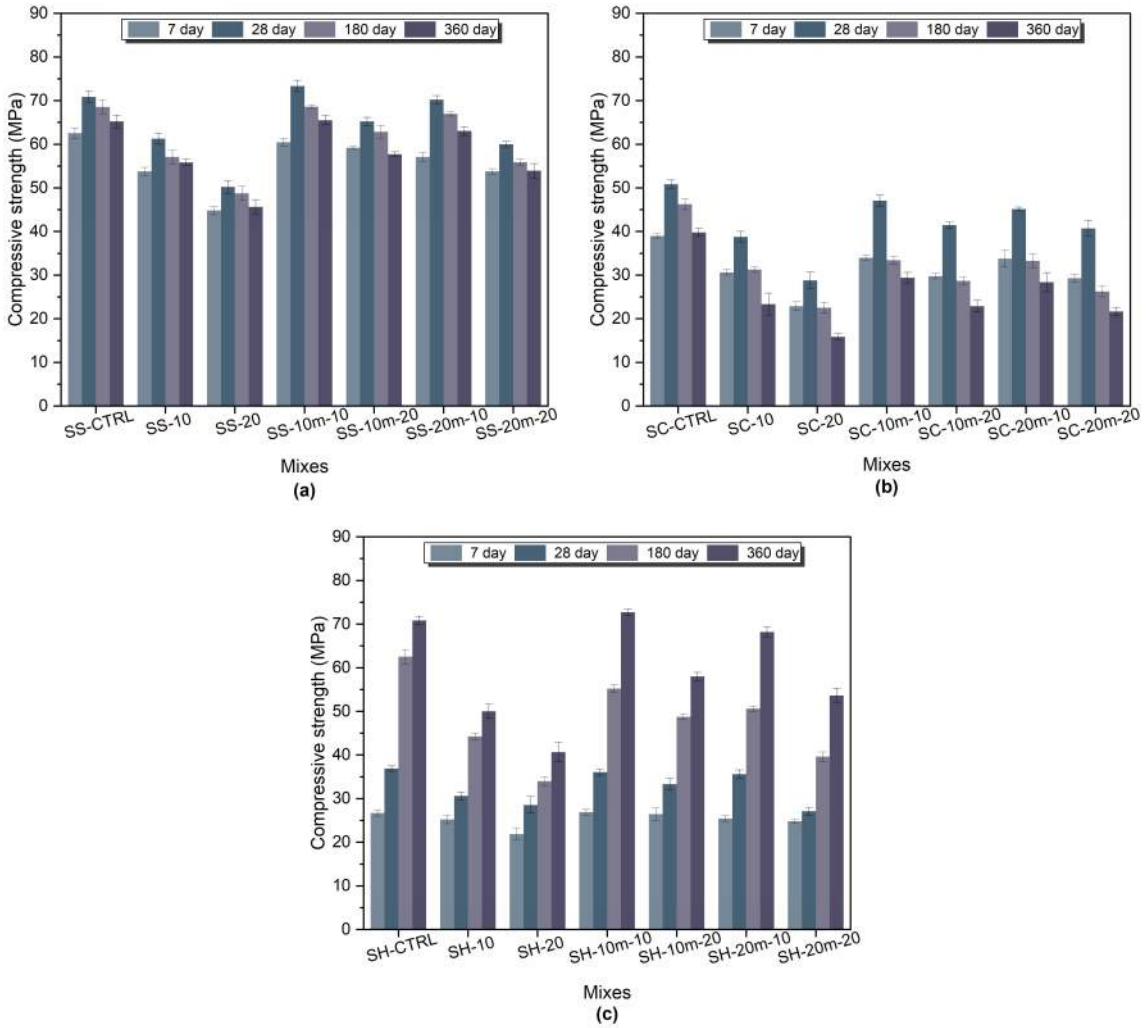

Figure 34. Compressive strength of **(a)** SS-, **(b)** SC-, **(c)** SH-activated mortars. Data adapted from Paper IV (Teker Ercan et al., 2023b).

At 10 wt% WA, 10 minutes of grinding increased 28-day strength by 19.72% for SS mixes, 21.39% for SC, and 17.82% for SH. Gains were smaller with 20 minutes of grinding. At 20 wt% WA, the benefits of grinding were more significant, with increases of 39.81% (SS), 43.97% (SC), and 32.52% (SH). For example, the SS-10m-10 mix reached 73.33 ± 1.3 MPa at 28 days, which is 3.5% higher than SS-CTRL. Compressive strength increases have

been linked to the alkaline content of wood ash, which promotes aluminosilicate dissolution (Samsudin et al., 2015). The higher early age performance of SS-activated mixes is consistent with the dissolved silica in the activator, supporting more polymerized C–A–S–H networks and denser microstructures (Fu et al., 2022; Provis et al., 2015). SC-activated mixes showed the most significant compressive strength gain from 7 to 28 days, because of the slower kinetics of SC activation, where early carbonate formation delays the development of C–A–S–H (Dai et al., 2023; Fu et al., 2022).

The long-term compressive strength showed three distinct patterns based on the activator used. SS-activated mixes showed reductions of 2.9–6.9% at 180 days, increasing to 7.9–11.5% by 360 days. For example, SS-CTRL decreased from 70.83 ± 1.30 MPa at 28 days to 68.54 ± 1.57 MPa at 180 days and 65.21 ± 1.44 MPa at 360 days, while SS-10m-10 dropped from 73.33 ± 1.30 MPa to 65.49 ± 1.00 MPa (−10.7% at 360 days). This pattern aligns with the generally higher carbonation susceptibility of SS-activated slag: under typical ambient exposure, it tends to carbonate more deeply and undergo greater C–A–S–H decalcification than NaOH-activated systems, which matches the observed long-term strength declines (Bernal et al., 2010; Lamaa et al., 2023; Nedeljković et al., 2018; Palacios & Puertas, 2006; Provis et al., 2015; Provis & Bernal, 2014).

SC-activated mixes experienced more significant long-term strength losses, typically 22–47% between 28 and 360 days, with an average decrease of 24.6% at 180 days. For example, SC-20m-20 dropped from 40.71 ± 1.80 MPa (28 days) to 26.25 ± 1.25 MPa (180 days) and 21.67 ± 0.95 MPa (360 days) (−46.8%). These losses are attributed to carbonation, which increases porosity and weakens the matrix at later ages. Similar patterns have been observed in studies on SC-activated slag under natural and accelerated carbonation conditions (Azar et al., 2024; Dai et al., 2023; Humad et al., 2021; Ke et al., 2016; Provis & van Deventer, 2014; Wang et al., 2022).

In contrast, SH-activated mixes gained strength throughout the testing period, increasing by 42–102% between 28 and 360 days, with an average of 46% at 180 days. For example, SH-10m-10 increased from 36.04 ± 0.72 MPa (28 d) to 55.21 ± 0.95 MPa (180 d) and 72.71 ± 0.72 MPa (360 d) (+101.7%). This ongoing development reflects sustained slag dissolution under highly alkaline conditions and gradual densification of Ca-rich C–A–S–H gels, with some of the alkali incorporated into the gel structure and some retained in the pore solution. Long-term strength increases and greater residual carbonation resistance have also been reported in independent studies of SH-activated slag (Cheah, Part, et al., 2017; Provis et al., 2015).

Mechanochemical activation of wood ash further improved later-age strength. At 10 wt% replacement, 10 minutes of grinding increased the 360-day strength by 13–17% in SS mixes, 22–26% in SC mixes, and 36–45% in SH mixes compared to unground WA. At 20 wt% replacement, gains were 18–26% (SS), 37–44% (SC), and 32–43% (SH). Notably, for SH-activated mixes at 20 wt% WA, 10 minutes of grinding yielded higher strength than 20 minutes at all ages, suggesting diminishing returns under highly alkaline conditions. These

improvements are mainly due to finer particle size providing additional nucleation sites and improved particle packing, with a secondary contribution from the slightly increased dissolution of the ground ash. The smaller particles at 20 minutes might result from excessive fineness, which increases activator demand, viscosity, and particle agglomeration, limiting dispersion and effective seeding (Marjanović et al., 2014; Senneca et al., 2011).

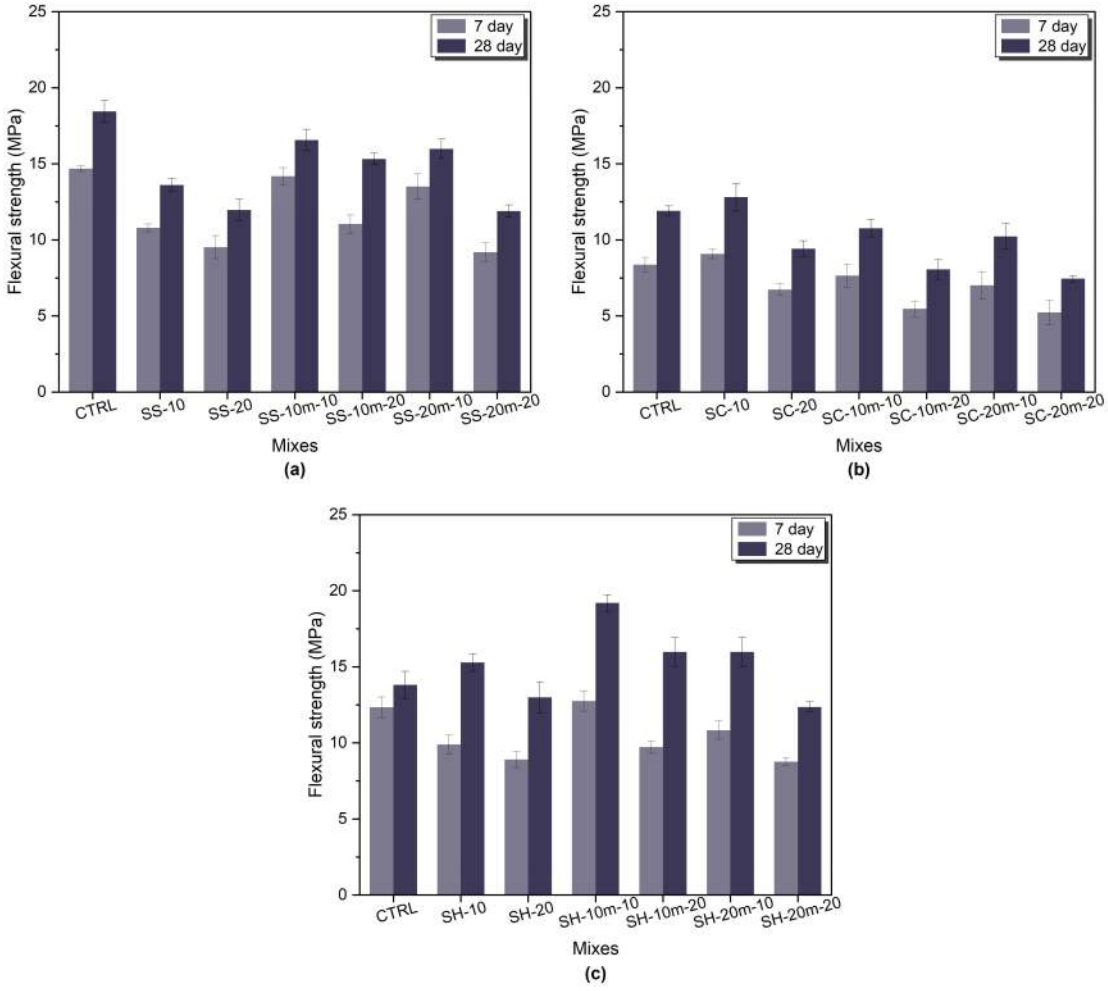

Figure 35. Flexural strength of **(a)** SS- **(b)** SC-, **(c)** SH-activated mortars. Data adapted from Paper IV (Teker Ercan et al., 2023b).

Figure 35 shows the results for flexural strength. The overall trend within each activator group was similar to that of compressive strength. However, the highest value was 19.19 ± 0.54 MPa for SH-10m-10 at 28 days. All SH mixes with 10 wt% WA exceeded the SH-CTRL at 28 days, while SC mixes showed the lowest values. Flexural strength is more sensitive than compressive strength to microcracking. This might explain why small improvements in defect distribution around ground WA particles led to comparatively higher flexural strength improvement, even when increases in compressive strength were moderate (Aydin & Baradan, 2014).

4.4.3. Heat of Hydration

To better understand the reaction kinetics and phase development in alkali-activated systems containing WA, isothermal calorimetry was conducted on selected mixes using SS, SC, and SH activators. Ground WA for 10 min was chosen for its superior mechanical performance across different activator types and replacement levels, with a 20 wt% replacement ratio selected to better capture the effect of WA. Heat release was monitored for over 168 hours, with cumulative heat release and heat flow curves shown in Figure 36.

The calorimetry results showed clear differences among the activator systems. In SS-activated pastes, the presence of ground WA (SS-10m-20) caused an earlier and more intense main peak compared with both the unground version and the control, indicating accelerated reaction kinetics. The shorter induction period and increased cumulative heat release (148.7 J/g) suggest that ground wood ash may promote nucleation, enhancing hydration. The appearance of a rare third peak also indicated possible activator gelation or early C–A–S–H formation, consistent with previous findings on hybrid binders (Bílek et al., 2023; Dai et al., 2020). The lower heat release of SS-20 compared to the SS-CTRL aligns with observations by Dai et al. (2020) for slag–fly ash blends, where lower depolymerization of the secondary precursor reduces early heat evolution.

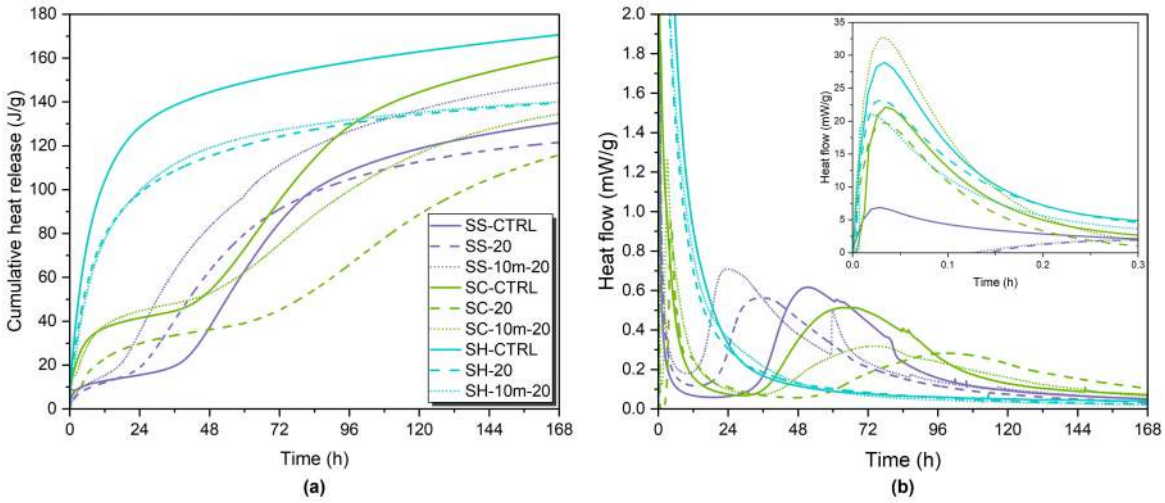

Figure 36. (a) Cumulative heat and **(b)** heat flow of SS-, SC-, SH-activated pastes. Data adapted from Paper IV (Teker Ercan et al., 2023b).

SC-activated pastes showed a longer induction stage and a later, less intense main peak, aligning with previous literature findings (Fu et al., 2022; Humad et al., 2019). While SC-10m-20 had the highest cumulative heat early on, SC-CTRL ultimately achieved the greatest total after 7 days (160.5 J/g). This delayed main peak might explain their low early-age strength and reduced 28-day flexural performance, likely due to a weaker early-age matrix.

SH-activated systems behaved differently, with no distinct second peak within the test period, likely due to limited formation of major reaction products at early ages. The high pH of NaOH solution can accelerate GGBFS dissolution and shorten the induction stage (Fu et

al., 2022; Provis & Bernal, 2014). Despite this, SH-CTRL released the highest cumulative heat overall (170.5 J/g). The absence of a secondary peak, combined with relatively high total heat release, suggests that SH activation promotes rapid initial dissolution but produces fewer stable hydrates in the early stage. This interpretation is consistent with the high alkalinity of SH activators (Gijbels et al., 2020; Provis & Bernal, 2014). Since heat release does not directly correlate with strength, these calorimetric patterns align with the observation that SH can achieve the highest flexural strength while remaining behind SS in compressive strength, likely due to differences in microstructure.

4.4.4. Microstructure and Phase Development

The XRD patterns of the 7-day-old alkali-activated pastes given in Figure 37 show crystalline phases formed during hydration, along with a broad amorphous hump typical of C–A–S–H. This aligns with reports for slag-based alkali-activated materials, where such humps are linked to poorly crystalline C–A–S–H (Kim & Kang, 2020; Provis et al., 2015) and aligns with the results of the EDS spot analyses.

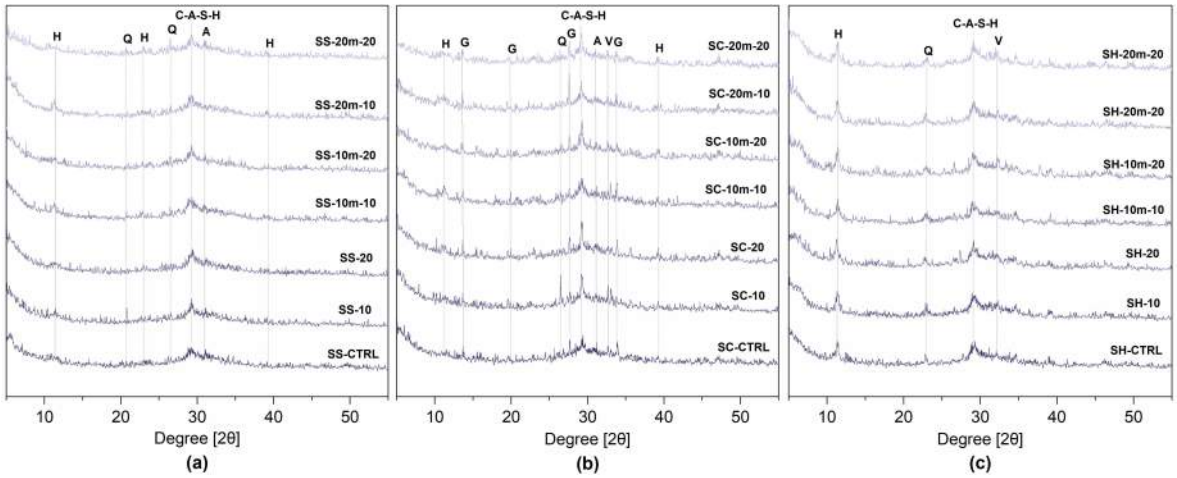

Figure 37. XRD patterns of 7-days old (**a**) SS-, (**b**) SC-, (**c**) SH-activated (H: Hydrotalcite, G: Gaylussite, V: Vaterite, Q: Quartz, M: Mullite, A: Akermanite). Data adapted from Paper IV (Teker Ercan et al., 2023b).

Hydrotalcite and quartz are found in all activator types; additional reflections include akermanite in SS, gaylussite, vaterite, mullite, and akermanite in SC, and vaterite in SH. The presence of hydrotalcite indicates Mg-bearing slag chemistry, and the early formation of gaylussite in SC-activated systems is commonly observed (Haha et al., 2011, 2012; Nguyen et al., 2022; Reddy et al., 2022).

The Ca/Si, Al/Si, Na/Si, and Ca/Al ratios of 28-day-old alkali-activated mortars are given in Figure 38 and 39. SEM-EDS analysis confirmed the gel identification: a mean Ca/Si ratio of about 0.6–1.5 with Al/Si around 0.15–0.35, characteristic of C–A–S–H (Tole et al., 2020). SS-activated samples generally have lower Ca/Si ratios compared to SC- and SH-activated samples, which aligns with increased dissolved silicate promoting Si incorporation into the gel and enhancing gel polymerization and alkali uptake capacity (Cao et al., 2020). SC pastes

exhibit higher Ca/Si ratios along with noticeable Na/Si ratios, corresponding to the delayed formation of Ca-rich C–A–S–H and the Na–Ca carbonate phases (e.g., gaylussite) identified by XRD. SH-activated samples show higher Na/Si ratios, consistent with a Na-rich pore solution.

Strength development is governed by C–A–S–H, consistent with Ca/Al > 2 (Cheah et al., 2017). For SS and SC pastes, Na/Si ratios (~0.3–0.7) align with alkali uptake in C–A–S–H rather than the formation of a distinct N-A-S-H network in these Ca-rich binders (Cheah et al., 2017). In SH-activated mortars, the higher Na/Si ratio (~1.15–3.79) may result from excess Na^+ remaining in the pore solution rather than the formation of sodium-polysialate, as noted by Cheah et al. (2017).

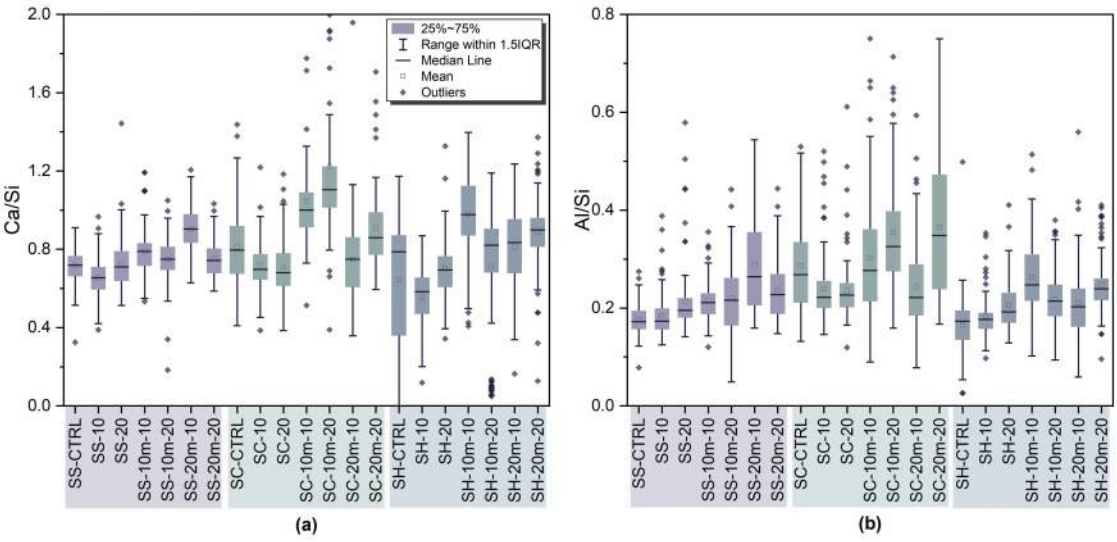

Figure 38. (a) Ca/Si and **(b)** Al/Si ratio of 28-day-old alkali-activated mortars.

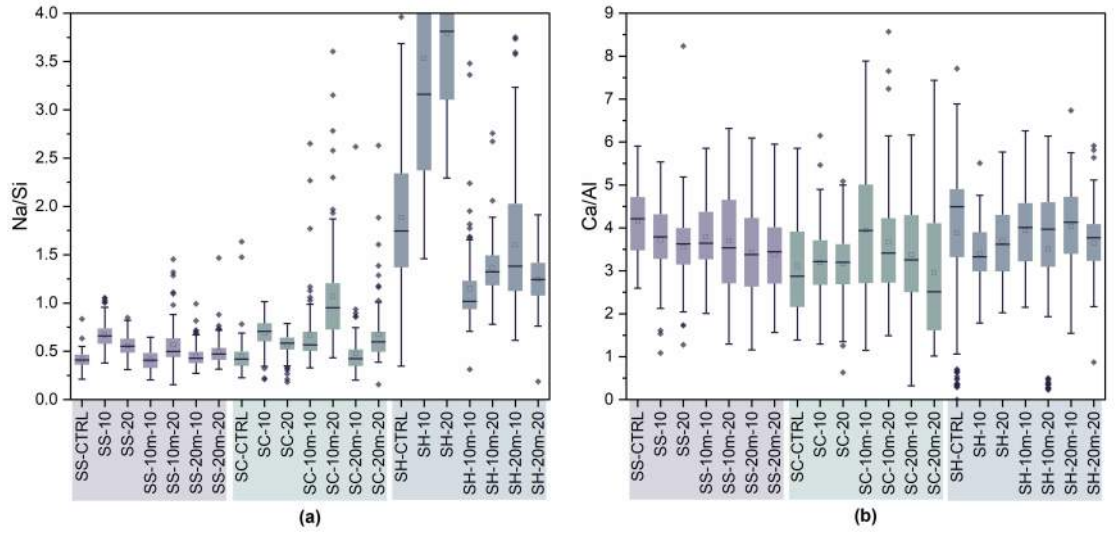

Figure 39. (a) Na/Si and **(b)** Ca/Al ratio of 28-day-old alkali-activated mortars.

SEM images of 28-day SS-, SC-, and SH-activated mortars are shown in Figures 40 and 41. CTRL samples and 10 wt% ground WA-containing samples exhibited a denser, more homogeneous microstructure, while higher WA increased unreacted particles and microcracks, likely due to drying shrinkage, potentially reducing strength (Candamano et al., 2017; Cheah et al., 2015)

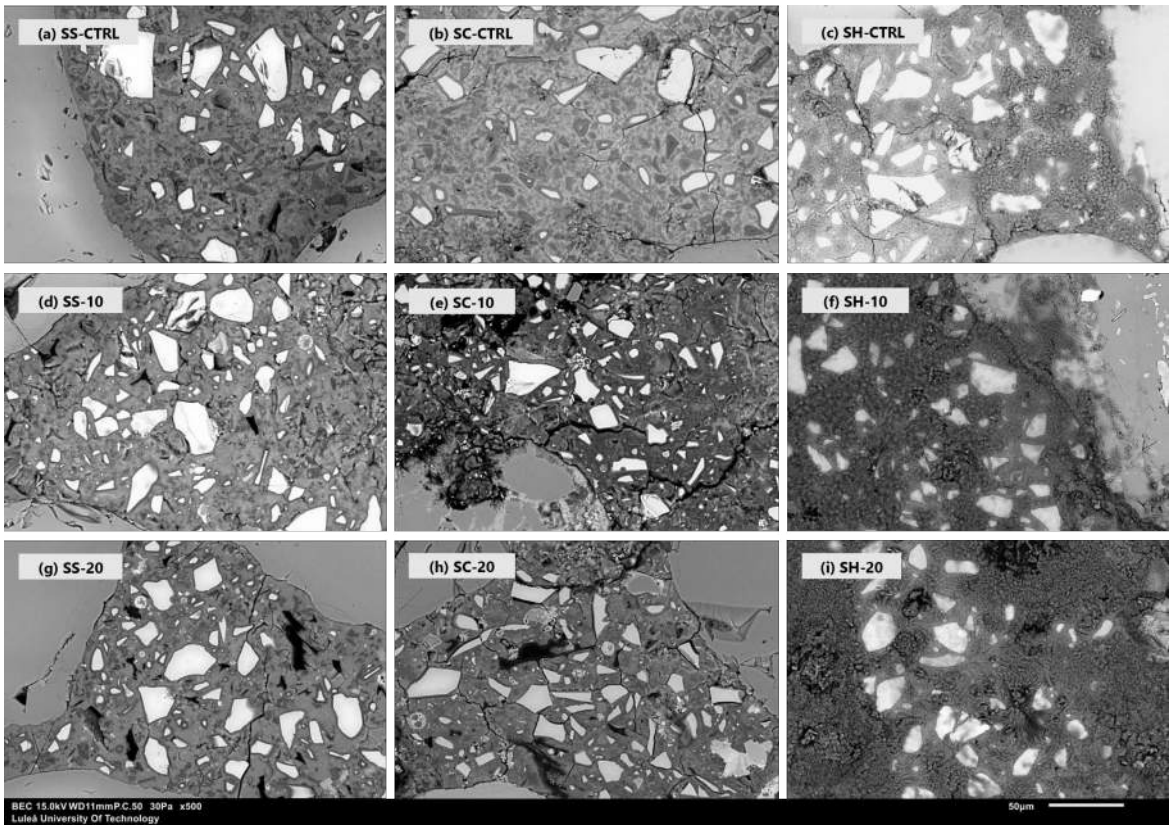

Figure 40. SEM images of 28-day-old SS-, SC-, and SH-activated mortars incorporating 100 wt% GGBFS or unground wood ash as a partial replacement (10 wt% and 20 wt%) for GGBFS at 500× magnification. Data adapted from Paper IV (Teker Ercan et al., 2023b).

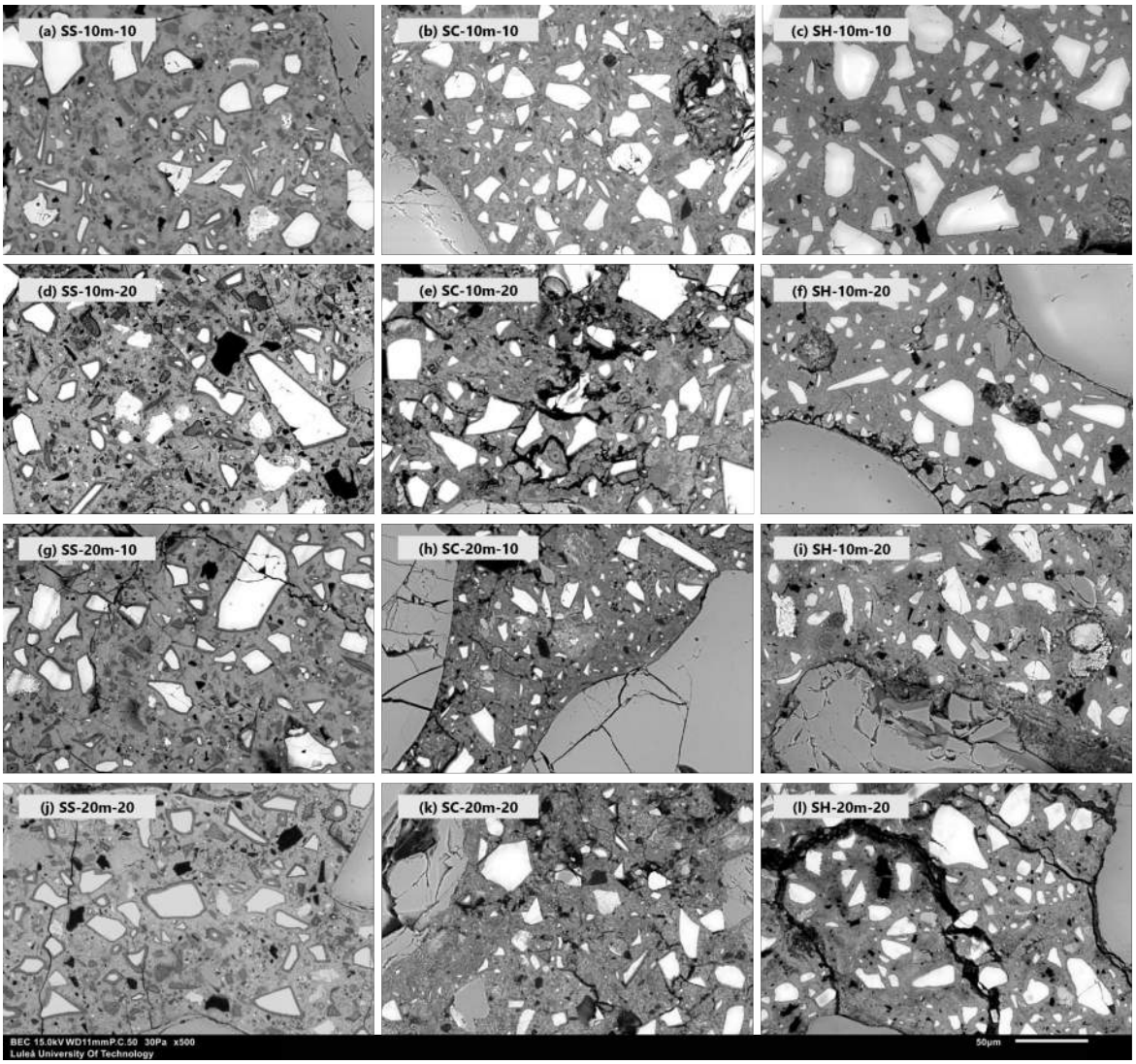

Figure 41. SEM images of 28-day-old SS-, SC-, and SH-activated mortars incorporating ground wood ash (10 and 20 minutes) as a partial replacement (10 wt% and 20 wt%) for GGBFS at 500× magnification. Data adapted from Paper IV (Teker Ercan et al., 2023b).

4.5. Multivariate Statistical Analysis

To identify dominant patterns among the tested samples and explore the relationships between physical, chemical, and pozzolanic properties, a multivariate statistical analysis was performed using Principal Component Analysis (PCA) and Hierarchical Cluster Analysis (HCA) (Jolliffe, 1986; Szczepanik et al., 2021; Ward, 1963).

PCA was used to reduce the dimensionality of the dataset and to extract the main sources of variation among samples (Jolliffe, 1986; Sigvardsen, 2020). By converting correlated variables into a smaller number of uncorrelated principal components, PCA helps visualize similarities and differences between samples based on their physical, chemical, and reactivity-related properties.

HCA was used to group the ash samples into clusters based on their overall similarity across all selected variables. The analysis was performed using Ward's linkage method with Euclidean distance as the dissimilarity metric (Simonsen et al., 2020; Ward, 1963). The resulting dendrogram illustrates that samples with similar profiles, considering both ash origin and grinding duration, cluster together, revealing underlying structure within the dataset.

The data used in this analysis were obtained from Study A and included fly ash (FA) and four types of wood ash (WA1–WA4), both in unground form and after 10 and 20 minutes of grinding. Each sample was characterized using a set of relevant parameters, including physical properties (median particle size, D50; specific surface area, SSA), chemical composition (pozzolanic oxides, PO; calcium oxide, CaO), and reactivity indicators (CH consumption, CH-cons; strength activity index, SAI; cumulative heat release, R3; and Frattini test CaO reduction, CaO-red). These variables were selected due to their strong relevance to pozzolanic performance and their responsiveness to MCA.

All statistical analyses were performed using OriginPro 2025 (v10.2.0.188). Before analysis, all variables were standardized (z-scores) to remove bias from differences in scale and units.

4.5.1. Principal Component Analysis (PCA)

The PCA results showed that the first two principal components (PC1 and PC2) explained 84.46% of the total variance (PC1 = 44.48%, PC2 = 39.98%), enabling a reliable two-dimensional representation of the multivariate data structure.

The PCA loading plot (Figure 42) showed a clear separation between variables predominantly associated with grinding variable, particle fineness and surface area (GD, D50, SSA) and those related to reactivity and composition (PO, R3, CaO-red, CH-cons, SAI). This distinction also reflects the dual role of MCA: while it directly influences physical parameters such as particle size and surface area and is associated with higher pozzolanic performance by enhancing dissolution rates, portlandite consumption, and cumulative heat release.

The GD was closely aligned with SSA, SAI, and CH-cons, suggesting that longer grinding time aligns with higher physical-reactivity indicators in the WAs. In contrast,

parameters like R3 and CaO-red were loaded along a different axis, reflecting a separate reactivity dimension associated with particle fineness and dissolution behaviour. PO was also located in this area of the loading plot, suggesting its importance to overall reactivity, but through a different mechanism. This orthogonal distribution of variables supports the idea that MCA affects both physical and reactivity properties, but not always in the same way.

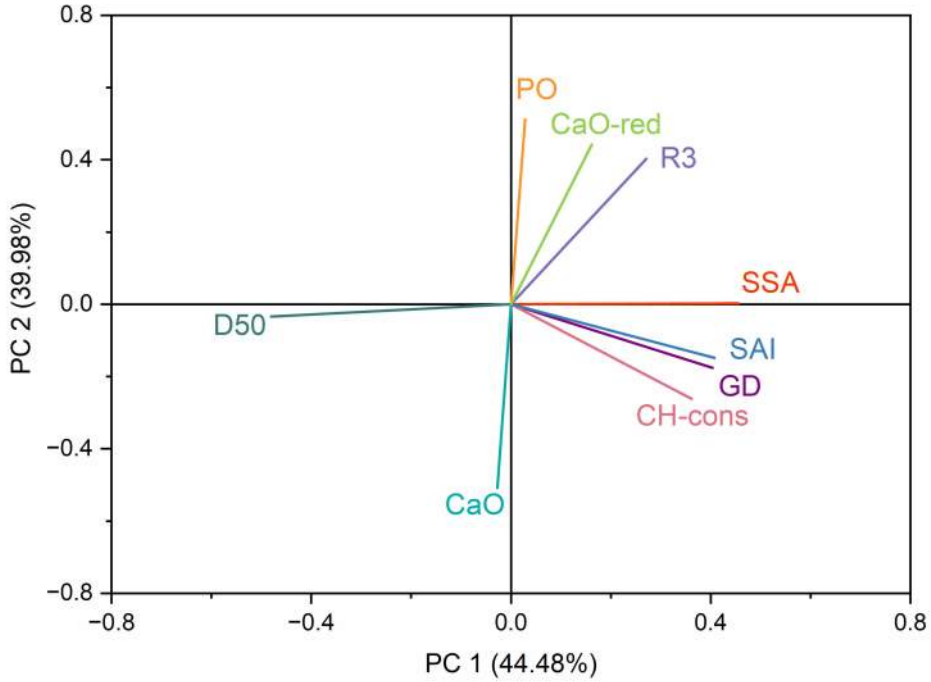

Figure 42. PCA Loading Plot illustrating the contributions of original variables to PC1 and PC2.

The PCA score plot (Figure 43) shows a clear trend among all wood ash samples in response to MCA. Initially, WA1 and WA3 are located in the upper-left area of the PCA space, indicating negative PC1 but positive PC2 scores. In contrast, WA2 and WA4 are found in the lower-left area, with both PC1 and PC2 scores being negative. This initial separation reflects differences in their chemical and physical properties, especially the higher CaO content and lower pozzolanic oxides in WA2 and WA4. After MCA, all WA samples shift toward the positive side along PC1, consistent with improvements in fineness and related reactivity response. This trend aligns with the observed increases in CH consumption and SAI and is consistent with the enhanced reactivity without changing the oxide composition. WA1 and WA3 shift to the upper-right area of the PCA plot, indicating increased pozzolanic activity. Meanwhile, WA2 and WA4 also move toward positive PC1 values in the lower part of the plot. As discussed earlier, this behaviour may be influenced by latent hydraulic properties rather than a pozzolanic reaction mechanism.

FA distinctly separates from all WA samples, occupying the far upper-right region with high positive scores on both principal components. This aligns with its high pozzolanic oxide content and reactivity. Notably, WA1-10m and WA3-10m are positioned close to FA,

suggesting that under optimized grinding conditions, WA1 and WA3 may approach the performance of FA.

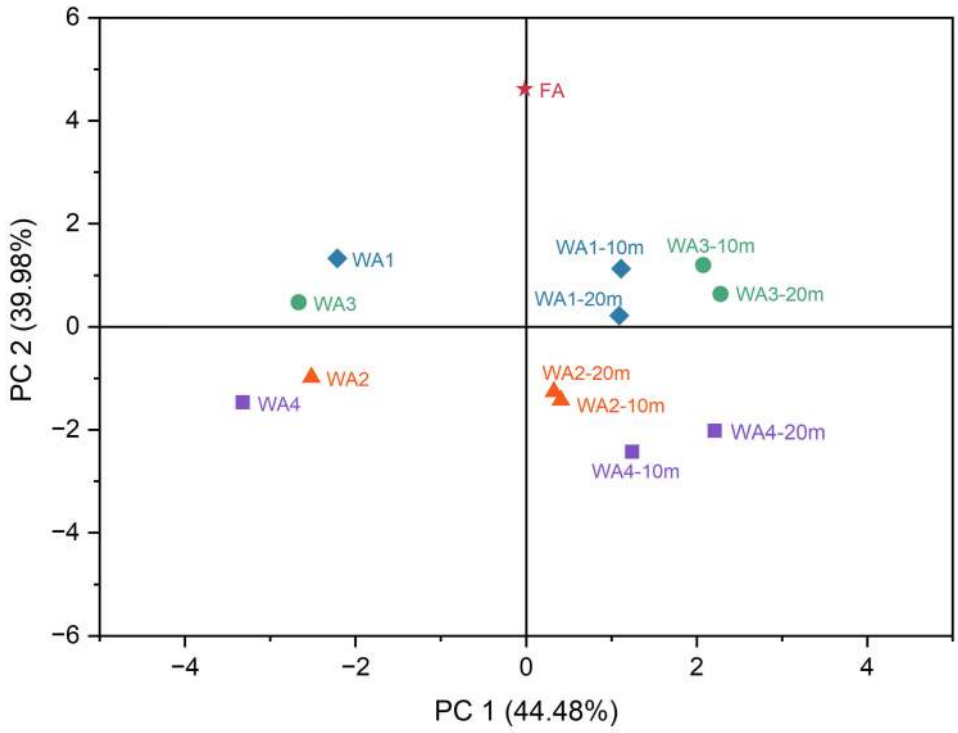

Figure 43. PCA Score Plot displaying the distribution of wood ash and fly ash samples along PC1 and PC2, showing the effect of grinding duration and ash type on sample clustering.

4.5.2. Hierarchical Cluster Analysis (HCA)

Hierarchical clustering was conducted to support the PCA results and provide deeper insight into the relationships among ash samples based on their comprehensive property profiles. The resulting dendrogram, presented in Figure 44, separates the FA at the largest distance, reflecting its distinct chemical and physical characteristics compared to the biomass-derived wood ashes.

The clustering pattern shows three main groups. The first group includes FA along with the ground samples of WA1 and WA3 (WA1-10m, WA1-20m, WA3-10m, WA3-20m), all of which demonstrate enhanced pozzolanic behaviour. Although WA1 and WA3 have relatively low inherent reactivity in their unground form, MCA is associated with improvements in their characteristics, shifting their position toward FA in the multivariate space. This indicates that fineness and particle morphology play a critical role in activating their latent reactivity.

The second cluster includes ground samples of WA2 and WA4 (WA2-10m, WA2-20m, WA4-10m, WA4-20m), which also show improved physical properties after grinding but still have lower pozzolanic reactivity. This indicates that compositional limitations, especially low silica and high calcium levels, may restrict their pozzolanic performance. However, as

discussed in earlier sections, these ashes may still display latent hydraulic behaviour, which may explain their distinct clustering despite their limited pozzolanic contribution.

Finally, the third cluster includes all unground wood ash samples (WA1–WA4), which are clearly separated and further divided into WA1–WA3 and WA2–WA4 subgroups. This separation reflects the inherent differences in their origin and composition and is consistent with their limited pozzolanic activity due to insufficient fineness and underdeveloped reactivity.

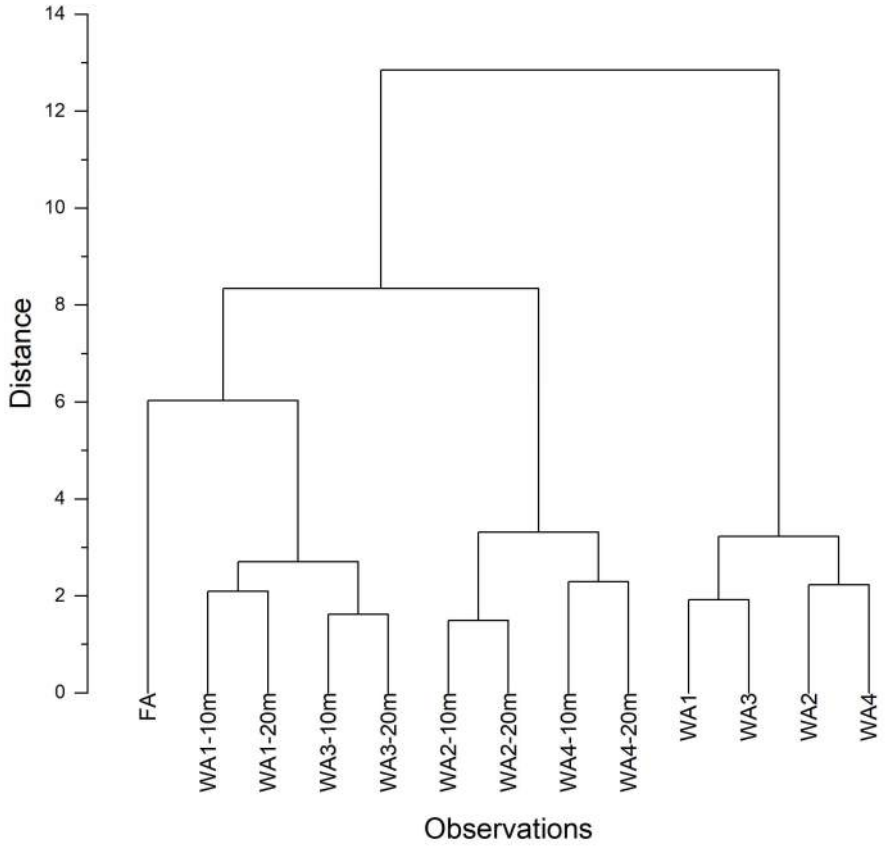

Figure 44. Dendrogram illustrating the hierarchical clustering of ash samples based on their chemical, physical, and reactivity-related properties.

Overall, the hierarchical clustering analysis supports the PCA findings and emphasizes the effectiveness of grinding in modifying and partially standardizing wood ash properties. However, it also shows that MCA alone cannot fully overcome the compositional barriers to reactivity in certain ash types.

Chapter 5

Conclusions

5.1. Concluding Remarks

The findings obtained from this study are summarized in the following conclusions:

- Mechanochemical activation significantly increased fineness and surface area of wood ashes, leading to improved reactivity, although the inherent oxide composition still controlled the overall potential.
- Wood ashes showed large variability in chemical composition; silica- and alumina-rich ashes were more pozzolanic, while calcium-rich ashes displayed latent hydraulic behaviour.
- At a 10 wt% replacement level of cement, concretes with ground wood ash showed comparable or improved strength compared to control mixes. In contrast, higher replacement levels tended to reduce both workability and strength.
- Mechanochemical activation promoted higher hydration heat release, faster early-age strength development, and denser microstructures in both cement-based and alkali-activated systems.
- Freeze–thaw resistance decreased in non-air-entrained concretes with wood ash but could be maintained or improved by combining with air-entraining admixtures.
- Leaching behaviour was generally improved after mechanochemical activation, with a reduced release of most heavy metals. However, the use of the stainless steel grinding media increased Cr concentrations in the wood ash.

- In alkali-activated mortars, partial replacement of ground granulated blast furnace slag with ground wood ash maintained comparable or higher strength at 10 wt% replacement, while the unground wood ashes resulted in reduced strength.
- Multivariate statistical analyses confirmed that wood ashes with higher pozzolanic oxide contents became more comparable to fly ash after mechanochemical activation.
- The findings demonstrate that wood ash has the potential to be valorised as a supplementary cementitious material, especially after mechanochemical activation, thereby contributing to both improved material performance and sustainability.

5.2. Answering the Research Questions

1. How does the utilization of wood ash in both cement-based and alkali-activated materials influence their mechanical properties, durability, and environmental impact? **(Paper I)**

   Wood ash can be utilized in both cement-based and alkali-activated systems. At lower levels of cement replacement (≤20%), compressive strength and durability can be maintained or even improved, while higher replacement levels generally result in reduced workability and strength loss. Similar effects have been observed in alkali-activated systems when wood ash was combined with reactive precursors such as fly ash or ground granulated blast furnace slag. From an environmental perspective, using wood ash can reduce cement consumption and CO_2 emissions, while also diverting biomass residues from landfills, thereby enhancing the overall sustainability of construction materials.

2. How do wood ashes with varying chemical compositions respond to mechanochemical activation in terms of pozzolanic reactivity? **(Paper II)**

   Wood ashes rich in silica and alumina showed increased pozzolanic reactivity after mechanochemical activation, while Ca-rich ashes exhibited limited response and tended to behave more hydraulically. Mechanochemical activation increased surface area and improved dissolution of reactive oxides, as demonstrated by the SAI, Frattini, and R3 tests. Multivariate analyses (PCA and HCA) further supported these findings, indicating that siliceous wood ashes clustered closer to fly ash after mechanochemical activation. Overall, mechanochemical activation effectively improved the pozzolanic potential of chemically suitable wood ashes.

3. How does mechanochemical activation of wood ash affect the strength of concrete and hydration when used as a partial cement replacement, and what is the optimum grinding duration? **(Paper II, III)**

   Mechanochemical activation of wood ash enhanced the compressive strength of concrete compared to unground wood ash, at a 10 wt% cement replacement level, where mixtures achieved values comparable to or higher than the control sample. It also

increased the cumulative heat release during hydration and enhanced the formation of hydration products. Considering these effects together, 10 minutes can be regarded as the optimum and balanced grinding duration, as it not only improves performance and hydration but also requires lower energy input than 20 minutes of grinding.

4. How does mechanochemical activation affect the leaching behaviour of heavy metals in wood ash and in concretes incorporating wood ash as a cement replacement? **(Paper III)**

   Mechanochemical activation generally reduced the leaching of most heavy metals from wood ash at a liquid-to-solid ratio of 10, with the extent depending on the ash mineralogy, and it improved the regulatory classification, although Cr contamination from stainless-steel grinding media was observed. In concretes with 20 wt% replacement, wood ash-containing mixes showed lower cumulative heavy metal leaching than the control sample. For Cr, mechanochemical activation caused a slight increase compared to the unground wood ash; nonetheless, leaching remained below the control and within the limits of the Dutch Building Materials Decree, confirming the environmental safety of concretes containing wood ash under the test conditions.

5. How do wood ash incorporation and mechanochemical activation affect the freeze–thaw durability of concrete? **(Paper III)**

   The incorporation of wood ash without air entrainment decreased the freeze–thaw durability of concrete, resulting in higher surface scaling compared to the control and fly ash mixes. Mechanochemical activation further compacted the matrix but also reduced entrapped air, leading to poor resistance in non-air-entrained systems. However, when combined with air-entraining admixtures (AEA), all mixes showed significantly improved durability. Notably, concrete with ground wood ash exhibited lower scaling than those with unground ash, indicating that mechanochemical activation improves the compatibility of wood ash with AEA and promotes a more efficient air-void system.

6. How does the incorporation of wood ash and mechanochemical activation affect the mechanical properties of alkali-activated mortars when used as a partial slag replacement, and what is the optimum grinding duration? **(Paper IV)**

   Mechanochemical activation of wood ash improved both compressive and flexural strength in alkali-activated mortars compared to unground wood ash, regardless of the activator type. Sodium silicate mixes achieved the highest compressive strength at 28 days, while sodium hydroxide mixes showed the highest flexural strength. At a 10 wt% replacement level, a 10-minute grinding duration was optimal, resulting in increased compressive strength in SS-activated mortars and flexural strength in SH-activated mortars compared to their respective controls. Over 360 days, SS- and SC-activated mixes experienced strength loss, while SH-activated mixes continued to gain strength

over time. Mechanochemical activation consistently enhanced long-term mechanical performance across all activator types.

5.3. Future Research

To strengthen the generalizability and long-term applicability of the findings, future work can focus on:

- **Feedstock diversity:** Investigate a broader range of wood ashes produced from different fuels, combustion technologies, and operating conditions to verify applicability across compositions.
- **Mechanochemical activation optimization:** Systematically vary grinding parameters such as speed, media type, residence time, and specific energy input, to optimize mechanochemical activation for different ash chemistries.
- **Long-term performance:** Expand testing to alkali–silica reaction, shrinkage, and other service-life indicators to clarify effects on the durability of concrete.
- **Environmental assessment:** Quantify energy use, CO_2 emissions, and life-cycle impacts associated with grinding to evaluate the overall sustainability of this approach.

References

Abdulkareem, M., Komkova, A., Havukainen, J., Habert, G., & Horttanainen, M. (2023). Identifying Optimal Precursors for Geopolymer Composite Mix Design for Different Regional Settings: A Multi-Objective Optimization Study. *Recycling*, *8*(2), 32. https://doi.org/10.3390/recycling8020032

Abdulkareem, O. A., Matthews, J. C., & Bakri, A. M. M. A. (2018). Strength and porosity characterizations of blended biomass wood ash-fly ash-based geopolymer mortar. *AIP Conference Proceedings 2045*, *2045*, 020096. https://doi.org/10.1063/1.5080909

Abdulkareem, O. A., Ramli, M., & Matthews, J. C. (2019). Production of geopolymer mortar system containing high calcium biomass wood ash as a partial substitution to fly ash: An early age evaluation. *Composites Part B: Engineering*, *174*, 106941. https://doi.org/10.1016/j.compositesb.2019.106941

Abdullahi, M. (2006). Characteristics of Wood ASH/OPC Concrete. *Leonardo Electronic Journal of Practices and Technologies* , *8*, 9–16. http://lejpt.academicdirect.org

Akinyemi, B. A., & Dai, C. (2020). Development of banana fibers and wood bottom ash modified cement mortars. *Construction and Building Materials*, *241*. https://doi.org/10.1016/j.conbuildmat.2020.118041

Akmalaiuly, K., Berdikul, N., Pundienė, I., & Pranckevičienė, J. (2023). The Effect of Mechanical Activation of Fly Ash on Cement-Based Materials Hydration and Hardened State Properties. *Materials*, *16*(8). https://doi.org/10.3390/ma16082959

Amaral, R. C., Rohden, A. B., Garcez, M. R., & Andrade, J. J. de O. (2022). Reuse of wood ash from biomass combustion in non-structural concrete: mechanical properties, durability, and eco-efficiency. *Journal of Material Cycles and Waste Management Volume*, *24*, 2439–2454.

Ashrafizadeh, H., & Ashrafizaadeh, M. (2012). Influence of processing parameters on grinding mechanism in planetary mill by employing discrete element method. *Advanced Powder Technology*, *23*(6), 708–716. https://doi.org/10.1016/j.apt.2011.09.002

ASTM-C1437. (2015). Standard Test Method for Flow of Hydraulic Cement Mortar. *ASTM International*, 6–7.

ASTM C1702-17. (2017). Standard Test Method for Measurement of Heat of Hydration of Hydraulic Cementitious Materials Using Isothermal Conduction Calorimetry. *ASTM International*.

ASTM C1897-20. (2020). Standard Test Methods for Measuring the Reactivity of Supplementary Cementitious Materials by Isothermal Calorimetry and Bound Water Measurements. *ASTM International, West Conshohocken, PA*, *04*(August), 7–11. https://doi.org/10.1520/C1897-20.2

ASTM C311-02. (2007). *Standard Test Methods for Sampling and Testing Fly Ash or Natural Pozzolans for Use in Portland-Cement Concrete*. http://www.aci-int.org.

ASTM C618-15. (2015). *Standard Specification for Coal Fly Ash and Raw or Calcined Natural Pozzolan for Use in Concrete*. www.astm.org

Avet, F., Li, X., Ben Haha, M., Bernal, S. A., Bishnoi, S., Cizer, Ö., Cyr, M., Dolenec, S., Durdzinski, P., Haufe, J., Hooton, D., Juenger, M. C. G., Kamali-Bernard, S., Londono-Zuluaga, D., Marsh, A. T. M., Marroccoli, M., Mrak, M., Parashar, A., Patapy, C., … Scrivener, K. (2022). Report of RILEM TC 267-TRM phase 2: optimization and testing of

the robustness of the R3 reactivity tests for supplementary cementitious materials. *Materials and Structures/Materiaux et Constructions*, *55*(3). https://doi.org/10.1617/s11527-022-01928-6

Avet, F., Snellings, R., Alujas Diaz, A., Ben Haha, M., & Scrivener, K. (2016). Development of a new rapid, relevant and reliable (R3) test method to evaluate the pozzolanic reactivity of calcined kaolinitic clays. *Cement and Concrete Research*, *85*, 1–11. https://doi.org/10.1016/j.cemconres.2016.02.015

Awoyera, P. O., Adesina, A., Sivakrishna, A., Gobinath, R., Kumar, K. R., & Srinivas, A. (2020). Alkali activated binders: Challenges and opportunities. *Materials Today: Proceedings*, *27*, 40–43. https://doi.org/10.1016/j.matpr.2019.08.199

Aydin, S., & Baradan, B. (2014). Effect of activator type and content on properties of alkali-activated slag mortars. *Composites Part B: Engineering*, *57*, 166–172. https://doi.org/10.1016/j.compositesb.2013.10.001

Azar, P., Patapy, C., Samson, G., Cussigh, F., Frouin, L., & Cyr, M. (2024). Effect of natural and accelerated carbonation on microstructure and pH of sodium carbonate alkali-activated slag. *Cement and Concrete Research*, *181*(April). https://doi.org/10.1016/j.cemconres.2024.107525

Bajare, D., Bumanis, G., Shakhmenko, G., & Justs, J. (2011). Obtaining composition of geopolymers (alkali activated binders) from local industrial wastes. *3rd International Conference CIVIL ENGINEERING`11 Proceedings* , 50–56.

Bakhoum, E. S., Amir, A., Osama, F., & Adel, M. (2023). Prediction model for the compressive strength of green concrete using cement kiln dust and fly ash. *Scientific Reports*, *13*(1). https://doi.org/10.1038/s41598-023-28868-7

Baki, V. A., Ke, X., Heath, A., Calabria-Holley, J., & Terzi, C. (2024). Improving the pozzolanic reactivity of clay, marl and obsidian through mechanochemical or thermal activation. *Materials and Structures/Materiaux et Constructions*, *57*(1), 1–21. https://doi.org/10.1617/s11527-023-02280-z

Baki, V. A., Ke, X., Heath, A., Calabria-Holley, J., Terzi, C., & Sirin, M. (2022). The impact of mechanochemical activation on the physicochemical properties and pozzolanic reactivity of kaolinite, muscovite and montmorillonite. *Cement and Concrete Research*, *162*(May), 106962. https://doi.org/10.1016/j.cemconres.2022.106962

Baláž, P. (2008). Mechanochemistry in nanoscience and minerals engineering. *Mechanochemistry in Nanoscience and Minerals Engineering*, 1–413. https://doi.org/10.1007/978-3-540-74855-7

Baláž, P., Achimovicová, M., Baláž, M., Billik, P., Zara, C. Z., Criado, J. M., Delogu, F., Dutková, E., Gaffet, E., Gotor, F. J., Kumar, R., Mitov, I., Rojac, T., Senna, M., Streletskii, A., & Krystyna, W. C. (2013). Hallmarks of mechanochemistry: From nanoparticles to technology. *Chemical Society Reviews*, *42*(18), 7571–7637. https://doi.org/10.1039/c3cs35468g

Baričević, A., Carević, I., Bajto, J. Š., Štirmer, N., Bezinović, M., & Kristović, K. (2021). Potential of using wood biomass ash in low-strength composites. *Materials*, *14*(5), 1–24. https://doi.org/10.3390/ma14051250

Bernal, S. A., de Gutierrez, R. M., Provis, J. L., & Rose, V. (2010). Effect of silicate modulus and metakaolin incorporation on the carbonation of alkali silicate-activated slags. *Cement and Concrete Research*, *40*(6), 898–907. https://doi.org/10.1016/j.cemconres.2010.02.003

Berodier, E., & Scrivener, K. (2014). Understanding the filler effect on the nucleation and growth of C-S-H. *Journal of the American Ceramic Society*, *97*(12), 3764–3773. https://doi.org/10.1111/jace.13177

Berra, M., Ippolito, N. M., Mangialardi, T., Paolini, A. E., & Piga, L. (2019). Leaching test procedure for assessing the compliance of the chemical and environmental requirements of hardened woody biomass fly ash cement mixtures. *Waste Management*, *90*, 10–16. https://doi.org/10.1016/j.wasman.2019.04.038

Berra, M., Mangialardi, T., & Paolini, A. E. (2015). Reuse of woody biomass fly ash in cement-based materials. *Construction and Building Materials*, *76*, 286–296. https://doi.org/10.1016/j.conbuildmat.2014.11.052

Berra, M., Paolini, A. E., & Mangialardi, T. (2016). Environmental quality of hardened wood fly ash-cement mixtures. *Proceedings of Institution of Civil Engineers: Waste and Resource Management*, *169*(1), 3–13. https://doi.org/10.1680/warm.15.00003

Bílek, V., Kalina, L., & Novotný, R. (2023). Structural build-up and breakdown of alkali-activated slag pastes with different order of lignosulfonate and activator addition. *Construction and Building Materials*, *386*(April). https://doi.org/10.1016/j.conbuildmat.2023.131557

Brazão Farinha, C., de Brito, J., & Veiga, R. (2019). Influence of forest biomass bottom ashes on the fresh, water and mechanical behaviour of cement-based mortars. *Resources, Conservation and Recycling*, *149*, 750–759. https://doi.org/10.1016/J.RESCONREC.2019.06.020

Bülbül, F., & Courard, L. (2025). Turning Waste into Greener Cementitious Building Material: Treatment Methods for Biomass Ashes—A Review. *Materials*, *18*(4), 834. https://doi.org/10.3390/ma18040834

Cagnetta, G., Huang, J., & Yu, G. (2018). A mini-review on mechanochemical treatment of contaminated soil: From laboratory to large-scale. *Critical Reviews in Environmental Science and Technology*, *48*(7–9), 723–771. https://doi.org/10.1080/10643389.2018.1493336

Candamano, S., De Luca, P., Frontera, P., & Crea, F. (2017). Production of geopolymeric mortars containing forest biomass ash as partial replacement of metakaolin. *Environments - MDPI*, *4*(4), 1–13. https://doi.org/10.3390/environments4040074

Cao, R., Zhang, S., Banthia, N., Zhang, Y., & Zhang, Z. (2020). Interpreting the early-age reaction process of alkali-activated slag by using combined embedded ultrasonic measurement, thermal analysis, XRD, FTIR and SEM. *Composites Part B: Engineering*, *186*(February), 107840. https://doi.org/10.1016/j.compositesb.2020.107840

Carević, I., Baričević, A., Štirmer, N., & Šantek Bajto, J. (2020). Correlation between physical and chemical properties of wood biomass ash and cement composites performances. *Construction and Building Materials*, *256*. https://doi.org/10.1016/j.conbuildmat.2020.119450

Carević, I., Pečur, I. B., & Štirmer, N. (2018). Durability Properties of Cement Composities with Wood Biomass Ash. *4th International Conference of Service Life Design for Infrastructures (SLD4), 27-30 August 2018, RILEM WEEK 2018 At: Delft, Netherlands*. https://www.researchgate.net/publication/327416681

Carević, I., Serdar, M., Štirmer, N., & Ukrainczyk, N. (2019). Preliminary screening of wood biomass ashes for partial resources replacements in cementitious materials. *Journal of Cleaner Production*, *229*, 1045–1064. https://doi.org/10.1016/j.jclepro.2019.04.321

Carević, I., Štirmer, N., Serdar, M., & Ukrainczyk, N. (2021). Effect of Wood Biomass Ash Storage on the Properties of Cement Composites. *Materials*, *14*(7), 1632. https://doi.org/10.3390/ma14071632

Carević, I., Štirmer, N., Trkmić, M., & Jurić, K. K. (2020). Leaching characteristics of wood biomass fly ash cement composites. *Applied Sciences (Switzerland)*, *10*(23), 1–17. https://doi.org/10.3390/app10238704

Castrillón, J. J., & Gil, H. (2020). Mechanical properties of mortars modified with wood waste ash. *Journal of the Indian Academy of Wood Science*, *17*(1), 90–99. https://doi.org/10.1007/s13196-020-00258-w

Castro, J., Varga, I. D. la, & Weiss, J. (2012). Using Isothermal Calorimetry to Assess the Water Absorbed by Fine LWA during Mixing. *Journal of Materials in Civil Engineering*, *24*(8), 996–1005. https://doi.org/10.1061/(asce)mt.1943-5533.0000496

Celik, I. B. (2009). The effects of particle size distribution and surface area upon cement strength development. *Powder Technology*, *188*(3), 272–276. https://doi.org/10.1016/J.POWTEC.2008.05.007

Celik, K., Meral, C., Petek Gursel, A., Mehta, P. K., Horvath, A., & Monteiro, P. J. M. (2015). Mechanical properties, durability, and life-cycle assessment of self-consolidating concrete mixtures made with blended portland cements containing fly ash and limestone powder. *Cement and Concrete Composites*, *56*, 59–72. https://doi.org/10.1016/j.cemconcomp.2014.11.003

CEN/TS 12390-9:2016. (2018). *Testing hardened concrete – Part 9: Freeze-thaw resistance with de-icing salts – Scaling*.

Chang, J. J. (2003). A study on the setting characteristics of sodium silicate-activated slag pastes. *Cement and Concrete Research*, *33*(7), 1005–1011. https://doi.org/10.1016/S0008-8846(02)01096-7

Cheah, C. B. (2011). Properties of high calcium wood ash and densified silica fume blended cement. *International Journal of the Physical Sciences*, *6*(28). https://doi.org/10.5897/ijps11.1485

Cheah, C. B., Part, W. K., & Ramli, M. (2015). The hybridizations of coal fly ash and wood ash for the fabrication of low alkalinity geopolymer load bearing block cured at ambient temperature. *Construction and Building Materials*, *88*, 41–55. https://doi.org/10.1016/j.conbuildmat.2015.04.020

Cheah, C. B., Part, W. K., & Ramli, M. (2017). The long term engineering properties of cementless building block work containing large volume of wood ash and coal fly ash. *Construction and Building Materials*, *143*, 522–536. https://doi.org/10.1016/j.conbuildmat.2017.03.162

Cheah, C. B., & Ramli, M. (2011). The implementation of wood waste ash as a partial cement replacement material in the production of structural grade concrete and mortar: An overview. *Resources, Conservation and Recycling*, *55*(7), 669–685. https://doi.org/10.1016/j.resconrec.2011.02.002

Cheah, C. B., & Ramli, M. (2012). Mechanical strength, durability and drying shrinkage of structural mortar containing HCWA as partial replacement of cement. *Construction and Building Materials*, *30*, 320–329. https://doi.org/10.1016/j.conbuildmat.2011.12.009

Cheah, C. B., & Ramli, M. (2013). The engineering properties of high performance concrete with HCWA-DSF supplementary binder. *Construction and Building Materials*, *40*, 93–103. https://doi.org/10.1016/j.conbuildmat.2012.10.010

Cheah, C. B., Samsudin, M. H., Ramli, M., Part, W. K., & Tan, L. E. (2017). The use of high calcium wood ash in the preparation of Ground Granulated Blast Furnace Slag and Pulverized Fly Ash geopolymers: A complete microstructural and mechanical characterization. *Journal of Cleaner Production*, *156*, 114–123. https://doi.org/10.1016/J.JCLEPRO.2017.04.026

Chen, H. J., Shih, N. H., Wu, C. H., & Lin, S. K. (2019). Effects of the loss on ignition of fly ash on the properties of high-volume fly ash concrete. *Sustainability (Switzerland)*, *11*(9). https://doi.org/10.3390/su11092704

Chen, Z., Lu, S., Tang, M., Lin, X., Qiu, Q., He, H., & Yan, J. (2019). Mechanochemical stabilization of heavy metals in fly ash with additives. *Science of the Total Environment*, *694*. https://doi.org/10.1016/j.scitotenv.2019.133813

Chowdhury, S., Maniar, A., & Suganya, O. M. (2015). Strength development in concrete with wood ash blended cement and use of soft computing models to predict strength parameters. *Journal of Advanced Research*, *6*(6), 907–913. https://doi.org/10.1016/j.jare.2014.08.006

Chowdhury, S., Mishra, M., & Suganya, O. (2014). The incorporation of wood waste ash as a partial cement replacement material for making structural grade concrete: An overview. *Ain Shams Engineering Journal*, *6*(2), 429–437. https://doi.org/10.1016/j.asej.2014.11.005

Chung, C. W., Shon, C. S., & Kim, Y. S. (2010). Chloride ion diffusivity of fly ash and silica fume concretes exposed to freeze-thaw cycles. *Construction and Building Materials*, *24*(9), 1739–1745. https://doi.org/10.1016/j.conbuildmat.2010.02.015

Council of the European Union. (2003). Council of the European Union. (2003). Council Decision 2003/33/EC of 19 December 2002 establishing criteria and procedures for the acceptance of waste at landfills pursuant to Article 16 of and Annex II to Directive 1999/31/EC. *Official Journal of the European Communities*, *L 11/27*, 27–49. https://eur-lex.europa.eu/legal-content/EN/TXT/?uri=CELEX:32003D0033

Couto, Á. F. Do, Sandoval, G. F. B., Schwantes-Cezario, N., Christoni, A. R. F., Cruz, R. J. P., Silva, P. R. C. Da, & Morales, G. (2024). Physicochemical evaluation of Eucalyptus Wood Ash as a mineral admixture in Portland cement matrices: A preliminary study. *Case Studies in Construction Materials*, *21*(October). https://doi.org/10.1016/j.cscm.2024.e03860

Cui, P., Wan, Y., Shao, X., Ling, X., Zhao, L., Gong, Y., & Zhu, C. (2023). Study on Shrinkage in Alkali-Activated Slag–Fly Ash Cementitious Materials. *Materials*, *16*(11). https://doi.org/10.3390/ma16113958

da Costa, T. P., Quinteiro, P., Tarelho, L. A. C., Arroja, L., & Dias, A. C. (2019). Environmental assessment of valorisation alternatives for woody biomass ash in construction materials. *Resources, Conservation and Recycling*, *148*, 67–79. https://doi.org/10.1016/j.resconrec.2019.04.022

Dai, X., Aydin, S., Yardimci, M. Y., Lesage, K., & de Schutter, G. (2020). Influence of water to binder ratio on the rheology and structural Build-up of Alkali-Activated Slag/Fly ash mixtures. *Construction and Building Materials*, *264*, 120253. https://doi.org/10.1016/j.conbuildmat.2020.120253

Dai, X., Ren, Q., Aydin, S., Yardimci, M. Y., & De Schutter, G. (2023). Accelerating the reaction process of sodium carbonate-activated slag mixtures with the incorporation of a small addition of sodium hydroxide/sodium silicate. *Cement and Concrete Composites*, *141*(January), 105118. https://doi.org/10.1016/j.cemconcomp.2023.105118

De Rossi, A., Simão, L., Ribeiro, M. J., Hotza, D., & Moreira, R. F. P. M. (2020). Study of cure conditions effect on the properties of wood biomass fly ash geopolymers. *Journal of*

Materials Research and Technology, *9*(4), 7518–7528. https://doi.org/10.1016/j.jmrt.2020.05.047

Demis, S., Tapali, J. G., & Papadakis, V. G. (2014). An investigation of the effectiveness of the utilization of biomass ashes as pozzolanic materials. *Construction and Building Materials*, *68*, 291–300. https://doi.org/10.1016/J.CONBUILDMAT.2014.06.071

Dimter, S., Zagvozda, M., Tonc, T., & Šimun, M. (2022). Evaluation of Strength Properties of Sand Stabilized with Wood Fly Ash (WFA) and Cement. *Materials*, *15*(9). https://doi.org/10.3390/ma15093090

Donatello, S., Freeman-Pask, A., Tyrer, M., & Cheeseman, C. R. (2010). Effect of milling and acid washing on the pozzolanic activity of incinerator sewage sludge ash. *Cement and Concrete Composites*, *32*(1), 54–61. https://doi.org/10.1016/j.cemconcomp.2009.09.002

Donatello, S., Tyrer, M., & Cheeseman, C. R. (2010). Comparison of test methods to assess pozzolanic activity. *Cement and Concrete Composites*, *32*(2), 121–127. https://doi.org/10.1016/j.cemconcomp.2009.10.008

Doudart de la Grée, G. C. H., Florea, M. V. A., Keulen, A., & Brouwers, H. J. H. (2016). Contaminated biomass fly ashes - Characterization and treatment optimization for reuse as building materials. *Waste Management*, *49*, 96–109. https://doi.org/10.1016/j.wasman.2015.12.023

Drljača, D. M., Vukić, L. M., Dragić, D. M., Borković, A. P., Botić, T. T., Dugić, P. T., Papuga, S. V., Šolić, M. D., Maletić, S. P., Gvero, P. M., & Savković, J. R. (2022). Leaching of heavy metals from wood biomass ash, before and after binding in cement composite. *Journal of the Serbian Chemical Society*, *87*(9), 1091–1108. https://doi.org/10.2298/JSC220217054D

Elinwa, A. U., & Ejeh, S. P. (2004). Effects of the Incorporation of Sawdust Waste Incineration Fly Ash in Cement Pastes and Mortars. *Journal of Asian Architecture and Building Engineering*, *3*(1), 1–7. https://doi.org/10.3130/JAABE.3.1

Elinwa, A. U., & Mahmood, Y. A. (2002). Ash from timber waste as cement replacement material. *Cement and Concrete Composites*, *24*(2), 219–222. https://doi.org/10.1016/S0958-9465(01)00039-7

Etiégni, L., & Campbell, A. G. (1991). Physical and Chemical Characteristics of Wood Ash*. *Bioresource Technology*, *37*, 173–178.

Fava, G., Naik, T. R., & Pierpaoli, M. (2018). Compressive strength and leaching behavior of mortars with biomass ash. *Recycling*, *3*(3). https://doi.org/10.3390/recycling3030046

Flower, D. J. M., & Sanjayan, J. G. (2017). Greenhouse Gas Emissions Due to Concrete Manufacture. *Handbook of Low Carbon Concrete*, *12*(5), 1–16. https://doi.org/10.1016/B978-0-12-804524-4.00001-4

Fořt, J., Šál, J., Žák, J., & Černý, R. (2020). Assessment of wood-based fly ash as alternative cement replacement. *Sustainability (Switzerland)*, *12*(22), 1–16. https://doi.org/10.3390/su12229580

Fu, Q., Bu, M., Zhang, Z., Xu, W., Yuan, Q., & Niu, D. (2022). Hydration Characteristics and Microstructure of Alkali-Activated Slag Concrete: A Review. *Engineering*, *20*, 162–179. https://doi.org/10.1016/j.eng.2021.07.026

Fu, X., Li, Q., Zhai, J., Sheng, G., & Li, F. (2008). The physical-chemical characterization of mechanically-treated CFBC fly ash. *Cement and Concrete Composites*, *30*(3), 220–226. https://doi.org/10.1016/j.cemconcomp.2007.08.006

Gabrijel, I., Rukavina, M. J., & Štirmer, N. (2021). Influence of wood fly ash on concrete properties through filling effect mechanism. *Materials*, *14*(23). https://doi.org/10.3390/ma14237164

Garcia, M. D. L., & Sousa-Coutinho, J. (2013). Strength and durability of cement with forest waste bottom ash. *Construction and Building Materials*, *41*, 897–910. https://doi.org/10.1016/j.conbuildmat.2012.11.081

Gaudreault, C., Lama, I., & Sain, D. (2020). Is the beneficial use of wood ash environmentally beneficial? A screening-level life cycle assessment and uncertainty analysis. *Journal of Industrial Ecology*, *24*(6), 1300–1309. https://doi.org/10.1111/jiec.13019

Gerges, N., Issa, C. A., Antoun, M., Sleiman, E., Hallal, F., Shamoun, P., & Hayek, J. (2021). Eco-friendly mortar: Optimum combination of wood ash, crumb rubber, and fine crushed glass. *Case Studies in Construction Materials*, *15*. https://doi.org/10.1016/j.cscm.2021.e00588

Ghufran, M., Khan, K. I. A., Ullah, F., Nasir, A. R., Al Alahmadi, A. A., Alzaed, A. N., & Alwetaishi, M. (2022). Circular Economy in the Construction Industry: A Step towards Sustainable Development. *Buildings*, *12*(7). https://doi.org/10.3390/buildings12071004

Gijbels, K., Pontikes, Y., Samyn, P., Schreurs, S., & Schroeyers, W. (2020). Effect of NaOH content on hydration, mineralogy, porosity and strength in alkali/sulfate-activated binders from ground granulated blast furnace slag and phosphogypsum. *Cement and Concrete Research*, *132*(April), 106054. https://doi.org/10.1016/j.cemconres.2020.106054

Global Cement and Concrete Association. (2022, June 8). *https://gccassociation.org*.

Grabias-Blicharz, E., & Franus, W. (2023). A critical review on mechanochemical processing of fly ash and fly ash-derived materials. *Science of The Total Environment*, *860*(September 2022), 160529. https://doi.org/10.1016/j.scitotenv.2022.160529

Grau, F., Choo, H., Hu, J. W., & Jung, J. (2015). Engineering behavior and characteristics of wood ash and sugarcane bagasse ash. *Materials*, *8*(10), 6962–6977. https://doi.org/10.3390/ma8105353

Haha, M. Ben, Lothenbach, B., Le Saout, G., & Winnefeld, F. (2011). Influence of slag chemistry on the hydration of alkali-activated blast-furnace slag - Part I: Effect of MgO. *Cement and Concrete Research*, *41*(9), 955–963. https://doi.org/10.1016/j.cemconres.2011.05.002

Haha, M. Ben, Lothenbach, B., Le Saout, G., & Winnefeld, F. (2012). Influence of slag chemistry on the hydration of alkali-activated blast-furnace slag - Part II: Effect of Al2O3. *Cement and Concrete Research*, *42*(1), 74–83. https://doi.org/10.1016/j.cemconres.2011.08.005

Hamid, Z., & Rafiq, S. (2020). A Comparative Study on Strength of Concrete Using Wood Ash as Partial Replacement of Cement. *IOP Conference Series: Materials Science and Engineering*, *955*(1). https://doi.org/10.1088/1757-899X/955/1/012043

Hewlett, P., & Liska, M. (2019). *Lea's Chemistry of Cement and Concrete* (Fifth Edit).

Hills, C. D., Tripathi, N., Singh, R. S., Carey, P. J., & Lowry, F. (2020). Valorisation of agricultural biomass-ash with CO2. *Scientific Reports*, *10*(1), 13801. https://doi.org/10.1038/s41598-020-70504-1

Hjerpe, K. (2008). *Recommendations for extraction of logging residues and ash recycling*. 31.

Huang, L., & Yan, P. (2019). Effect of alkali content in cement on its hydration kinetics and mechanical properties. *Construction and Building Materials*, *228*, 116833. https://doi.org/10.1016/j.conbuildmat.2019.116833

Humad, A. M., Habermehl-Cwirzen, K., & Cwirzen, A. (2019). Effects of fineness and chemical composition of blast furnace slag on properties of Alkali-Activated Binder. *Materials*,

12(20), 1–16. https://doi.org/10.3390/ma12203447

Humad, A. M., Provis, J. L., Habermehl-Cwirzen, K., Rajczakowska, M., & Cwirzen, A. (2021). Creep and Long-Term Properties of Alkali-Activated Swedish-Slag Concrete. *Journal of Materials in Civil Engineering*, *33*(2), 04020475. https://doi.org/10.1061/(ASCE)MT.1943-5533.0003381

IEA. (2025). *Cement*. International Energy Agency. https://www.iea.org/energy-system/industry/cement

Ilić, B., Radonjanin, V., Malešev, M., Zdujić, M., & Mitrović, A. (2016). Effects of mechanical and thermal activation on pozzolanic activity of kaolin containing mica. *Applied Clay Science*, *123*, 173–181. https://doi.org/10.1016/j.clay.2016.01.029

International Energy Agency (IEA). (2024). *World Energy Outlook 2024*.

James, A. K., Thring, R. W., Helle, S., & Ghuman, H. S. (2012). Ash management review-applications of biomass bottom ash. *Energies*, *5*(10), 3856–3873. https://doi.org/10.3390/en5103856

Jiang, M., Chen, X., Rajabipour, F., & Hendrickson, C. T. (2014). Comparative Life Cycle Assessment of Conventional, Glass Powder, and Alkali-Activated Slag Concrete and Mortar. *Journal of Infrastructure Systems*, *20*(4), 1–9. https://doi.org/10.1061/(asce)is.1943-555x.0000211

Jolliffe, I. T. (1986). *Principal Component Analysis* (1st ed.). Springer. https://doi.org/10.1007/978-0-387-98135-2

Juenger, M. C. G., Snellings, R., & Bernal, S. A. (2019). Supplementary cementitious materials: New sources, characterization, and performance insights. *Cement and Concrete Research*, *122*(May 2019), 257–273. https://doi.org/10.1016/j.cemconres.2019.05.008

Jurić, K. K., Carević, I., Serdar, M., & Štirmer, N. (2021). Feasibility of using pozzolanicity tests to assess reactivity of wood biomass fly ashes. *Journal of the Croatian Association of Civil Engineers*, *72*(12), 1145–1153. https://doi.org/10.14256/JCE.2950.2020

Kalina, R. D., Al-Shmaisani, S., Ferron, R. D., Juenger, M. C. G., Ryan D. Kalina Raissa Douglas Ferron, and Maria C. G. Juenger, S. A.-S., Kalina, R. D., Al-Shmaisani, S., Ferron, R. D., & Juenger, M. C. G. (2019). False positives in ASTM C618 specifications for natural pozzolans. *ACI Materials Journal*, *116*(1), 165–172. https://doi.org/10.14359/51712243

Kaminskas, R., & Cesnauskas, V. (2014). Influence of activated biomass fly ash on portland cement hydration. *Ceramics - Silikaty*, *58*(4), 260–268.

Kannan, V., & Raja Priya, P. (2021). Evaluation of the permeability of high strength concrete using metakaolin and wood ash as partial replacement for cement. *SN Applied Sciences*, *3*(1). https://doi.org/10.1007/s42452-020-04024-y

Kapeluszna, E., Kotwica, Ł., Malata, G., Murzyn, P., & Nocuń-Wczelik, W. (2020). The effect of highly reactive pozzolanic material on the early hydration of alite – C3A – gypsum synthetic cement systems. *Construction and Building Materials*, *251*, 118879. https://doi.org/10.1016/J.CONBUILDMAT.2020.118879

Kara De Maeijer, P., Craeye, B., Snellings, R., Kazemi-Kamyab, H., Loots, M., Janssens, K., & Nuyts, G. (2020). Effect of ultra-fine fly ash on concrete performance and durability. *Construction and Building Materials*, *263*, 120493. https://doi.org/10.1016/j.conbuildmat.2020.120493

Kato, K., Xin, Y., Hitomi, T., & Shirai, T. (2019). Surface modification of fly ash by mechano-

chemical treatment. *Ceramics International*, *45*(1), 849–853. https://doi.org/10.1016/j.ceramint.2018.09.254

Ke, X., Baki, V. A., & Skevi, L. (2023). Mechanochemical activation for improving the direct mineral carbonation efficiency and capacity of a timber biomass ash. *Journal of CO2 Utilization*, *68*(August 2022), 102367. https://doi.org/10.1016/j.jcou.2022.102367

Ke, X., Bernal, S. A., & Provis, J. L. (2016). Controlling the reaction kinetics of sodium carbonate-activated slag cements using calcined layered double hydroxides. *Cement and Concrete Research*, *81*, 24–37. https://doi.org/10.1016/j.cemconres.2015.11.012

Kim, T., & Kang, C. (2020). The Mechanical Properties of Alkali-Activated Slag-Silica Fume Cement Pastes by Mixing Method. *International Journal of Concrete Structures and Materials*, *14*(1). https://doi.org/10.1186/s40069-020-00416-x

Kim, T., & Olek, J. (2012). Effects of sample preparation and interpretation of thermogravimetric curves on calcium hydroxide in hydrated pastes and mortars. *Transportation Research Record*, *2290*, 10–18. https://doi.org/10.3141/2290-02

Kothari, A., Habermehl-Cwirzen, K., Hedlund, H., & Cwirzen, A. (2020). A review of the mechanical properties and durability of ecological concretes in a cold climate in comparison to standard ordinary portland cement-based concrete. *Materials*, *13*(16). https://doi.org/10.3390/MA13163467

Koufany, I., De la Torre, A. G., Redondo-Soto, C., Santacruz, I., Cuesta, A., Gastaldi, D., Canonico, F., Mazanec, O., & Aranda, M. A. G. (2025). General correlation between R3 test results and compressive strengths for five families of supplementary cementitious materials. *Cement and Concrete Composites*, *163*(March), 106166. https://doi.org/10.1016/j.cemconcomp.2025.106166

Kramar, S., & Ducman, V. (2018). Evaluation of ash pozzolanic activity by means of the strength activity index test, frattini test and DTA/TG analysis. *Tehnicki Vjesnik*, *25*(6), 1746–1752. https://doi.org/10.17559/TV-20171203193229

Kumar, M., Xiong, X., Wan, Z., Sun, Y., Tsang, D. C. W., Gupta, J., Gao, B., Cao, X., Tang, J., & Ok, Y. S. (2020). Ball milling as a mechanochemical technology for fabrication of novel biochar nanomaterials. *Bioresource Technology*, *312*(June), 123613. https://doi.org/10.1016/j.biortech.2020.123613

Kumar, S., & Kumar, R. (2011). Mechanical activation of fly ash: Effect on reaction, structure and properties of resulting geopolymer. *Ceramics International*, *37*(2), 533–541. https://doi.org/10.1016/j.ceramint.2010.09.038

Lamaa, G., Duarte, A. P. C., Silva, R. V., & de Brito, J. (2023). Carbonation of Alkali-Activated Materials: A Review. *Materials*, *16*(8). https://doi.org/10.3390/ma16083086

Lanzerstorfer, C. (2017). Fly Ash from the Combustion of Post-Consumer Waste Wood: Distribution of Heavy Metals by Particle Size. *International Journal of Environmental Science*, *2*, 438–442.

Lao, J. C., Huang, B. T., Fang, Y., Xu, L. Y., Dai, J. G., & Shah, S. P. (2023). Strain-hardening alkali-activated fly ash/slag composites with ultra-high compressive strength and ultra-high tensile ductility. *Cement and Concrete Research*, *165*(November 2022), 107075. https://doi.org/10.1016/j.cemconres.2022.107075

Lazik, P.-R., Bošnjak, J., Cetin, E., & Kücük, A. (2020). Application of Wood Ash as a Substitute For Fly Ash And Investigation of Concrete Properties. *Otto-Graf-Journal*, *19*.

Lescinskis, O., Sapata, A., Bumanis, G., Sinka, M., Zhou, X., & Bajare, D. (2025). The Potential

of Wood Ash to Be Used as a Supplementary Cementitious Material in Cement Mortars. *Buildings*, *15*(9), 1507. https://doi.org/10.3390/buildings15091507

Lessard, J.-M., Omran, A., Tagnit-Hamou, A., & Gagne, R. (2017). Feasibility of Using Biomass Fly and Bottom Ashes to Produce RCC and PCC. *Journal of Materials in Civil Engineering*, *29*(4), 04016267. https://doi.org/10.1061/(asce)mt.1943-5533.0001796

Li, M. G., Sun, C. J., Gau, S. H., & Chuang, C. J. (2010). Effects of wet ball milling on lead stabilization and particle size variation in municipal solid waste incinerator fly ash. *Journal of Hazardous Materials*, *174*(1–3), 586–591. https://doi.org/10.1016/j.jhazmat.2009.09.092

Li, Y., & Sun, Y. (2000). Preliminary study on combined-alkali-slag paste materials. *Cement and Concrete Research*, *30*(6), 963–966. https://doi.org/10.1016/S0008-8846(00)00269-6

Londono-Zuluaga, D., Gholizadeh-Vayghan, A., Winnefeld, F., Avet, F., Ben Haha, M., Bernal, S. A., Cizer, Ö., Cyr, M., Dolenec, S., Durdzinski, P., Haufe, J., Hooton, D., Kamali-Bernard, S., Li, X., Marsh, A. T. M., Marroccoli, M., Mrak, M., Muy, Y., Patapy, C., … Scrivener, K. L. (2022). Report of RILEM TC 267-TRM phase 3: validation of the R3 reactivity test across a wide range of materials. *Materials and Structures/Materiaux et Constructions*, *55*(5). https://doi.org/10.1617/s11527-022-01947-3

Long, H. V. (2021). Optimizing mixtures of alkali aluminosilicate cement based on ternary by-products. *Civil Engineering Journal (Iran)*, *7*(7), 1264–1274. https://doi.org/10.28991/cej-2021-03091724

Lothenbach, B., Scrivener, K., & Hooton, R. D. (2011). Supplementary cementitious materials. *Cement and Concrete Research*, *41*(12), 1244–1256. https://doi.org/10.1016/j.cemconres.2010.12.001

Luo, L., Yao, W., Liang, G., & Luo, Y. (2023). Workability, autogenous shrinkage and microstructure of alkali-activated slag/fly ash slurries: Effect of precursor composition and sodium silicate modulus. *Journal of Building Engineering*, *73*(May), 106712. https://doi.org/10.1016/j.jobe.2023.106712

Luukkonen, T., Abdollahnejad, Z., Yliniemi, J., Kinnunen, P., & Illikainen, M. (2018). One-part alkali-activated materials: A review. *Cement and Concrete Research*, *103*, 21–34. https://doi.org/10.1016/J.CEMCONRES.2017.10.001

Makó, É., Frost, R. L., Kristóf, J., & Horváth, E. (2001). The effect of quartz content on the mechanochemical activation of kaolinite. *Journal of Colloid and Interface Science*, *244*(2), 359–364. https://doi.org/10.1006/jcis.2001.7953

Maresca, A., Hansen, M., Ingerslev, M., & Astrup, T. F. (2018). Column leaching from a Danish forest soil amended with wood ashes: fate of major and trace elements. *Biomass and Bioenergy*, *109*, 91–99. https://doi.org/10.1016/J.BIOMBIOE.2017.12.014

Marion, A. M., De Lanève, M., & De Grauw, A. (2005). Study of the leaching behaviour of paving concretes: Quantification of heavy metal content in leachates issued from tank test using demineralized water. *Cement and Concrete Research*, *35*(5), 951–957. https://doi.org/10.1016/j.cemconres.2004.06.014

Marjanović, N., Komljenović, M., Baščarević, Z., & Nikolić, V. (2014). Improving reactivity of fly ash and properties of ensuing geopolymers through mechanical activation. *Construction and Building Materials*, *57*, 151–162. https://doi.org/10.1016/j.conbuildmat.2014.01.095

Michalchuk, A. A. L., Boldyreva, E. V., Belenguer, A. M., Emmerling, F., & Boldyrev, V. V. (2021). Tribochemistry, Mechanical Alloying, Mechanochemistry: What is in a Name? *Frontiers in Chemistry*, *9*(May), 1–29. https://doi.org/10.3389/fchem.2021.685789

Monteiro, P. J. M., Miller, S. A., & Horvarth, A. (2017). Towards sustainable concrete. *Nature Materials*, *16*, 698–699. https://doi.org/https://doi.org/10.1038/nmat4930

Montinaro, S., Concas, A., Pisu, M., & Cao, G. (2008). Immobilization of heavy metals in contaminated soils through ball milling with and without additives. *Chemical Engineering Journal*, *142*(3), 271–284. https://doi.org/10.1016/j.cej.2007.12.003

Moraes, J. C. B., Cordeiro, G. C., Akasaki, J. L., Vieira, A. P., & Payá, J. (2021). Improving the reactivity of a former ground sugarcane bagasse ash produced by autogenous combustion through employment of two different additional grinding procedures. *Construction and Building Materials*, *270*, 121471. https://doi.org/10.1016/j.conbuildmat.2020.121471

Mucsi, G. (2016). Mechanical activation of power station fl y ash by grinding – A review. *Epitoanyag - Journal of Silicate Based and Composite Materials*, *68*(2), 56–61. https://doi.org/10.14382/epitoanyag-jsbcm.2016.10

Nader, V., Awwad, E., Wakim, J., & Haya, L. B. (2020). A study on cement-based mixes with partial wood bottom ash replacement. *Proceedings of Institution of Civil Engineers: Waste and Resource Management*, *173*(1), 15–23. https://doi.org/10.1680/jwarm.19.00005

Naik, T. R., Kraus, R. N., & Siddique, R. (2002). Demonstration of manufacturing technology for concrete and CLSM utilizing wood ash from Wisconsin. *UWM Centre for By Product Utilization*, *538*, 124.

National Institute for Public Health and the Environment of The Netherlands (RIVM). (2022). *Critical emission limit values for building materials: technical background, interpretation and reconstruction*.

Ndahirwa, D., Zmamou, H., Lenormand, H., Chenot, E., Potel, S., & Leblanc, N. (2024). Wood ash-based binders for lightweight building materials: Evaluating the influence of hydraulic lime and cement on the setting and mechanical properties of wood ash pastes. *Results in Engineering*, *24*(August). https://doi.org/10.1016/j.rineng.2024.102738

Nedeljković, M., Zuo, Y., Arbi, K., & Ye, G. (2018). Carbonation Resistance of Alkali-Activated Slag Under Natural and Accelerated Conditions. *Journal of Sustainable Metallurgy*, *4*(1), 33–49. https://doi.org/10.1007/s40831-018-0166-4

Ngueyep, M., & Leroy, L. (2019). Valorization of Wood Ashes as Partial Replacement of Portland Cement: Mechanical Performance and Durability. *European Journal of Scientific Research* , *151*, 468–478. http://www.

Nguyen, T. N., Phung, Q. T., Yu, Z., Frederickx, L., Jacques, D., Sakellariou, D., Dauzeres, A., Elsen, J., & Pontikes, Y. (2022). Alteration in molecular structure of alkali activated slag with various water to binder ratios under accelerated carbonation. *Scientific Reports*, *12*(1), 1–16. https://doi.org/10.1038/s41598-022-09491-4

Nomura, Y., Fujiwara, K., Terada, A., Nakai, S., & Hosomi, M. (2010). Prevention of lead leaching from fly ashes by mechanochemical treatment. *Waste Management*, *30*(7), 1290–1295. https://doi.org/10.1016/j.wasman.2009.11.025

Norouzi, M., Chàfer, M., Cabeza, L. F., Jiménez, L., & Boer, D. (2021). Circular economy in the building and construction sector: A scientific evolution analysis. *Journal of Building Engineering*, *44*. https://doi.org/10.1016/j.jobe.2021.102704

Ohenoja, K., Tanskanen, P., Peltosaari, O., Wigren, V., Österbacka, J., & Illikainen, M. (2016). Effect of particle size distribution on the self-hardening property of biomass-peat fly ash from a bubbling fluidized bed combustion. *Fuel Processing Technology*, *148*, 60–66. https://doi.org/10.1016/j.fuproc.2016.02.023

Omran, A., Soliman, N., Xie, A., Davidenko, T., & Tagnit-Hamou, A. (2018). Field trials with concrete incorporating biomass-fly ash. *Construction and Building Materials*, *186*, 660–669. https://doi.org/10.1016/j.conbuildmat.2018.07.084

Ottosen, L. M., Hansen, E. Ø., Jensen, P. E., Kirkelund, G. M., & Golterman, P. (2016). Wood ash used as partly sand and/or cement replacement in mortar. *International Journal of Sustainable Development and Planning*, *11*(5), 781–791. https://doi.org/10.2495/SDP-V11-N5-781-791

Ottosen, L. M., & Sigvardsen, N. M. (2024). Heavy metal leaching from wood ash before and after hydration and carbonation. *Environmental Science and Pollution Research*, *2023*. https://doi.org/10.1007/s11356-024-33221-0

Ouyang, X., Ma, Y., Liu, Z., Liang, J., & Ye, G. (2020). Effect of the sodium silicate modulus and slag content on fresh and hardened properties of alkali-activated fly ash/slag. *Minerals*, *10*(1). https://doi.org/10.3390/min10010015

Owaid, H. M., Al-Rubaye, M. M., & Al-Baghdadi, H. M. (2021). Use of waste paper ash or wood ash as substitution to fly ash in production of geopolymer concrete. *Scientific Review Engineering and Environmental Sciences*, *30*(3), 464–476. https://doi.org/10.22630/PNIKS.2021.30.3.39

Palacios, M., & Puertas, F. (2006). Effect of carbonation on alkali-activated slag paste. *Journal of the American Ceramic Society*, *89*(10), 3211–3221. https://doi.org/10.1111/J.1551-2916.2006.01214.X

Pálková, H., Barlog, M., Madejová, J., Hronský, V., Petra, L., Šimon, E., Billik, P., & Zimowska, M. (2021). Structural changes in smectites subjected to mechanochemical activation: The effect of the occupancy of the octahedral sites. *Applied Clay Science*, *213*(August). https://doi.org/10.1016/j.clay.2021.106214

Pantić, V., Šupić, S., Vučinić-Vasić, M., Nemeš, T., Malešev, M., Lukić, I., & Radonjanin, V. (2023). Effects of Grinding Methods and Water-to-Binder Ratio on the Properties of Cement Mortars Blended with Biomass Ash and Ceramic Powder. *Materials*, *16*(6). https://doi.org/10.3390/ma16062443

Parashar, A., & Bishnoi, S. (2020). A comparison of test methods to assess the strength potential of plain and blended supplementary cementitious materials. *Construction and Building Materials*, *256*, 119292. https://doi.org/10.1016/j.conbuildmat.2020.119292

Patil, A. G., & Anandhan, S. (2015). Influence of planetary ball milling parameters on the mechano-chemical activation of fly ash. *Powder Technology*, *281*, 151–158. https://doi.org/10.1016/j.powtec.2015.04.078

Provis, J. L. (2014). Geopolymers and other alkali activated materials: Why, how, and what? *Materials and Structures/Materiaux et Constructions*, *47*(1–2), 11–25. https://doi.org/10.1617/s11527-013-0211-5

Provis, J. L., & Bernal, S. A. (2014). Geopolymers and Related Alkali-Activated Materials. *Annual Review of Materials Research*, *44*(1), 299–327. https://doi.org/10.1146/annurev-matsci-070813-113515

Provis, J. L., Palomo, A., & Shi, C. (2015). Advances in understanding alkali-activated materials. *Cement and Concrete Research*, *78*, 110–125. https://doi.org/10.1016/j.cemconres.2015.04.013

Provis, J. L., & van Deventer, J. S. J. (2014). Alkali Materials Activated State-of-the-Art Report. In *RILEM State-of-the-Art Reports* (Vol. 13).

Puertas, F., González-Fonteboa, B., González-Taboada, I., Alonso, M. M., Torres-Carrasco, M., Rojo, G., & Martínez-Abella, F. (2018). Alkali-activated slag concrete: Fresh and hardened behaviour. *Cement and Concrete Composites*, *85*, 22–31. https://doi.org/10.1016/j.cemconcomp.2017.10.003

Rajamma, R., Ball, R. J., Tarelho, L. A. C., Allen, G. C., Labrincha, J. A., & Ferreira, V. M. (2009). Characterisation and use of biomass fly ash in cement-based materials. *Journal of Hazardous Materials*, *172*(2–3), 1049–1060. https://doi.org/10.1016/j.jhazmat.2009.07.109

Rajamma, R., Senff, L., Ribeiro, M. J., Labrincha, J. A., Ball, R. J., Allen, G. C., & Ferreira, V. M. (2015). Biomass fly ash effect on fresh and hardened state properties of cement based materials. *Composites Part B: Engineering*, *77*, 1–9. https://doi.org/10.1016/j.compositesb.2015.03.019

Raju, R., Paul, M. M., & Aboobacker, K. A. (2014). Strength performance of concrete using bottom ash as fine aggregate. *Impact Journals*, *2*(9), 111–122. www.impactjournals.us

Ramos, T., Matos, A. M., & Sousa-Coutinho, J. (2013). Mortar with wood waste ash: Mechanical strength carbonation resistance and ASR expansion. *Construction and Building Materials*, *49*, 343–351. https://doi.org/10.1016/j.conbuildmat.2013.08.026

Reddy, K. C., Seo, J., Yoon, H. N., Kim, S., Kim, G. M., Son, H. M., Park, S., & Park, S. (2022). Supercritical CO2-Induced Evolution of Alkali-Activated Slag Cements. *Materials*, *15*(17). https://doi.org/10.3390/ma15175873

Rissanen, J., Ohenoja, K., Kinnunen, P., & Illikainen, M. (2020). *Peat-Wood Fly Ash as Cold-Region Supplementary Cementitious Material: Air Content and Freeze-Thaw Resistance of Air-Entrained Mortars*. https://doi.org/10.1061/(ASCE)MT.1943

Rissanen, J., Ohenoja, K., Kinnunen, P., Romagnoli, M., & Illikainen, M. (2018). Milling of peat-wood fly ash: Effect on water demand of mortar and rheology of cement paste. *Construction and Building Materials*, *180*, 143–153. https://doi.org/10.1016/J.CONBUILDMAT.2018.05.014

Rosales, J., Cabrera, M., Beltrán, M. G., López, M., & Agrela, F. (2017). Effects of treatments on biomass bottom ash applied to the manufacture of cement mortars. *Journal of Cleaner Production*, *154*(2017), 424–435. https://doi.org/10.1016/j.jclepro.2017.04.024

Rossen, J. E., Lothenbach, B., & Scrivener, K. L. (2015). Composition of C-S-H in pastes with increasing levels of silica fume addition. *Cement and Concrete Research*, *75*, 14–22. https://doi.org/10.1016/j.cemconres.2015.04.016

Rossen, J. E., & Scrivener, K. L. (2017). Optimization of SEM-EDS to determine the C–A–S–H composition in matured cement paste samples. *Materials Characterization*, *123*, 294–306. https://doi.org/10.1016/j.matchar.2016.11.041

Rumman, R., & Alam, M. S. (2025). Does wood fly ash (WFA) have pozzolanic property? A study on low- and high-temperature partially burnt WFA compared to classes C and F coal fly ash (CFA). *Construction and Building Materials*, *471*(November 2024), 140700. https://doi.org/10.1016/j.conbuildmat.2025.140700

Samsudin, M. H., & Chee Ban, C. (2015). Granulated Blast Furnace Slag and High Calcium Wood Ash (GGBS-HCWA) for the Fabrication of Geopolymer Mortar. *Advances in Environmental Biology*, *9*(4), 22–25. http://www.aensiweb.com/AEB/

Şanal, İ. (2018). Significance of Concrete Production in Terms of Carbondioxide Emissions: Social and Environmental Impacts. *Journal of Polytechnic*, *0900*(2), 369–378. https://doi.org/10.2339/politeknik.389590

Sanna, A. L., Pia, G., & Delogu, F. (2023). Kinetics of Grain Size Reduction in Minerals Undergoing Ball Milling. *Transactions of the Indian Institute of Metals*, *0123456789*. https://doi.org/10.1007/s12666-023-03034-9

Šantek Bajto, J., Štirmer, N., Cerković, S., Carević, I., & Kostanić Jurić, K. (2021). Pilot Scale Production of Precast Concrete Elements with Wood Biomass Ash. *Materials*, *14*(21), 6578. https://doi.org/10.3390/ma14216578

Scrivener, K. L., John, V. M., & Gartner, E. M. (2018). Eco-efficient cements: Potential economically viable solutions for a low-CO2 cement-based materials industry. *Cement and Concrete Research*, *114*(June), 2–26. https://doi.org/10.1016/j.cemconres.2018.03.015

Scrivener, K., Snellings, R., & Lothenbach, B. (2016). A practical guide to microstructural analysis of cementitious materials. In *A Practical Guide to Microstructural Analysis of Cementitious Materials*. https://doi.org/10.1007/978-1-4684-6282-1_8

Seco, A., Martín-Antunes, M. A., Espuelas, S., Fernández, A., & Prieto, E. (2025). Mechanochemical activation of non-conventional precursors for use as suplementary cementitious materials. *Applied Clay Science*, *266*(April 2024). https://doi.org/10.1016/j.clay.2025.107705

Senneca, O., Salatino, P., Chirone, R., Cortese, L., & Solimene, R. (2011). Mechanochemical activation of high-carbon fly ash for enhanced carbon reburning. *Proceedings of the Combustion Institute*, *33*(2), 2743–2753. https://doi.org/10.1016/j.proci.2010.07.067

Sharma, M., & Lalotra, S. (2022). An experimental study on strength of concrete with partial replacement of cement by wood ash and fine aggregate by copper slag. *International Research Journal of Engineering and Technology*, *9*(4), 412–418. www.irjet.net

Siddique, R. (2012). Utilization of wood ash in concrete manufacturing. *Resources, Conservation and Recycling*, *67*, 27–33. https://doi.org/10.1016/j.resconrec.2012.07.004

Šídlová, M., Šulc, R., Rak, P., Formáček, P., Pulcová, K., & Snop, R. (2023). Comparison of different methods for assessing the pozzolanic activity of fly ash and bottom ash. *AIP Conference Proceedings*, *2780*(1). https://doi.org/10.1063/5.0137066

Sigvardsen, N. M. (2020). Utilisation of Wood Ash in Cement-Based Materials. In *Downloaded from orbit.dtu.dk on: Oca* (Vol. 17).

Sigvardsen, N. M., Geiker, M. R., & Ottosen, L. M. (2021a). Phase development and mechanical response of low-level cement replacements with wood ash and washed wood ash. *Construction and Building Materials*, *269*, 121234. https://doi.org/10.1016/J.CONBUILDMAT.2020.121234

Sigvardsen, N. M., Geiker, M. R., & Ottosen, L. M. (2021b). Reaction mechanisms of wood ash for use as a partial cement replacement. *Construction and Building Materials*, *286*. https://doi.org/10.1016/j.conbuildmat.2021.122889

Sigvardsen, N. M., Kirkelund, G. M., Jensen, P. E., Geiker, M. R., & Ottosen, L. M. (2019). Impact of production parameters on physiochemical characteristics of wood ash for possible utilisation in cement-based materials. *Resources, Conservation and Recycling*, *145*, 230–240. https://doi.org/10.1016/j.resconrec.2019.02.034

Sigvardsen, N. M., & Ottosen, L. M. (2019). Characterization of coal bio ash from wood pellets and low-alkali coal fly ash and use as partial cement replacement in mortar. *Cement and Concrete Composites*, *95*, 25–32. https://doi.org/10.1016/j.cemconcomp.2018.10.005

Silva, G. J. B., Santana, V. P., & Wójcik, M. (2021). Investigation on mechanical and microstructural properties of alkali-activated materials made of wood biomass ash and glass

powder. *Powder Technology*, *377*, 900–912. https://doi.org/10.1016/j.powtec.2020.09.048

Silva, T. H., Lara, L. F. S., Silva, G. J. B., Provis, J. L., & Bezerra, A. C. S. (2022). Alkali-activated materials produced using high-calcium, high-carbon biomass ash. *Cement and Concrete Composites*, *132*. https://doi.org/10.1016/j.cemconcomp.2022.104646

Simonsen, A. M. T., Pedersen, K. B., & Jensen, P. E. (2020). Applying Chemometrics to Evaluate Mine Tailings' Potential As Partial Cement Replacement. *KnE Engineering*, *2020*, 178–187. https://doi.org/10.18502/keg.v5i4.6808

Skevi, L., Baki, V. A., Feng, Y., Valderrabano, M., & Ke, X. (2022). Biomass Bottom Ash as Supplementary Cementitious Material: The Effect of Mechanochemical Pre-Treatment and Mineral Carbonation. *Materials*, *15*(23). https://doi.org/10.3390/ma15238357

Skibsted, J., & Snellings, R. (2019). Reactivity of supplementary cementitious materials (SCMs) in cement blends. *Cement and Concrete Research*, *124*(May), 105799. https://doi.org/10.1016/j.cemconres.2019.105799

Sklivaniti, V., Tsakiridis, P. E., Katsiotis, N. S., Velissariou, D., Pistofidis, N., Papageorgiou, D., & Beazi, M. (2017). Valorisation of woody biomass bottom ash in Portland cement: A characterization and hydration study. *Journal of Environmental Chemical Engineering*, *5*(1), 205–213. https://doi.org/10.1016/j.jece.2016.11.042

Snellings, R., Kazemi-Kamyab, H., Nielsen, P., & Van den Abeele, L. (2021). Classification and Milling Increase Fly Ash Pozzolanic Reactivity. *Frontiers in Built Environment*, *7*(April), 1–13. https://doi.org/10.3389/fbuil.2021.670996

Snellings, R., Mertens, G., & Elsen, J. (2012). Supplementary Cementitious Materials. *Reviews in Mineralogy and Geochemistry*, *74*(1), 211–278. https://doi.org/10.2138/rmg.2012.74.6

SS-EN 12350-2:2019. (2019). *Testing Fresh Concrete—Part 2: Slump Test*.

SS-EN 12350-7:2019. (2019). *Testing fresh concrete – Part 7: Air content – Pressure methods*.

SS-EN 12390-3:2019. (2019). *Testing Hardened Concrete Part 3: Compressive Strength of Test Specimens*.

SS-EN 12457-2. (2003). *Characterisation of waste - Leaching - Compliance test for leaching of granular waste materials and sludges - Part 2: One stage batch test at a liquid to solid ratio of 10 l/kg for materials with particle size below 4 mm (without or with size reduction)*.

SS-EN 16637-2:2023. (2023). *Construction products: Assessment of release of dangerous substances – Part 2: Horizontal dynamic surface leaching test*.

SS-EN 196-1. (2005). *Methods of testing cement - Part 1: Determination of strength*.

SS-EN 196-11:2019. (2019). *Methods of testing cement – Part 11: Heat of hydration – Isothermal Conduction Calorimetry method*.

SS-EN 196-5. (2011). *Methods of testing cement - Part 5 - Pozzolanicity test for pozzolanic cement*.

SS-EN 197-1. (2011). *Cement – Part 1 : Composition, specifications and conformity criteria for common cements*.

SS-EN 450-1. (2012). *Fly ash for concrete - Part 1: Definition, specifications and conformity criteria*.

SS 137244:2019. (2019). *Concrete testing – Hardened concrete – Scaling at freezing*.

Štirmer, N., & Carević, I. (2022). Utilization of Wood Biomass Ash in Concrete Industry. *Biomass,*

Biorefineries and Bioeconomy. https://doi.org/10.5772/intechopen.102549

Štirmer, N., Carević, I., Milovanović, B., & Baricevic, A. (2018). Market potential of wood biomass ash utilisation in cement composites-Croatian case study. *SynerCrete'18 International Conference on Interdisciplinary Approaches for Cement-Based Materials and Structural Concrete At: Funchal, Madeir, Portugal.*, 24–26.

Subramaniam, P., Subasinghe, K., & Fonseka, W. R. K. (2015). Wood Ash As an Effective Raw Material for Concrete Blocks. *International Journal of Research in Engineering and Technology*, *04*(02), 228–233. https://doi.org/10.15623/ijret.2015.0402030

Šupić, S., Malešev, M., Radonjanin, V., Bulatović, V., & Milović, T. (2021). Reactivity and pozzolanic properties of biomass ashes generated by wheat and soybean straw combustion. *Materials*, *14*(4), 1–20. https://doi.org/10.3390/ma14041004

Suraneni, P. (2021). Recent developments in reactivity testing of supplementary cementitious materials. *RILEM Technical Letters*, *6*, 131–139. https://doi.org/10.21809/rilemtechlett.2021.150

Suraneni, P., Hajibabaee, A., Ramanathan, S., Wang, Y., & Weiss, J. (2019). New insights from reactivity testing of supplementary cementitious materials. *Cement and Concrete Composites*, *103*(May), 331–338. https://doi.org/10.1016/j.cemconcomp.2019.05.017

Suraneni, P., & Weiss, J. (2017). Examining the pozzolanicity of supplementary cementitious materials using isothermal calorimetry and thermogravimetric analysis. *Cement and Concrete Composites*, *83*, 273–278. https://doi.org/10.1016/j.cemconcomp.2017.07.009

Sverige. Naturvårdsverket., & CM gruppen). (2010). Återvinning av avfall i anläggningsarbeten. Handbok. In *Naturvådsverket*.

Szczepanik, M., Szyszlak-Bargłowicz, J., Zajaç, G., Koniuszy, A., Hawrot-Paw, M., & Wolak, A. (2021). The use of multivariate data analysis (HCA and PCA) to characterize ashes from biomass combustion. *Energies*, *14*(21). https://doi.org/10.3390/en14216887

Szczesniak, B., Borysiuk, S., Choma, J., & Jaroniec, M. (2020). Mechanochemical synthesis of highly porous materials. *Materials Horizons*, *7*(6). https://doi.org/10.1039/d0mh00081g

Taylor, H. F. W. (1997). *Cement Chemistry* (2nd ed.). Thomas Telford Publishing.

Teixeira, E. R., Mateus, R., Camões, A. F., Bragança, L., & Branco, F. G. (2016). Comparative environmental life-cycle analysis of concretes using biomass and coal fly ashes as partial cement replacement material. *Journal of Cleaner Production*, *112*, 2221–2230. https://doi.org/10.1016/J.JCLEPRO.2015.09.124

Teixeira, E. R. R., Camões, A., & Branco, F. G. G. (2019). Valorisation of wood fly ash on concrete. *Resources, Conservation and Recycling*, *145*(February), 292–310. https://doi.org/10.1016/j.resconrec.2019.02.028

Teker Ercan, E. E., Andreas, L., Cwirzen, A., & Habermehl-Cwirzen, K. (2023). Wood Ash as Sustainable Alternative Raw Material for the Production of Concrete—A Review. *Materials*, *16*(7), 2557. https://doi.org/10.3390/ma16072557

Teker Ercan, E. E., Andreas, L., Cwirzen, A., & Habermehl-Cwirzen, K. (2025). Ground Wood Ash as a Supplementary Cementitious Material: Effects on Strength, Durability and Environmental Performance of Concrete. *Construction and Building Materials*, *Under Revi*.

Teker Ercan, E. E., Cwirzen, A., & Habermehl-Cwirzen, K. (2023). The Effects of Partial Replacement of Ground Granulated Blast Furnace Slag by Ground Wood Ash on Alkali-Activated Binder Systems. *Materials*, *16*(15), 5347.

Teker Ercan, E. E., Panek, R., Szeląg, M., Cwirzen, A., & Habermehl-Cwirzen, K. (2025). The Impact of the High-Energy Grinding of Wood Ash on Its Pozzolanic Activity. *Materials*, *18*(13).

The European Commission's Knowledge Centre for Bioeconomy. (2018). *Brief on biomass for energy in the European Union*.

Tironi, A., Trezza, M. A., Scian, A. N., & Irassar, E. F. (2013). Assessment of pozzolanic activity of different calcined clays. *Cement and Concrete Composites*, *37*(1), 319–327. https://doi.org/10.1016/j.cemconcomp.2013.01.002

Tole, I. (2022). *PhD thesis: Revalorization of poorly reactive sources by mechanochemical activation*.

Tole, I., Delogu, F., Qoku, E., Habermehl-Cwirzen, K., & Cwirzen, A. (2022). Enhancement of the pozzolanic activity of natural clays by mechanochemical activation. *Construction and Building Materials*, *352*(July), 128739. https://doi.org/10.1016/j.conbuildmat.2022.128739

Tole, I., Habermehl-Cwirzen, K., Rajczakowska, M., & Cwirzen, A. (2018). Activation of a raw clay by mechanochemical process-effects of various parameters on the process efficiency and cementitious properties. *Materials*, *11*(10), 6–8. https://doi.org/10.3390/ma11101860

Tole, I., Rajczakowska, M., Humad, A., Kothari, A., & Cwirzen, A. (2020). Geopolymer based on mechanically activated air-cooled blast furnace slag. *Materials*, *13*(5). https://doi.org/10.3390/ma13051134

Tosti, L., van Zomeren, A., Pels, J. R., & Comans, R. N. J. (2018). Technical and environmental performance of lower carbon footprint cement mortars containing biomass fly ash as a secondary cementitious material. *Resources, Conservation and Recycling*, *134*(March), 25–33. https://doi.org/10.1016/j.resconrec.2018.03.004

Tripathi, N., Hills, C. D., Singh, R. S., & Atkinson, C. J. (2019). Biomass waste utilisation in low-carbon products: harnessing a major potential resource. *Npj Climate and Atmospheric Science*, *2*(1). https://doi.org/10.1038/s41612-019-0093-5

Tripathi, N., Hills, C. D., Singh, R. S., & Singh, J. S. (2020). Offsetting anthropogenic carbon emissions from biomass waste and mineralised carbon dioxide. *Scientific Reports*, *10*(1). https://doi.org/10.1038/s41598-020-57801-5

Turk, J., Cotič, Z., Mladenovič, A., & Šajna, A. (2015). Environmental evaluation of green concretes versus conventional concrete by means of LCA. *Waste Management*, *45*, 194–205. https://doi.org/10.1016/j.wasman.2015.06.035

Udoeyo, F. F., Inyang, H., David, Y. T., & Oparadu, E. E. (2006). Potential of Wood Waste Ash as an Additive in Concrete. *Journal of Materials In Civil Engineering*. https://doi.org/10.1061/ASCE0899-1561200618:4605

Ukrainczyk, N., Vrbos, N., & Koenders, E. A. B. (2016). Reuse of Woody Biomass Ash Waste in Cementitious Materials. *Chemical and Biochemical Engineering Quarterly*, *30*(2), 137–148. https://doi.org/10.15255/CABEQ.2015.2231

Usta, M. C., Yörük, C. R., Uibu, M., Hain, T., Gregor, A., & Trikkel, A. (2022). CO2 Curing of Ca-Rich Fly Ashes to Produce Cement-Free Building Materials. *Minerals*, *12*(5). https://doi.org/10.3390/min12050513

Vassilev, S. V., Baxter, D., Andersen, L. K., & Vassileva, C. G. (2010). An overview of the chemical composition of biomass. *Fuel*, *89*(5), 913–933. https://doi.org/10.1016/j.fuel.2009.10.022

Vassilev, S. V., Baxter, D., Andersen, L. K., Vassileva, C. G., & Morgan, T. J. (2012). An overview of the organic and inorganic phase composition of biomass. *Fuel*, *94*, 1–33. https://doi.org/10.1016/j.fuel.2011.09.030

Vdovic, N., Jurina, I., Škapin, S. D., & Sondi, I. (2010). The surface properties of clay minerals modified by intensive dry milling - revisited. *Applied Clay Science*, *48*(4), 575–580. https://doi.org/10.1016/j.clay.2010.03.006

Vu, V. A., Cloutier, A., Bissonnette, B., Blanchet, P., & Duchesne, J. (2019). The effect of wood ash as a partial cement replacement material for making wood-cement panels. *Materials*, *12*(7). https://doi.org/10.3390/ma12172766

Wang, H., Wang, L., Xu, Y., Cao, K., Ge, Y., Wang, X., & Li, Q. (2022). Accelerating the Reaction Kinetics of Na2CO3-Activated Slag Mortars by Calcined Recycled Concrete Fines. *Materials*, *15*(15), 1–17. https://doi.org/10.3390/ma15155375

Wang, N., Sun, X., Zhao, Q., Yang, Y., & Wang, P. (2020). Leachability and adverse effects of coal fly ash: A review. *Journal of Hazardous Materials*, *396*(April). https://doi.org/10.1016/j.jhazmat.2020.122725

Wang, S., Llamazos, E., Baxter, L., & Fonseca, F. (2008). Durability of biomass fly ash concrete: Freezing and thawing and rapid chloride permeability tests. *Fuel*, *87*(3), 359–364. https://doi.org/10.1016/j.fuel.2007.05.027

Wang, Y., Ramanathan, S., Burris, L., Hooton, R. D., Shearer, C. R., & Suraneni, P. (2022). Reactivity of Unconventional Fly Ashes, SCMs, and Fillers: Effects of Sulfates, Carbonates, and Temperature. *Advances in Civil Engineering Materials*, *11*(2), 639–657. https://doi.org/10.1520/ACEM20220003

Ward, J. H. (1963). Hierarchical Grouping to Optimize an Objective Function. In *Journal of the American Statistical Association* (Vol. 58, Issue 301, pp. 236–244). https://doi.org/10.1080/01621459.1963.10500845

Wembe, J. T., Ngueyep, L. L. M., Elat, E., Pliya, P., Telefouet, A. J. P., Ndjaka, J. M. B., & Noumowe, A. (2024). Valorization of ashes from different wood species in cementitious materials. *Discover Sustainability*, *5*(1). https://doi.org/10.1007/s43621-024-00460-7

Wu, F., Li, H., & Yang, K. (2021). Effects of mechanical activation on physical and chemical characteristics of coal-gasification slag. *Coatings*, *11*(8). https://doi.org/10.3390/coatings11080902

Xu, W., Lo, Y. T., Ouyang, D., Memon, S. A., Xing, F., Wang, W., & Yuan, X. (2015). Effect of rice husk ash fineness on porosity and hydration reaction of blended cement paste. *Construction and Building Materials*, *89*, 90–101. https://doi.org/10.1016/j.conbuildmat.2015.04.030

Yang, Z., Huddleston, J., & Brown, H. (2016). Effects of Wood Ash on Properties of Concrete and Flowable Fill. *Journal of Materials Science and Chemical Engineering*, *04*(07), 101–114. https://doi.org/10.4236/msce.2016.47013

Yuan, Q., Zhang, Y., Wang, T., Wang, J., & Romero, C. E. (2021). Mechanochemical stabilization of heavy metals in fly ash from coal-fired power plants via dry milling and wet milling. *Waste Management*, *135*(October), 428–436. https://doi.org/10.1016/j.wasman.2021.09.029

Zając, G., Szyszlak-Bargłowicz, J., Gołębiowski, W., & Szczepanik, M. (2018). Chemical characteristics of biomass ashes. *Energies*, *11*(11), 1–15. https://doi.org/10.3390/en11112885

Zhang, J., Yan, J., & Sheng, J. (2015). Dry grinding effect on pyrophyllite-quartz natural mixture and its influence on the structural alternation of pyrophyllite. *Micron*, *71*, 1–6. https://doi.org/10.1016/j.micron.2014.12.005

Department of Civil, Environmental and Natural Resources Engineering
Division of Structural and Fire Engineering

ISSN 1402-1544
ISBN 978-91-8048-887-7 (print)
ISBN 978-91-8048-888-4 (pdf)

Luleå University of Technology 2025

LULEÅ
UNIVERSITY
OF TECHNOLOGY